Sclerochronologic and oxygen isotope analysis of growth increments in shells of the bivalve *Arctica islandica* from southwest off Iceland

Master thesis in Physical Geography

Vilde Melvik

Department of Geography

University of Bergen

May 2017

Front page picture: photographed during the Ice2ice cruise expedition GS16-204, in August 2016.

Abstract

The marine bivalve mollusc *Arctica islandica* is presently known as the longest-living non-colonial animal, and considered to be a valuable paleo proxy and recorder of past environmental variability. This study presents the first absolutely dated, statistically robust master shell chronology from the southwest Icelandic shelf (64 °N). The chronology is based on annual growth increments in ten live-collected specimens from the same population, which is combined to form a 141-year long chronology, covering AD 1873-2014. The selected study site is strategically located in the pathway of the relatively warm and saline Irminger Current, a branch of the North Atlantic Current. The Irminger Current carries North Atlantic water masses, and assembling data from *A. islandica* specimens in this area is therefore a promising tool for the reconstruction of past marine environmental conditions in the North Atlantic beyond instrumental records. The chronology was successfully constructed by sclerochronological procedures, an approach very similar to dendrochronology, by statistical age-detrending, transformation, averaging and standardization of the annual growth increment width series in the selected specimens. The seasonal stable oxygen isotope composition within the increments was also measured, which reflects seasonal variability of the water temperature at the study site. It was found that the main growing season occurs during the period of increasing water temperatures, between February/March and August/September. Comparisons between the master shell chronology and environmental records, both instrumental and proxy based, from the same region revealed that the growth signal of the population is likely to be directly or indirectly linked to certain environmental factors. Comparison with the growth data indicate that the bivalves are positively linked to the abundance of diatom phytoplankton, and negatively linked to the abundance of herbivorous copepods. These links are, however, probably weakened by the influence of other interfering environmental variables at the study location, particularly changes in stratification of the water column. A co-variability on multiannual (7-year) timescales between sea surface temperature and shell growth was also found, and the data indicate that the bivalve population has recorded low-frequency Atlantic multidecadal sea surface temperature variability over the last 140 years. The statistically strong chronology constructed in this study may potentially be used as a reference to which additionally increment data from live-collected and sub-fossil specimens from the same area can be included to extend the chronology.

Acknowledgements

First and foremost, I want to thank my supervisors Carin Andersson Dahl (Researcher I) and Professor Svein Olaf Dahl for involving me in this interesting project. Carin, being my main supervisor, has been a great support throughout my master project. She has provided me with space and confidence to independent thinking. At the same time she has always been available for discussions, advice and guidance, and she has challenged me to perform to the best of my capability. She has also made great efforts to facilitate my participation at various scientific arrangements; a paleoclimate workshop in Esporles, Mallorca; the 4th International Sclerochronology Conference in Portland, Maine, USA; and last but definitely not least, a three weeks' research cruise expedition on board the *G/O Sars* sailing between Iceland and Greenland in August 2016.

I will also express my deepest gratitude to the PhD students Fabian Bonitz and Tamara Trofimova who both have been of invaluable support and help. They have generously shared their experience, guided me in laboratory techniques, and have always been there to answer my questions. In addition to this they contribute to a friendly and motivating work environment at Uni Research Climate. Most of the work is done on the premises of Uni Research, utilising their laboratory facilities and their office accommodation allocating me my own desk at the department of Uni Research Climate, an offer I very much appreciate. I will like to thank "colleagues" at Uni Research, particularly Martin W. Miles and Odd Helge Otterå for sharing data and for fruitful discussions. I will also thank all the people who travelled with me on the Ice2ice expedition in August 2016 for making it a great and memorable experience.

I am grateful for the motivating conversations, encouragement and support given by my mom and dad, and for their interest in my work with this thesis, and for being available for discussions during my research and writing of my thesis. I want to thank my dear friend Caroline Skar Mjønes for being an essential conversation partner, sharing her own experiences from her own master project process, motivating me and always making me feel encouraged after our talks. I will also like to thank Pål for his kindness and support, and on the days my work with the thesis felt too demanding, for making me laugh.

Bergen, May 2017

Vilde Melvik

Contents

List of Figures

List of Tables

List of Abbreviations

Abbreviation	Word
AD	Anno Domini
AMO/AMV	Atlantic Multidecadal Oscillation/ Atlantic Multidecadal Variability
AMOC	Atlantic Meridional Overturning Circulation
APT	Data-adaptive power transformation
BP	Before Present (before 1950)
BWT	Bottom Water Temperature
[Chl-a]	Chlorophyll a
CPR	Continuous Plankton Recorder
CTD	Conductive Temperature Depth
EPS	Expressed Population Signal
ERSST	Extended Reconstructed Sea Surface Temperature
FX	Faxaflói station
GI	Growth Index
HadISST	Hadley Centre Sea Ice and Sea Surface Temperature
HadSST	Hadley Centre Sea Surface Temperature
IC	Irminger Current
ICOADS	International Comprehensive Ocean-Athmosphere Dataset
IPCC	Intergovernmental Panel on Climate Change
IRMS	Isotope Ratio Mass Spectrometer
KNMI	Royal Netherlands Meteorological Institute
L	*A. islandica* (Linnaeus, 1767)
MAR	Mid Atlantic Ridge
MSC	Master Shell Chronology
MRI	(Icelandic) Marine Research Institute
NAC	North Atlantic Current
NAO	North Atlantic Oscillation
NAW	North Atlantic water
NIIC	North Icelandic Irminger Current
NOAA	National Oceanic and Atmospheric Administration
PCI	Phytoplankton Colour Index
PSU	Practical Salinity Unit
RCS	Regional curve standardization
SST	Sea Surface Temperature
SGI	Standardized Growth Index
SPG	Subpolar gyre
Sv	Sverdrup measuring unit (1 Sv = 10^6 m^3/s)
$\delta^{18}O$	Stable oxygen isotope composition (in ‰)
VPDB	Vienna Pee Dee Belemnite
VSMOW	Vienna Standard Mean Ocean Water

1 Introduction

The extratropical marine settings of the North Atlantic plays a prominent role in the global heat exchange and it therefore recognized as a key location for climate research (Hansen and Østerhus, 2000). The prevailing ocean currents in this region form an intricate system which, combined with atmospheric forcing, have major impact on the regional climate system in the northern North Atlantic. In addition, deep-water formation in the Arctic, due to salinity and temperature driven water density variability, drives the global ocean thermohaline circulation and has a significant influence on the global climate system (Hopkins, 1991). The Nordic Seas are principally influenced by relatively warm and saline Atlantic water masses (> 3°C and >35 PSU; Mauritzen, 1996) which arrives from the tropics and are carried into the Nordic Seas by three branches of the North Atlantic Current (NAC), also called the North Atlantic Drift. These currents, transporting North Atlantic water masses (NAW), greatly affect the oceanic climate system, as well as the biological production and sea ice extent, in various parts of the North Atlantic region all the way up to the Arctic Ocean (Hansen and Østerhus, 2000, Mork and Blindheim, 2000). A north-western continuation of the NAC, the Irminger Current (IC), has with its Atlantic relatively warm and salty water a significant impact on the oceanic climatic conditions surrounding Iceland (Hansen and Østerhus, 2000). The prevailing favourable climate on Iceland is mostly due to the IC, which also contributes to an increased biological production in the Icelandic coastal areas (Astthorsson et al., 2007). Studies of the IC variability, such as changes in NAW transport and properties, is of great interest as it can lead to an increased understanding of the influence of the NAC in the North Atlantic region in general (Mork and Blindheim, 2000).

Currently, predictions of weather and climate beyond a timescale of only a few days in the northern North Atlantic are practically impossible (Holland et al., 2014). Reasons why this is so challenging are due to the dynamic behaviour of atmospheric and oceanic circulation patterns such as the North Atlantic Oscillation (NAO) (Hurrell, 1995), the Atlantic Multidecadal Oscillation, and the Atlantic Meridional Overturning Circulation (AMOC) that govern this region. The first instrumental climate recordings are from the terrestrial environment and date back to around AD 1860 (Gray et al., 2004). These recordings are usually marked by both temporal and spatial gaps, meaning that valuable climate information is missing. Instrumental data from marine environments are even more limited, both spatially and temporally, and only

extend back to around AD 1940 (Smith et al., 2003). Prior to the availability of instrumental records, information about environmental parameters (e.g. air temperatures, water temperatures and salinity) must be obtained by other measures such as historical documents and proxy records. Climate proxies are defined as naturally preserved physical features of the environment which can be applied as indirect substitutes for the lacking instrumental measurements of past climate variability. Dendrochronological studies of growth-rings in trees are for example a frequently used proxy method (Stokes and Smiley, 1996, p. 3). Dendrochronology is described by Stokes and Smiley (1996) as the study of the chronological sequence of annual growth rings in trees, and provides high-resolution paleoclimate archives which reveals valuable information about past terrestrial climate variability. However, as these proxies relate to terrestrial climate variability associated with atmospheric properties, they cannot reliably reflect variations which are bound to the marine environment.

Acknowledging the major impact the ocean has on the climate system in the North Atlantic, the lack of long-term, high-resolution paleoclimate archives from marine settings in this region constitute a great obstacle for further reliable climate reconstructions (Justwan et al., 2008, Holland et al., 2014). This large gap in our knowledge on how marine settings influence the climate system has resulted in an increased interest in acquiring more information from extratropical marine settings. Long-term, high-resolution proxy paleo data is considered as a criterion to establish well-confined predictive numerical climate models and thereby improve climate predictions (Justwan et al., 2008, Schöne, 2013). The Intergovernmental Panel on Climate Change (IPCC) has in its 4th Assessment Report (2007) recognized the importance of gathering more information about the climate variability in the North Atlantic region over the last two millennia. The report also acknowledges the value of data from marine proxy records extending to the present day. Several climate scientists also stress the importance of obtaining additional high-resolution proxy archives from marine settings to be in a better position to understand the processes and mechanisms of global climate change (e.g. Sicre et al., 2008, Mann et al., 2009, Wanamaker et al., 2011). Proxies from marine settings include for instance sediment cores taken from the seafloor. It is a scarcity of such archives from extratropical settings that are annually resolved, and those that are available are associated with considerable dating uncertainties (Reynolds et al., 2016). Marine sediment archives usually have a lower

frequency (multi-decadal to centennial) and temporal resolutions of maximum 5-10 years (Andersson et al., 2003, Andersson et al., 2010).

In the tropics, several high-resolution marine paleoclimate records have been established using shallow water corals (Jones et al., 2009). Similar proxy archives with the same temporal resolution from extratropical settings, using proxies such as coralline algae, cold water corals, fish otoliths and shells of bivalve molluscs, are currently quite uncommon (Schöne and Gillikin, 2013, Marali and Schöne, 2015). During the last decade, the interest in using shells of bivalve molluscs to study climate variations of the past has increased considerably (Jones, 1980), with special attention to the exceptionally long-lived marine bivalve mollusc *Arctica islandica* (Linnaeus, 1767). This particular species is considered to have great potential as a marine proxy in the North Atlantic shelf seas (Butler et al., 2009a). *Arctica islandica* has been proven to cover many of the required criteria, of which some are outlined by Thompson and Jones (1977), for the use in shell based chronology constructions (Butler et al., 2009b). 1) The *A. islandica* has an unusual great longevity, commonly >100 years (e.g. Weidman et al., 1994, Wanamaker et al., 2008). 2) The mollusc has a wide geographic distribution in the North Atlantic coastal waters (Jones, 1980, Dahlgren et al., 2000). 3) It has been shown to have a synchronous growth within a population (Jones, 1980, Thompson et al., 1980). 4) The species forms annual growth lines (Jones, 1980), and 5) the effects of past environmental influences are imprinted in their hard parts (shell) (e.g. Schöne et al., 2003, Wanamaker et al., 2011, Butler et al., 2013).

The method of analysing physical and chemical variations in the growth bands in shells of bivalve molluscs, and other marine organisms with skeletal hard parts (e.g. corals), is called sclerochronology. The term was introduced in the 1970s (Oschmann, 2009), and the methodology of sclerochronology is derived from dendrochronology, as the principle between annually formed growth lines/rings is almost identical (Witbaard et al., 2003). Growth lines separate the annually formed growth bands, often referred to as increments, and these can be measured, counted, sampled and geochemically analysed. Due to these growth increments the bivalve *A. islandica* has been referred to as 'the tree of the north Atlantic shelf' (Thompson and Jones, 1977). The ontogenetic age of the animal is determined by studying these growth increments, and precise calendar dates are assigned to each increment by counting back in time from the date of which the animal died (Thompson et al., 1980). In live-collected specimens the date of death is known and one is provided with a reference point in time to start the

counting. If this date is unknown, as is the case with sub-fossil specimens, the specimens needs to be compared, or cross-matched, with live-collected specimens to place it in time. Studies of shells of *A. islandica* have been found to enable both annual and seasonal resolution (Jones, 1980, Thompson et al., 1980, Wanamaker et al., 2011) and give a unique insight into how the shell growth of the bivalves from the same population has responded to past changes in their surrounding environment. This high-resolution response signal can be analysed together with existing environmental and climatic records attempting to decipher its origin.

As emphasised by Schöne (2013), it is essential for the understanding of past climate in the northern North Atlantic to establish a sclerochonological network based on *A. islandica* from this area, combining both the study of incremental growth patterns and geochemical analysis. To better understand the spatiotemporal variability of ocean dynamics, and to recognise forcing and feedback mechanisms operating within the climate system, statistically robust and long paleo archives from several strategically chosen sites with various climate sensitivity is required (Justwan et al., 2008). Such archives should be statistically sound region- or population-specific composite chronologies, and are also called master chronologies (Schöne, 2013). Scourse et al. (2006) emphasises how such high-resolution master chronologies from the marine environment can be applied and lead to advances in various fields of research, e.g. the history of water mass ventilation, radiocarbon reservoir corrections, and geochemical properties (stable isotopes) as indicator of water temperature and salinity. Additionally, a combination of several shell based master chronologies from key optimal locations can be used to establish a tool for assessing how anthropogenic activity impacts the marine environment (Scourse et al., 2006). Records of past climate, reflected by variations in environmental parameters such as water temperature, primary productivity and sea ice extent from around Iceland will provide a better understanding of the climatic history of this region. A paleorecord based on shells from an *A. islandica* population situated in an area bathed in North Atlantic water are of interest considering the major impact the NAC has in the North Atlantic region. Additional paleoclimate information from the area of investigation can therefore act as an indicator for a much wider region (Bryson, 1974, Ogilvie, 1983).

1.1 Objectives

The main objective of this study is to explore the potential of using *A. islandica* as a paleo environmental tool for the study of marine paleoclimate off the southwest coast of Iceland.

The working hypotheses are 1) that the growth of *A. islandica* in the population in the Faxaflói area southwest off Iceland are synchronous over a wide area making it possible to construct long master chronologies from this area, and 2) that stable oxygen isotopic composition within the growth increment reflects seasonal changes in water temperature in the Faxaflói area.

The hypotheses will be tested by:

1. Using established sclerochonological techniques to construct a continuous, absolutely-dated master chronology based on analysis of annual growth increments in live-collected specimens of the bivalve *A. islandica*.

2. Analysing the stable oxygen isotopic composition of growth increments in *A. islandica* at seasonal resolution.

An evaluation will also be performed to test whether there are any relationships between the master shell chronology and existing instrumental, historical and proxy records of various environmental variables such as sea water temperature, primary productivity, secondary productivity, sea ice extent, AMO index and NAO index, in the North Atlantic region.

2 Background

2.1 *Arctica islandica*

The marine bivalve mollusc *Arctica islandica* (Linnaeus, 1767) (Figure 1), more commonly called the ocean quahog, is considered to be a valuable paleo proxy and natural archive of the marine environment (Butler et al., 2009b). The *A. islandica* is acknowledged to be the longest-living non-colonial animal currently known of (> 500 years; Schöne et al., 2005a, Wanamaker et al., 2008, Butler et al., 2013) and is considered as a paleo proxy with great potential for climate reconstruction (Butler et al., 2013). Another essential trait of this bivalve species is its broad biogeographic distribution, confirming its ability to live in different environments: from shallow (about 5 m) to deeper water (about 500 m) (Scourse et al., 2006), with a various range of temperatures of 1°C to 16°C (Witbaard et al., 1997a) and salinity of 22 to 35 PSU (Practical Salinity Units) (Oeschger and Storey, 1993). *Arctica islandica* seem to be thriving in the coastal shelf seas of the North Atlantic, and has done so throughout the Holocene (Dahlgren et al., 2000). The species are often found at locations that are characterized by central oceanographic fronts, such as the Icelandic shelf seas (Scourse et al., 2006, Butler et al., 2013).

The physical growth rate of the bivalves are shown not to be uniform throughout the year; with usually fast growth rate during late spring and early summer, and slower growth rate in both the warmest and the coldest months (Jones, 1980). This growth variation is associated with food availability and food quality (Witbaard et al., 1997b, Schöne et al., 2005b), the duration of the growing season (Weidman et al., 1994, Butler et al., 2009b), and variability in sea water temperature (Schöne et al., 2005a). The observed synchronous growth within a population (Jones, 1980, Marchitto et al., 2000) indicate that the bivalves respond to certain environmental factors resulting in a shared environmental signal recorded in the shell of the bivalves. This implies that the bivalves are sensitive to variations in the surrounding environmental conditions, and therefore can both the growth and geochemical properties of the shells function as recorders of past environmental variabilities (Schöne et al., 2005be.g.). As first recognized by Thompson et al. (1980) the organism forms annual and even seasonal growth patterns in its shell (Weidman et al., 1994, Witbaard et al., 1994, Schöne et al., 2004, Schöne et al., 2005a, Butler et al., 2009b). The growth of the bivalve shell involves the calcification and production of aragonite calcium carbonate which leads to an expansion in both shell margin height, and in the inner shell surface

thickness (Stemmer et al., 2013). Regular changes in the rate of shell development result in the formation of growth lines (i.e. time interval of slower growth) and growth increments (i.e. time intervals of faster growth). The growth lines are possible to identify, and these mark the end of a growth increment, hence the end of the growing period of the bivalve (e.g. Weidman et al., 1994). The width of single growth increments can be measured. The variability of the growth increment widths from several specimens can be compared and, in case of overlapping lifespans and similar patterns, crossdated. This method is referred to as sclerochronology (Jones, 1980, Reynolds et al., 2016).

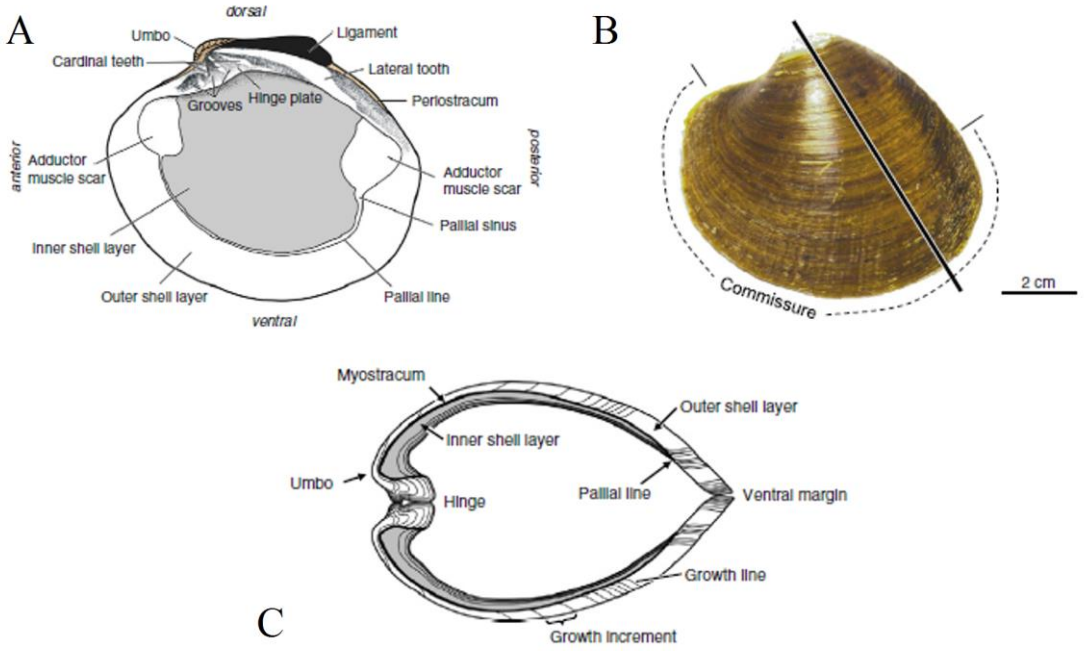

Figure 1: Morphological structures of an *A. islandica* shell. A) Interior view of the right (dextral) valve. Note that the coloured area of the hinge plate is part of the outer shell layer. B) Outer shell surface of the left (sinistral) valve. C) Umbo-ventral margin cross section as indicated in B. Modified after Schöne (2013).

During its lifetime, the growth rate of the bivalve changes a great deal, which is observed by the differing in increment widths along the longest axes from umbo to the end of the ventral margin (Figure 2). During the first few years of the bivalve's life the increment widths gradually increase until about five to ten years of age, after which the increments widths decreases exponentially, due to biological aging (e.g. Weidman et al., 1994). Growth increment series used in sclerochronological analysis can be obtained by performing exact measurements of the

consecutive increment widths from the shell margin or in the hinge plate region of the shell of each specimen (Butler et al. 2013). The shell margin is often used in addition to the hinge plate for long-lived specimens (> 300 years) because narrow increments can merge and make it impossible to visually distinguish the growth lines in the outermost part of the hinge plate region (Schöne, 2013). On the other hand, performing measurements in the margin of short lived individuals (< 50 years) can be challenging due to the geometry of the shell deposition in the wide early bands. In such cases, it is often better to use the hinge plate region (Butler et al. 2013). The morphology of the shell can also make the perpendicular measurements difficult, given this is the selected way of measuring, because the curvature of the earliest formed increments in the ventral margin makes it impossible to obtain consistent measurements. Visual cross-matching of growth increments are based on investigation of the growth between so-called 'marker-years' or marker layers. Particularly narrow or wide increments, but also distinct patterns, such as for instance several relatively narrow or wide increments in a row, can serve as marker layers. Within the same population, the most distinct marker layers are in general recognizable in all specimens studied. The growth patterns are identified based on comparing the same time interval (defined by the marker years) in all the selected specimens.

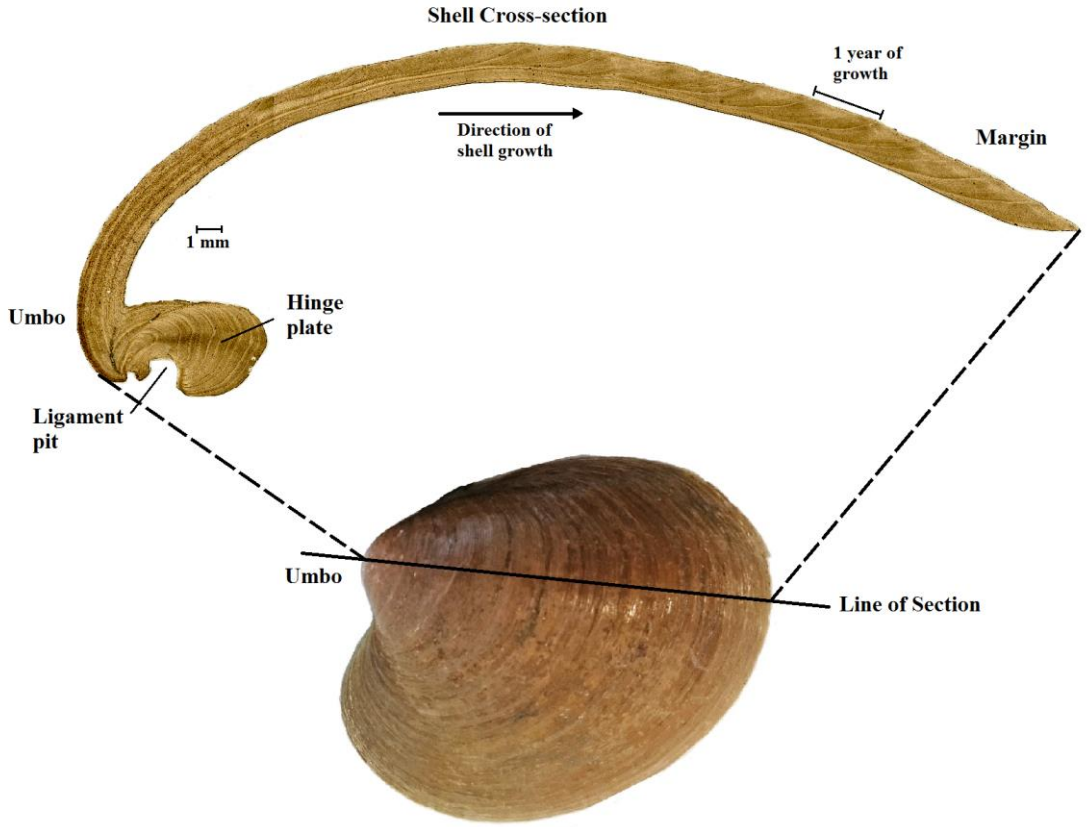

Figure 2: Composite digital microscope image (top) of the shell cross section of an *A. islandica* valve (bottom) with visible annual increments.

Precise processing procedures of the shells are required before the growth patterns of the *A. islandica* shells can be studied (Scourse et al., 2006). The bivalve mollusc has two valves which mainly differ from each other in the hinge region, where the left valve has a prominent tooth not present in the right valve (Ropes, 1987). Growth increments are formed in both this tooth and in the outer ventral shell margin, and the same relative growth pattern are found in both areas. The left valve is therefore the preferred valve for further examination, since it enables comparison of growth patterns in both areas of the shell if necessary. The left valve from all the live-collected specimens are processed to make a cross section of the longest growth axes (max height) of the shell margin, revealing the growth increments in both the outer ventral shell margin and the hinge tooth.

The growth lines imprinted in the shells and which marks the end of the growing season of the specimens being examined, represent very slow growth and eventually a total halt in the growth, usually in late autumn/early winter (Jones, 1980, Weidman et al., 1994, Witbaard et al., 1994).

It is valuable to know the approximate growth rate of the shells during different periods of the year to enable further interpretations of the geochemical and sclerochronological data from the *A. islandica* specimens (Schöne et al., 2005a). By analysing whole seasonal cycles the aim is to determine the approximate growing season of the *A. islandica* population, meaning the period when the bivalve is usually growing each year and the period when environmental variability is recorded during the shell formation.

Arctica islandica specimens of the same population usually grow at similar rates and this allows calculation of the population growth response to a common environmental signal or to some combination of some environmental drivers (Lohmann and Schöne, 2013, Butler et al., 2013). Specimens of which life-spans overlap can be cross-matched by comparing the annual growth increment series, and when combined they form a master chronology; a statistically sound region- or population-specific composite chronology (Schöne, 2013). Several *A. islandica* annually-resolved master shell chronologies of different lengths have been established for the North Atlantic region and used for the purpose of identifying possible shell growth responses to climate in the North Atlantic (Witbaard et al., 1997a, Marchitto et al., 2000, Schöne et al., 2002, Scourse et al., 2006, Wanamaker et al., 2008, Butler et al., 2009b, Wanamaker et al., 2009a, Butler et al., 2010, Wanamaker et al., 2012, Butler et al., 2013, Holland et al., 2014, Marali and Schöne, 2015, Mette et al., 2015). More specifically, *Arctica islandica* from Icelandic waters, mostly from north off Iceland, have been investigated in several studies (Schöne et al., 2005a, Wanamaker et al., 2008, Wanamaker et al., 2012, Butler et al., 2013, Lohmann and Schöne, 2013, Marali and Schöne, 2015). These studies have resulted in three shell based chronologies using *A. islandica* populations situated on the North Icelandic shelf (Butler et al., 2013, Marali and Schöne, 2015, Lohmann and Schöne, 2013). No such shell-based chronology exists from the shelf area southwest off Iceland, prior to this study.

2.2 Oceanographic and climatic setting

2.2.1 The northern North Atlantic region

The northern North Atlantic is a climatically important region which is greatly influenced by both oceanographic and atmospheric forcing (Hansen et al., 2008). The Nordic Seas (the Greenland, Iceland and Norwegian Seas) are situated in the northern North Atlantic and are all separated by deep submarine ridges. The water movement in this area is mostly topographically steered and these ridges therefore have a major influence on the direction of the ocean currents (Hansen and Østerhus, 2000, Mork and Blindheim, 2000). The Nordic Seas are dominated by warm saline North Atlantic Water and/or cold, low salinity Polar water arriving from the Arctic (Hopkins, 1991). The Nordic seas receive Atlantic inflow water from the North Atlantic Current (NAC), also called the North Atlantic drift, which transports relatively warm saline water (>3°C and >35 PLU (Mauritzen, 1996)) originating from the tropical North Atlantic Ocean (Hansen and Østerhus, 2000). The NAC flows northwards and crosses to the eastern side of the Mid-Atlantic Ridge, after which it divides into three separate branches termed by Hansen et al. (2008) as the Iceland Branch, the Shetland Branch and the Faroe Branch. The Iceland Branch, the smallest and also somewhat cooler and less salty than the other branches, flows north-eastward along The Mid-Atlantic Ridge (MAR). This current almost reaches Iceland before it shifts course and crosses to the western side of the Reykjanes Ridge, part of the MAR, into the Irminger Sea, traveling northwards along the ridge and the west coast of Iceland (Mauritzen, 1996, Hansen and Østerhus, 2000). This westward flowing branch commonly known as the Irminger Current (IC) is in scope for this project. The IC is measured to be on average 200 km wide and reaching 1500 m isobath (Våge et al., 2011).

The average water transport of the IC above 500 m is estimated to be about 7 Sv (Sverdrup measuring unit), however, there are considerable inter-annual variability (Våge et al., 2011). Without the relatively warm IC, the climatic conditions on and around Iceland, which is situated adjacent to the Arctic Circle at 63-67°N and 18-23°W, would be considerably cooler than it is (Hansen and Østerhus, 2000). The IC continues northward through the Denmark Strait, the channel between Greenland and Iceland (Hansen and Østerhus, 2000), which connects the Atlantic Ocean and the Arctic Ocean, where it divides into two branches. The main branch flows towards the west, turns southwards and flows parallel to the cold East Greenland Current

(Hansen and Østerhus, 2000). The minor branch, constituted of about 5-10 % of the IC, named the North Icelandic Irminger Current (NIIC), flows eastwards over the North Icelandic shelf and partly also towards the east coast (Vilhjálmsson, 2002). The NIIC is accountable for the relatively mild climate in the northern Iceland area and greatly influence the productivity of the marine ecosystems in this area (Logemann et al., 2013, and references therein).

The various ocean currents present in this region **(**Figure 3) and variability in atmospheric properties like pressure gradients and wind fields, have a combined effect on the climate conditions on and in the area surrounding Iceland (Hansen and Østerhus, 2000). The IC is under the influence of the changing water composition of the Nordic Seas, and both the strength and the shape of the North Atlantic subpolar gyre (SPG) greatly influence the temperature and salinity of the IC (Hátún et al., 2005). The subpolar gyre is an anticlockwise rotating body of relatively cold and low-salinity water in the central northern North Atlantic south off Iceland, which ration is due to strong winds moving with the earths' rotation (Hátún et al., 2009), known as the Coriolis effect. The NAC also gets stronger during substantial deep water formation, which is associated with a strong Atlantic Meridional Overturning Circulation (AMOC), and weaker during periods dominated by freshening of the sea surface, when polar meltwater arrives from the East Icelandic Current and East Greenland Current (Knudsen et al., 2004).

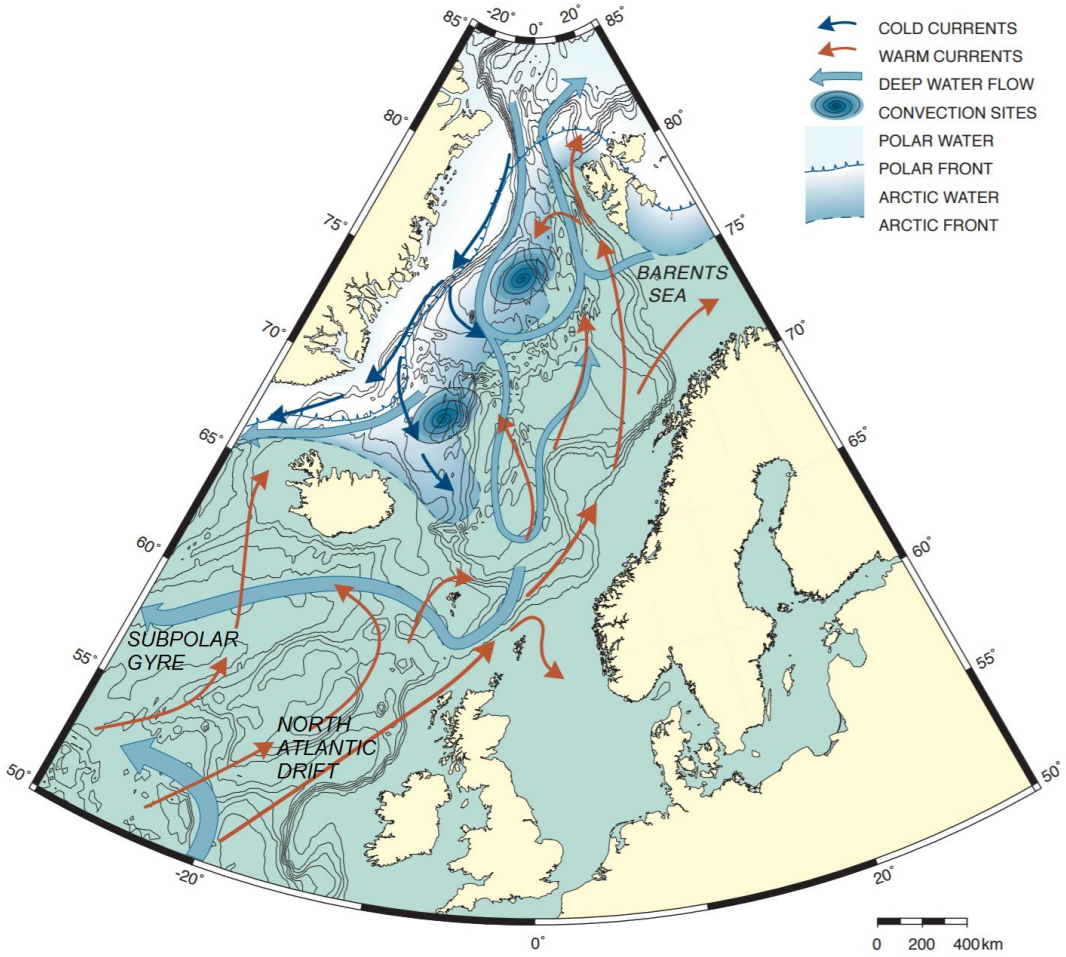

Figure 3: General oceanography of the Nordic Seas. The North Atlantic drift is illustrated by red arrows. Modified after Eva Bjørseth, Dept. Earth Science, University of Bergen.

2.2.2 The North Atlantic Oscillation and the Atlantic Multidecadal Oscillation

The North Atlantic Oscillation (NAO) is the dominant mode of atmospheric variability in the North Atlantic region (Hurrell, 1995) , and involves the difference of atmospheric pressure at sea level between the Icelandic low-pressure and the Azores (Portugal) high-pressure (Hurrell, 2001). A positive NAO phase indicates the presence of strong winds blowing across the Atlantic from the west, also known as westerlies, which bring warm and moist air to Europe. This typically leads to a shift towards milder winters and increased precipitation in Northern Europe. In the event of the opposite and thus negative NAO index where the westerlies are suppressed, the temperatures are more extreme, frequent heatwaves during summer, unusually cold winters

with reduced precipitation rate. Strong westerlies associated with a positive NAO mode has been shown to boost the AMOC by increasing convection and deep-water formation (Drinkwater et al., 2014, and references therein). The combination of differences in ocean water density, hence deep-water formation, at high northern latitudes and variability in Southern Ocean winds result in the AMOC (Marshall et al., 2001, Drinkwater et al., 2014). A strong AMOC results in enhanced NAC transport and thereby more heat into the North Atlantic (Mahajan et al., 2011). It is recognized that the internal AMOC variability to some extent is reflected by the Atlantic Multidecadal Oscillation (AMO), and an abnormally strong overturning is linked to warm temperatures in the North Atlantic (Drinkwater et al., 2014, and references therein).

The AMO, a reference first used by Kerr (2000), is a mode of observed multidecadal climate variability with fluctuations between cool and warm phases in the Northern Hemisphere (Knight et al., 2006). It can be described as the dominant mode of low-frequency, North Atlantic (0-70°) Sea Surface Temperature (SST) variability (Kerr et al., 2000, Gray et al., 2004). By examining available instrumental records over the last 150 years it is shown that the SST in the North Atlantic varies on multidecadal time scales (Drinkwater et al., 2014, and references therein). However, it is not yet determined if the variability is a true oscillation (Drinkwater et al., 2014, and refernces therein), meaning that data from 150 years of observations is not sufficient to state with certainty that the SST in the North Atlantic always is an repetitive phenomenon. In recent studies this climate mode is therefore referred to as the Atlantic Multidecadal Variability (AMV) (e.g. Ba et al., 2014). Despite this new interpretation and terminology, I will refer to this mode as the AMO. The connection between AMO and other factors besides the AMOC, such as wind forcing and aerosols, is not yet fully understood (Drinkwater et al., 2014). It is of relevance to mention that until recently the understanding of multidecadal variability in SST prior to 1950 was mainly based on high-resolution proxy records from the terrestrial environment, due to the scarcity in high resolution marine proxy records (Drinkwater et al., 2014).

The AMO signal has been observed to be relatively strong in the area around Iceland and southern Greenland since the 1990s, and the anomalously high SSTs are probably due to an enhanced NAW transport by the Irminger current (Drinkwater et al., 2014). The strengthening of the Irminger Current in the recent years has for instance been shown to contribute to

submarine melting and fast retreat of the south-east Greenland Ice-sheet glaciers, and the spatial extent of this melting is shown to be related to the northern limit of the IC (Drinkwater et al., 2014, and references therein). A weakening of the NAC is associated with the strengthening of the subpolar gyre (SPG), when cold water masses from the gyre dominates the northern northeast Atlantic due to its suppression of the NAC, which prevent some of the warm saline North Atlantic water (NAW) to reach higher latitudes (Hátún et al., 2005, Nye et al., 2014). In contrast, when the subpolar gyre weakens, coinciding with positive AMO phases, this allows for NAW to flow more freely into the northern North Atlantic (Nye et al., 2014). Abrupt shifts in the intensity of the SPG has also been associated with the reversal of the NAO index (Lohmann et al., 2009). The impact of varying SPG intensity is most pronounced in the Iceland Basin (Hátún et al., 2005), and the dynamics of primary productivity in this area has been shown to be influenced by the subpolar gyre in this region (Hátún et al., 2009). It is therefore reasonable to expect that the overall consequence of a weaker subpolar gyre, leading to increased NAC transport to the northern North Atlantic, will have a positive effect on the marine ecosystem as a whole, including the *A. islandica* south west off Iceland.

3 Study area

3.1 Area of investigation

In this project, several specimens of the bivalve *A. islandica* were collected from about 100 m depth at the southwest Icelandic shelf in the Faxaflói area (Figure 4). This study site is selected due to the existence of *A. islandica* populations in this area, and because the location is essentially affected by Atlantic water carried by the Irminger Current (IC) (Stefánsson and Guðmundsson, 1976). Iceland in general is located in a climatically sensitive area which is influenced by major features of the oceanic and atmospheric circulations (Ogilvie, 1983). Climatic changes influencing the North Atlantic Current, and thereby also the IC is expected to have an impact on the ecosystems situated within its path, including the *A. islandica* population studied in this project. These North Atlantic water masses are highly productive, and the primary productivity of the Icelandic shelf is therefore influenced by the IC due to the favourable temperature of the water and its transportations of large quantities of nutrients (Phosphor and Nitrate) from the tropics (Astthorsson et al., 2007). Iceland is also situated close to the main stream of North Atlantic westerlies (westerly winds) which have a strong influence on the climate in the North Atlantic (the 'Iceland Low') (Ogilvie, 1983). The instrumental records from this area are temporally and spatially incomplete. This becomes an obstacle when trying to develop a better understanding of environmental internal drivers, such as the North Atlantic Oscillation (NAO) and the Atlantic Multidecadal Oscillation (AMO), which contribute to ecosystem changes in the IC southwest off Iceland.

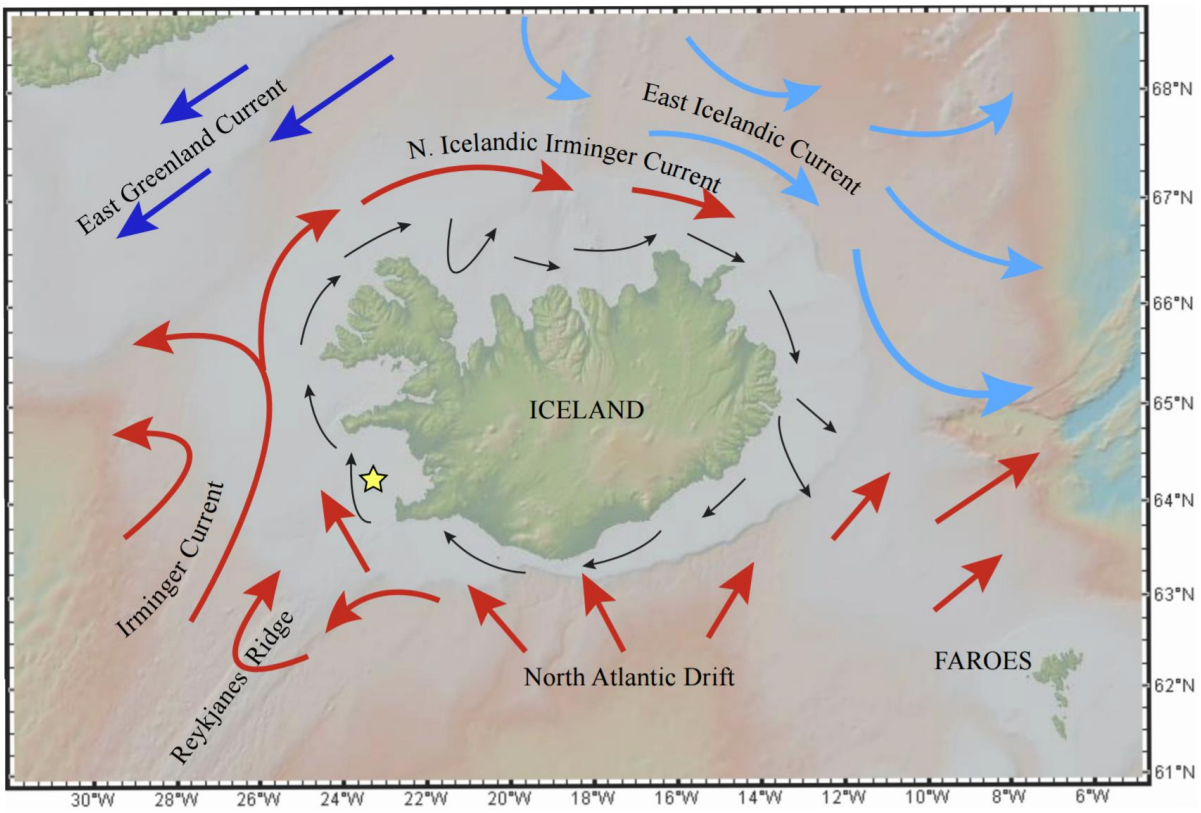

Figure 4: Location of the shell collection site (yellow star) off the southwest coast of Iceland, in the Faxaflói area. Arrows indicating the major surface ocean currents (red and blue) and coastal currents (black).

Records of meteorological observations on Iceland are limited. The IC has been monitored by Icelandic researchers for years and measurements are documented, however these records are limited to the most recent decades (Hansen and Østerhus, 2000). The first instrumental observations from the area around Iceland were carried out and documented from 1749-1751 near Reykjavik, and later similar observations were made temporarily at several locations. Continuous systematic weather observations on Iceland was initiated when a meteorological station was established at Stykkishólmur in 1845 (Ogilvie, 1983). Long term records of bottom water properties are very scarce, but these are the instrumental records that best reflect the ambient environment of the benthic fauna (Butler et al., 2010). Most of the existing instrumental records from the area around Iceland are gathered and presented on the online Oceanographic Group home page of the Icelandic Marine Research Institute (Valdimarsson, http://www.hafro.is/Sjora/). The data collection is done spatially systematically by dividing the

coastline of Iceland into sections (Figure 5) where the sampling stations form transects extending away from the coast.

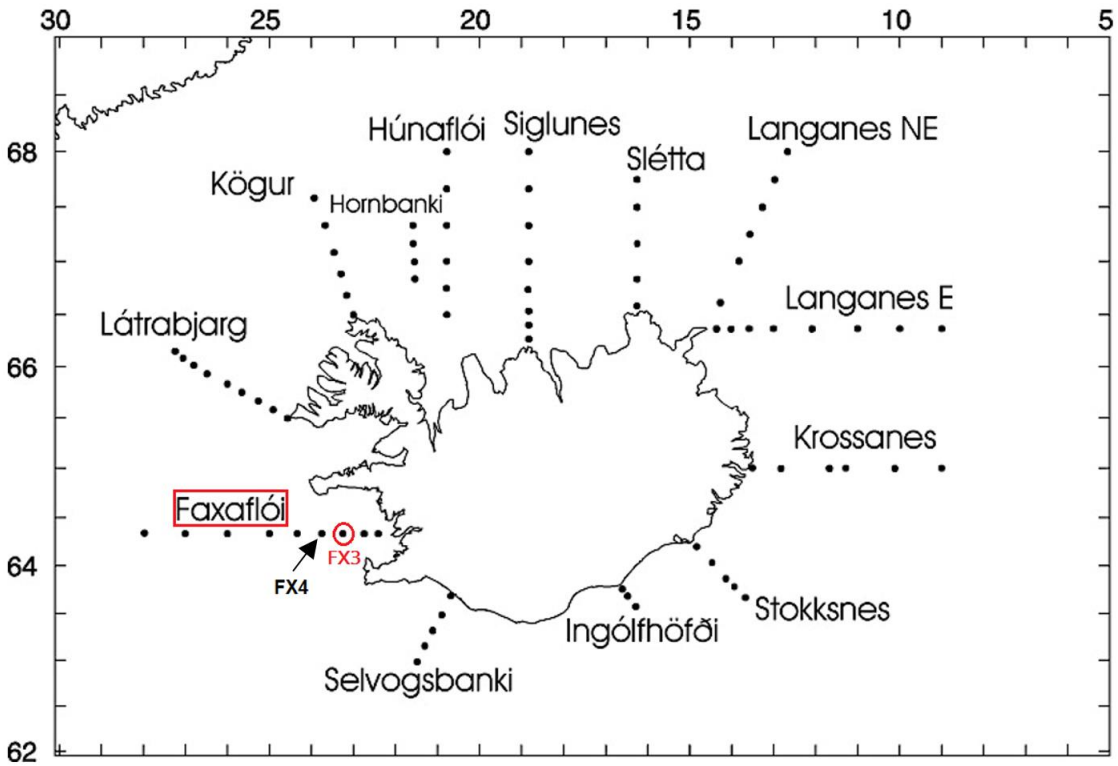

Figure 5: Hydrographic sections around Iceland. Shell material used in this study was collected close to station FX3 in the Faxaflói area. Modified after Hafrannsóknastofnun, Marine Research Institute, Reykjavík.

Since 1947, regular cruises have been carried out with varying intervals. After 1984, cruises have usually been done three to four times a year, most often in February, May, August and November, and Conductive Temperature Depth (CTD) profiles is obtained from several stations along the transects. Instrumental measurements of sea water temperature and salinity are obtained at 9 standard stations on the Faxaflói hydrographic section which is the section crossing the site of the *A. islandica* population in this study. A hydrographic station along this transect, Faxaflói station FX3 (64° 20´ N 23° 15´ W), is located 6.7 km from the shell collection site and has measurements from depths of 0 m, 20 m, 50 m and 100 m **(**Figure 5). Measurements recorded at 100 m are used for comparison with the data produced in this project. There are many gaps in the records, and the measurements are done with irregular intervals throughout

the different years. There is a particularly large gap in the instrumental record at station FX3, meaning no data available between1996-2005. The neighbouring station located ca 30 km further west of the shell collection site, FX4 (64° 20´ N 23° 45´ W), has data from this period. Mean salinity and temperature at the two stations (based on measurements taken during the period 2008-2015) differ by 0.07 PSU and 0.08°C, respectively and it is therefore assumed that data from both FX3 and FX4 adequately represents the approximate local growing environment of the bivalve population investigated in this study. Hence, data from both stations can give an as correct representation as possible of the water masses of which the current *A. islandica* population is living in.

According to Schöne et al. (2005b) it is advantageous to study specimens of *A. islandica* populations situated above the thermocline for the purpose of comparison with records of environmental variability, as such records mostly exists for surface waters. However, bivalve population situated in shallower water are influenced by the freshwater input from the terrestrial environment and the shell growth will therefore probably be influenced by more local, both month-month and year-to-year, variations. The site used for collection of the shells should therefore preferably not be subject to local influence of freshwater runoff or be located in an estuary (Butler et al., 2010) because this can influence the shell growth and possibly hide other signals of the changing properties of the North Atlantic water itself. To better be able to argue which environmental variability is affecting the bivalve growth it is important to have an overview of the various properties of the waters at the study location. The salinity, water temperature and the ecosystem composition in the area are therefore investigated more thoroughly based on available instrumental data and literature which describes the area.

3.2 The environmental conditions of the study area

3.2.1 Salinity

Varying water density, which are a result of the varying sea water temperature and salinity, causes the water masses to differ both vertically and horizontally (Hopkins, 1991). The study site is located quite close to the coast and it is natural to expect that different water masses with varying properties is present. The freshwater input to the Faxaflói area is a combination of direct runoff from land, surplus precipitation and the advection of low-salinity water carried by the

clockwise coastal current present around Iceland (Figure 4) (Stefánsson and Guðmundsson, 1976, Valdimarsson and Malmberg, 1999). Freshwater thickness was measured by Stefánsson and Guðmundsson (1976) between February 1966 and March 1967 to be at its thickest of 1.5 m in the Faxaflói area, and the direct freshwater run off into the Faxaflói Bay average of 29.28×10^6 m^3 per day. The freshwater input to the coastal water is at its highest during the late autumn which affects the water properties of the area. The dispersion of coastal waters both down in the water column and further away from the coast vary between seasons **(**Figure 6), where the boundary between coastal and open water occurs to be at maximum 50 m depth during spring (May) and mostly above 80 m during autumn (October/November). However, this coastal current and freshwater input is not likely to greatly interfere with the contribution the IC has at the site where the shell population is situated. This is determined by studying instrumental measurements of salinity of the water masses at the study site.

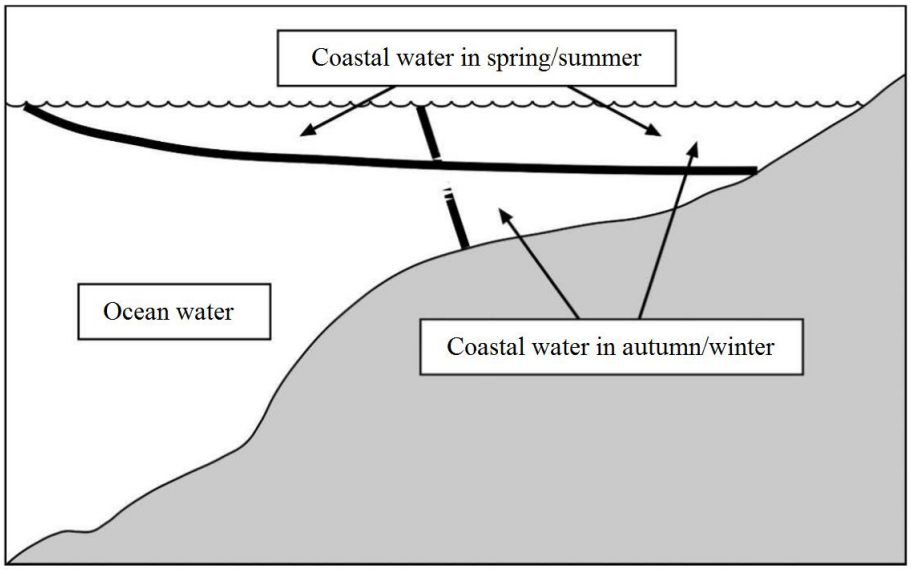

Figure 6: Standard summer and winter restrictions of coastal water at the coast of Iceland. Modified after Hanna et al. (2006, p. 5656, Fig. 3).

Hydrographic sections of the water masses in the Faxaflói area indicates the mean salinity at different stations for certain months and years (Figure 7). By studying such vertical sections from the station FX3 together with numerical records of salinity from the same area, it is possible to get a good overview of the principal water masses influencing this area. Based on these measurements the location and depth of the *A. islandica* population studied in this project

are submerged primarily by high salinity (> 35 PSU) North Atlantic water transported by the IC (Table 1).

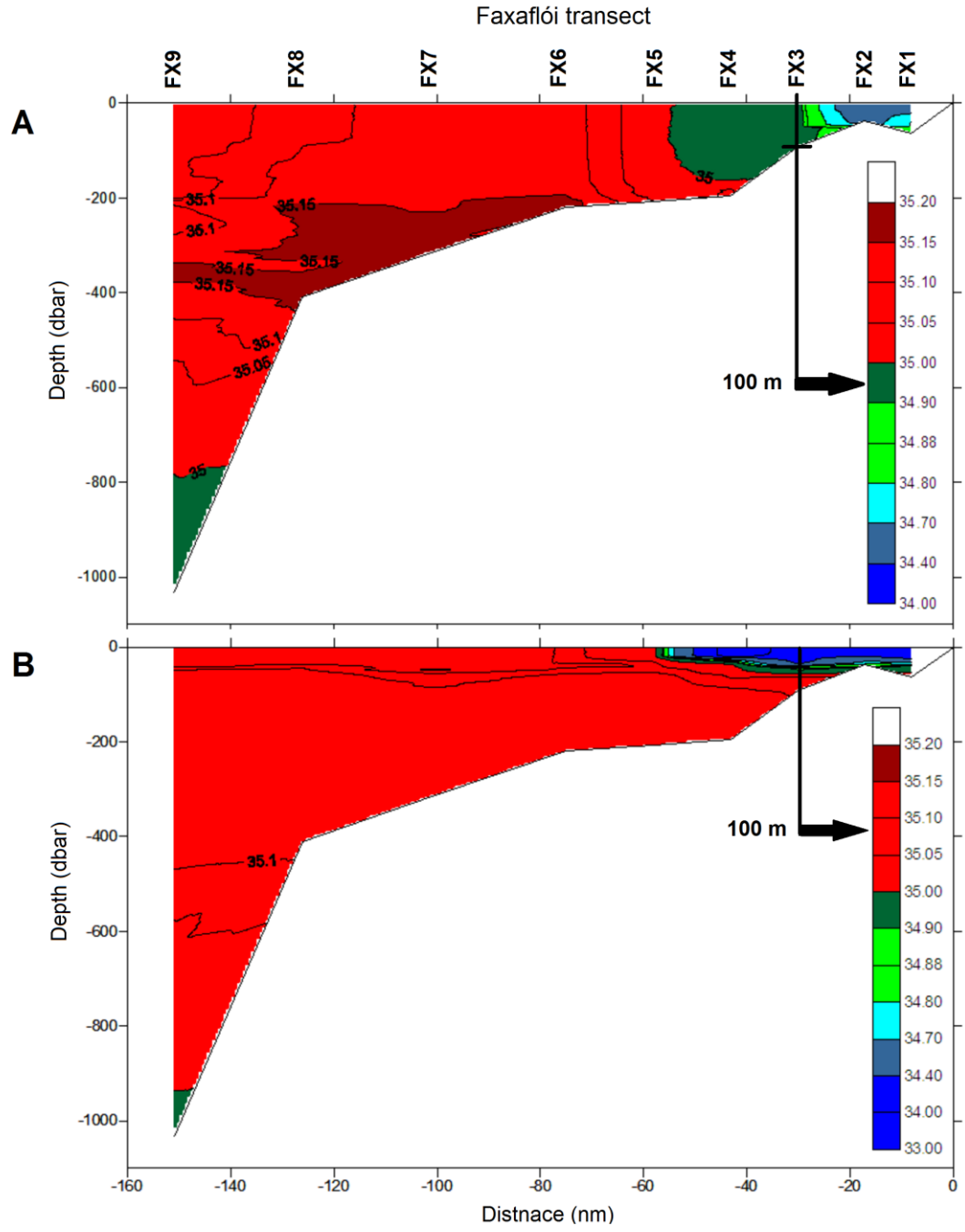

Figure 7: Hydrographic sections of the Faxaflói transect, black arrows indicate the salinity at 100 m depth at FX3. A) Anomalous low salinity recordings in November 2012. B) Hydrographic section from August 2014 illustrating how the approximately average salinity of FX3 and FX4 would appear, showing a more uniform temperature of the water column and less stratification. Hydrographic sections were only available from the period 1997-2016. Modified after Hafrannsóknastofnun, Marine Research Institute, Reykjavík (http://www.hafro.is/Sjora/).

Table 1: Salinity data comparison of Marine Research Institute (MRI) data from Faxaflói station FX3 and FX4 (100 m depth). NB. Measurements taken at the two stations were not always made at the same time of the year or even during the same year. It is therefore not always possible to compare the same years or months throughout the records.

Month	*Min salinity (PSU)*		*Max salinity (PSU)*		*Average salinity (PSU)*	
	FX3	*FX4*	*FX3*	*FX4*	*FX3*	*FX4*
February	34.99	35.03	35.11	35.21	35.06 (2008-2015)	35.14 (2000-2015)
May	35.04	35.12	35.21	35.22	35.12 (2008-2015)	35.15 (2001-2015)
August	35.08	35.12	35.20	35.24	35.13 (2008-2015)	35.14 (1999-2015)
November	34.89	34.82	35.17	35.16	35.04 (2008-2015)	35.14 (2000-2013)
Yearly	34.71	34.82	35.21	35.24	35.09 (2008-2015)	35.16 (2008-2015)

PSU (Practical salinity Unit)

Lower salinities than what is the case for North Atlantic water (NAW) are occasionally observed in the existing salinity record. During the period of instrumental salinity recording at FX3 (inconsistent measurements since March 1947), there are only eight values that are slightly below 35 PSU. The lowest recorded salinity occurred in April 2015 (34.713 PSU), and November 2012 (34.992 PSU). It is a recurring event that the lowest salinity of the year occurs between November and April. These values indicate periods of some years when the *A. islandica* population has been bathed in a mixture NAW and coastal water with lower salinity. Throughout the Faxaflói transect, stations FX3-FX9, there are temporal and spatial variations in salinity (Figure 8). The salinity throughout the transect have a maximum range of 0.22 PSU between FX3 and FX9, in November 2012. Thus, the salinity at FX3 deviates the most compared to the other stations further away from the coast along the Faxaflói transect. Nonetheless, the average salinity at FX3 is > 35 PSU which indicates mainly North Atlantic water masses at the site of shell collection.

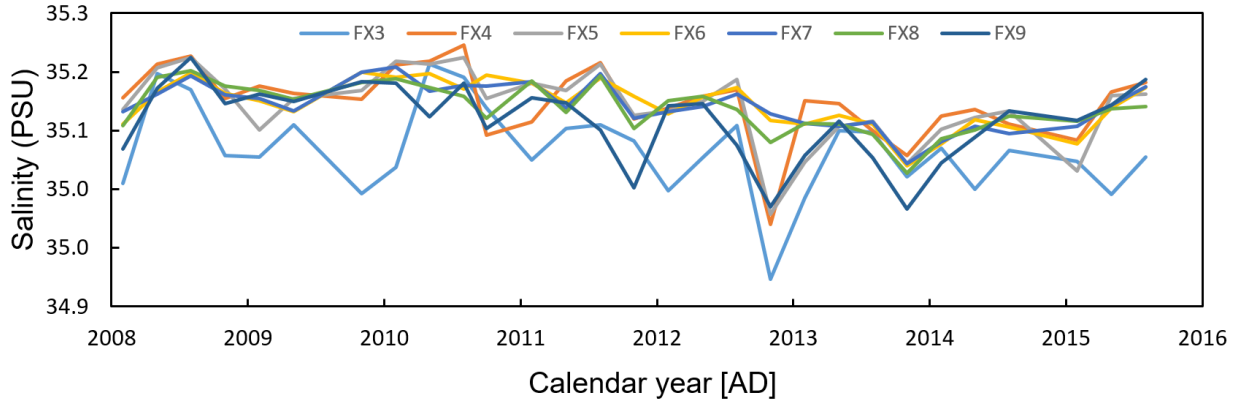

Figure 8: Salinity at 100 m depths at Faxaflói stations FX3 to FX9. Data from FX1 and FX are not included because these stations are situated in water depths shallower than 100 m depth and there are therefore no recordings from this depth.

3.2.2 Temperature

Throughout the Faxaflói transect the highest temperatures occur (based on the available monthly recordings) in August to November, and the lowest temperatures are usually found in February (Figure 9). There are generally less variations in temperature at 100 m depth at the stations further away from the coast. This indicate more mixing of water masses and heat exchange between different layers of the water column closer to the coast, which is probably because the water gets shallower towards the coast (Figure 10). The temperatures at the different stations vary about 1.5°C at the most which is usually during the summer, where the warmest temperature often occur at FX3 and FX4.

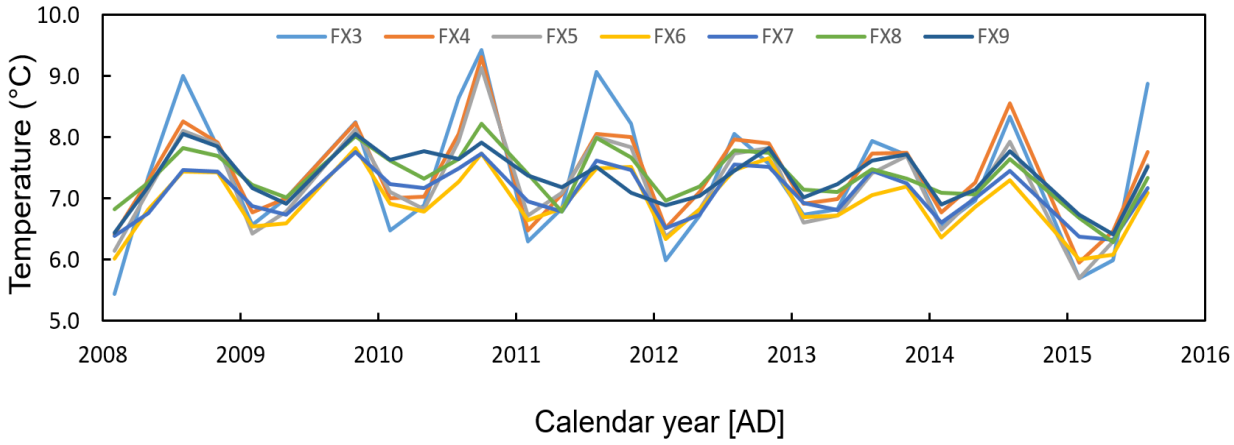

Figure 9: Temperatures at 100 m depth from the Faxaflói stations FX3 to FX9. Station FX1 and FX2 have no data at 100 m depth.

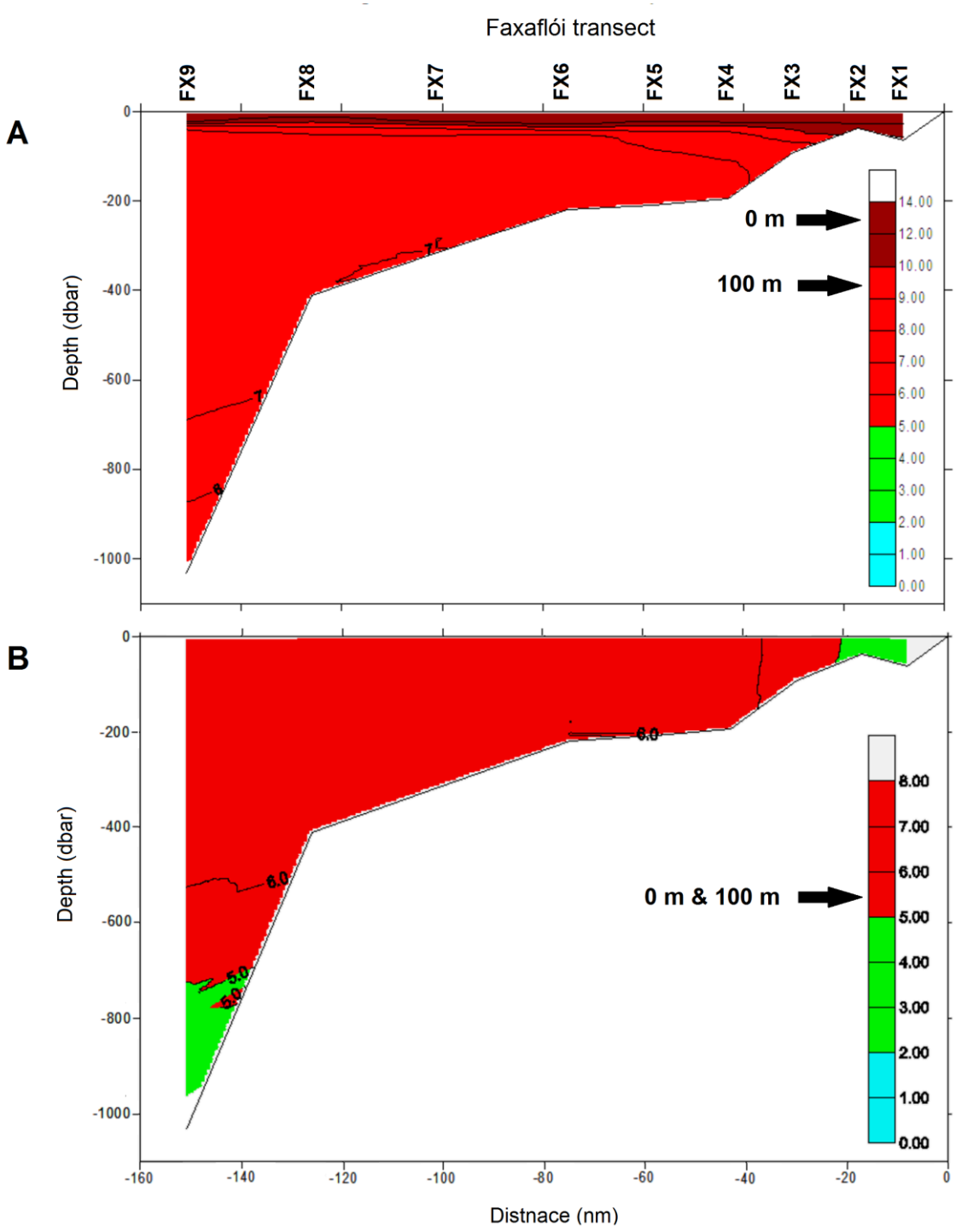

Figure 10: Hydrographic sections of the Faxaflói transect, black arrows indicate the temperature at FX3 at 0 m and 100 m depth, respectively. A) Year with high sea surface temperature during August 2010. B) Year with lowest temperatures during February 2008. Modified after Hafrannsóknastofnun, Marine Research Institute, Reykjavík (http://www.hafro.is/Sjora/).

The inconsistency in temperature data from the study area must be taken into consideration when analysing the data as it can be a source for bias. There are more data available for the surface waters throughout the Faxaflói transect compared to the measurements from other depths. When comparing bottom water temperature (BWT) measurements with the monthly sea surface temperature (SST) (HadlSST1) record one will get an indication of which month is probable to be the warmest also at100 m depth (Table 2). The highest SST occur in August, and this is sometimes also the case for the BWT, although the temperature rise is not as evident. However, the highest temperature at 100 m depth often occur later in the year than August. The timing of when the warmest temperature occurs at 100 m depth depend on the water mixing and the heat exchange between different depths. The recordings are inconsistent and thus it is not possible to identify which of the months is mainly the warmest. However, the data indicate that the highest temperature at 100 m depth occur in the months between August-November depending on when the heat transfer from the surface reaches further down in the water column.

Table 2: Highest and lowest MRI recorded temperature measurements at FX3 and FX4, at both the surface and at 100 m depth, in the period between 2008-2015.

Water depths	*Min. temp.*	*Max. temp.*	*Average*
FX3 (100 m)	5.44°C (February 2008)	9.42°C (October 2010) *8.4 °C (August 2010)*	7.29°C
FX4 (100 m)	5.95°C (February 2015)	9.31°C (October 2010) *8.05°C (August 2010)*	7.37°C
FX3 (0 m) SST	5.41°C (February 2008)	12.95°C (August 2010)	8.22°C
FX4 (0 m) SST	5.94°C (February 2015)	13.52°C (August 2010)	8.35°C
HadlSST1 SST (2004-2010)	5.66°C (February 2015)	12.33°C (August 2010)	9.23°C

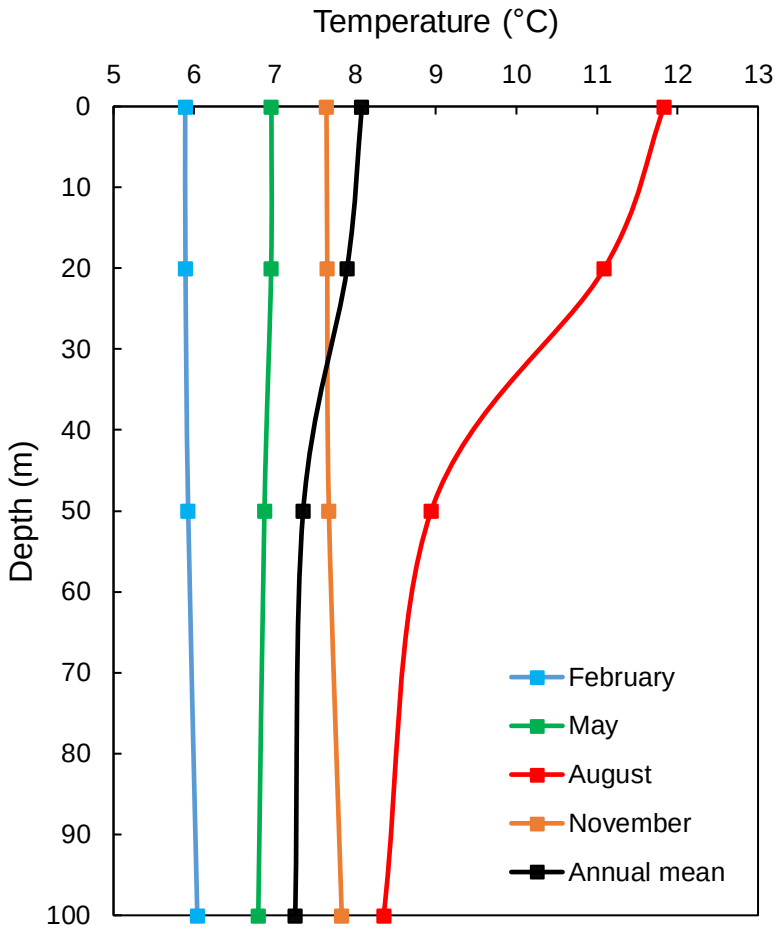

Figure 11: Records of water temperatures at FX3 demonstrate water stratification. Average of 2011-2013 at the sea surface, 20 m, 50 m and at 100 m depth, in February (blue line), May (green line), August (red line), November (orange line), and for the whole year (black line).

It is enough data recordings from August collected over the same years to calculate the average of both SST and BWT (100 m) at FX3 for August in the period 2010-2015. This available data demonstrates a high seasonal temperature gradient with a mean temperature difference in August between surface water and water at 100 m depth of 3.29°C, varying between 11.74°C and 8.45 °C, respectively. The temperatures are much more uniform throughout the water column in February, May and November (Figure 11). The average temperature difference in August indicates a higher degree of stratification of the water column during the summer, with a thermocline separating the deeper calm water from the surface well-mixed water (Figure 11). The months with lowest SST is February/March, which is also the case for the water at 100 m depth. The SST at FX3 is shown to deviate by a few degrees higher during the summer/autumn than the BWT at 100 m depth.

3.3 The ecosystem in the study area

The marine ecosystem of the Icelandic shelf seas is considered to be highly sensitive to climate variations (Astthorsson et al., 2007). The Irminger Sea seems to be an area with a high biological productivity (Gislason, 2003). Estimates show that there is a higher mean annual primary production in the west of Iceland, which is mostly affected by NAW, compared with the area in the north and east which have more variable water masses (Astthorsson et al., 2007). The primary productivity is also usually higher closer to the coast than farther offshore (Astthorsson et al., 2007). Understanding the biological production in the area is of importance when analysing the ecosystem, and the distribution of the phytoplankton in the area is one of the most important factors and therefore must be considered. The vertical phytoplankton distribution is mainly influenced by the supply of light, which is highest at the uppermost, well-mixed surface layer. The phytoplankton tend to stay within this level provided sufficient nutrient supply (Mellard et al., 2011). If low nutrient supply at the surface, however, the phytoplankton can live closer to the seafloor provided sufficient light (Mellard et al., 2011). The water column is often due to physical stratification, divided into distinct layers, a poorly mixed deep layer below a well-mixed surface layer (Mellard et al., 2011, and references therein). This boundary, the thermocline, separates the surface water from the calmer water beneath and to what degree these layers are separated is dependent on the temperature and salinity difference between the upper and the lower level. When the temperature difference is significant, as during summer months, a strong thermocline is established hindering the upward flux of nutrients from the bottom. During the winter and/or early spring, the temperature differences between surface and deeper water is low and the flux of nutrients upwards is not hindered and the sea surface is fertilized (Drinkwater et al., 2014). The consequence is an initiation of the spring phytoplankton bloom and increased primary production in the sea surface when the supply of sunlight decrease. Increased transport by the North Atlantic Current (NAC) will also result in higher temperatures and increased level of nutrients to the Icelandic waters, thereby contributing to the phytoplankton boost (Astthorsson et al., 2007).

The phytoplankton has a key role in the marine ecosystem. They make up nearly half of the global net primary production, being a major food supply of several zooplankton and fish species, and are also an important contributor to the carbon cycle (Field et al., 1998, Richardson and Schoeman, 2004). Phytoplankton also constitute most of the means of subsistence of the *A.*

islandica (Morton, 2011). As mentioned earlier, the growth of the bivalve is considered mainly to be affected by food availability and food quality. The abundance of phytoplankton in the water surrounding the bivalve population is therefore considered to influence the growth of the *A. islandica*. The bivalves are assumed to start growing in response to the phytoplankton spring bloom which determines when new potential supplies of food are available for the bivalves (Witbaard et al., 1997b). This link between phytoplankton and *A. islandica* is of importance when investigating the environmental influences which determine the growth of the bivalve.

The marine ecosystem is in general better monitored in the northern parts of Iceland than in the south and western parts where the ecosystem seems to be more complex (Astthorsson et al., 2007). In the north there are good indications that the food chain is simply controlled by a bottom-up transfer of biomass from phytoplankton through the copepods, and further via for example capelin and to the Icelandic cod (Astthorsson et al., 2007). The higher primary production on the west Icelandic shelf is known to result in higher copepod abundance compared with the north Icelandic shelf (Astthorsson et al., 2007). Higher zooplankton abundance can have a ripple effect further up in the food chain, affecting e.g. Icelandic capelin (*Mallotus villosus*) which mainly prays on the copepod and euphausiid stocks in the area (Gislason and Silva, 2012). Furthermore, capelin are the main single item in the diet of Icelandic cod (*Gadus morhua*) and is an important source of nutrition for several other commercial fish species in Icelandic waters (Vilhjálmsson, 2002).

4 Materials and methods

4.1 Ethics Statement

No endangered or protected species were involved during the sampling of the research material.

4.2 Sampling

Live and sub-fossil/dead *A. islandica* specimens were dredged from the sandy seafloor of the southwest Icelandic shelf during two cruises of the *R/V G.O. Sars*, in July 2015 and August 2016. Material used in this project are in all collected from three different stations with nearly the same coordinates (Table 3), at a depth of approximately 100 meter. A customized rigid-toothed dredge, big *Arctica* dredge, is used to trawl the seabed for both live and dead *A. islandica* shells. The dredge is a metal cage with an opening in one end (Figure 12). The opening has metal "teeth" at both top and bottom enabling the dredge to dig into the sand regardless of which of the two sides it settles on at the seafloor. The dredge is fastened to a wire and lowered to the bottom, and thereafter dragged after the ship along the seafloor for 5-10 minutes at a speed of 2 knots. The "big *Arctica* dredge" was originally designed in Bangor, Wales, and two of these dredges were manufactured in Bergen based on photos and measurements made by Paul Butler, School of Ocean Sciences, Bangor, Wales.

Figure 12: Big *Artcica* shell dredge used to collect shell material from the sea floor. Photo: taken by me during the Ice2ice cruise expedition GS16-204 in August 2016.

After the shells were brought on board on the ship the live-collected specimens (Figure 13) were stored in a freezer (-20°C) for a couple of hours, then thawed before the flesh was removed and the valves were properly cleaned manually. Each specimen was air-dried, assigned a unique ID and sorted in correctly labelled plastic bags and boxes. All samples chosen for further examination had their picture taken and morphometric details recorded: width, height (along maximum growth axes) and length (anterior-posterior axis). The dry weight of a single valve, and the condition indicators of the shell were also recorded using the following parameters: periostracum preservation, ligament preservation, condition of the shell margin, degree of bioerosion and boring, and condition of nacre (interior shell wall).

Figure 13: Live collected specimens of *A. islandica* from southwest off Iceland

Most of the specimens used in building of the chronology were collected from the same station, Stn. 31 during the cruise GS15-195 (64° 22.01′ N, 23° 07.64′ W), at the depth of 105 meters. A couple of additional specimens from Stn. 23 (64° 21.97′ N, 23° 07.45′ W) at a water depth of 103 m was added to the chronology. Two specimens from GS16-204 station 10 (64° 21.54′ N, 23° 07.20′ W, 101 m water depth) were used for stable oxygen isotope analysis.

Table 3: Overview of the stations where *A. islandica* specimens were collected

Cruise	*Station no.*	*Coordinates, Longitude [°] Minutes (decimal)*	*Water depth (m)*	*Specimens used*
GS15-198	31	64° 22.01′ N, 23° 07.64′ W	105	9
GS15-198	23	64° 21.97′ N, 23° 07.45′ W	103	2
GS16-204	10	64° 21.54′ N, 23° 07.20′ W	101	2

The 2016-expedition returned to the same area as visited during the 2015-cruise to compliment the material collected in 2015. In this project, most of the material used originate from the cruise of 2015. However, two of the specimens collected in 2016 were used for isotope analysis and determination of the growing season. For the chronology construction, only live-collected specimens were selected. The year of the specimen's death (AD 2015) is known. This makes it possible to build the chronology backwards in time from a known year which for the shells used in this project is AD 2014 assuming this is the last growth increment completed. An absolutely dated master chronology could be constructed using statistical tools.

4.3 Shell preparation

The shell preparation is a multistep process and begins with the sectioning of the left valve (Figure 14) using a high speed geological saw. The middle part of the sectioned valve with both hinge region and ventral margin intact is placed in silicon mould and soaked in epoxy resin to support the quite fragile valve section.

Figure 14: Sectioned left shell valve. The middle part is chosen for further processing.

The epoxy is made by carefully mixing a 4:1 ratio of BUEHLER EpoxiCure™2 Epoxy Resin and EpoxiCure™2 Epoxy Hardener, respectively, for approximately 2 minutes making sure the solution is properly mixed. The solution made is poured in the mould in two rounds, first to cover half of the valve, and second after a few hours when the epoxy has started to solidify to cover the rest of the valve. This stepwise preparation is done to ensure that the epoxy solution will not get too warm and start boiling. If boiling occurs, bubbles will be produces in the epoxy and/or potentially changing the isotopic composition of the aragonite. The epoxy solution is left to solidify in air temperature, often overnight, before the epoxy block containing the valve section is removed from the mould. Thereafter a BUEHLER IsoMet 5000 Linear Precision Saw with a IsoMet Diamond Wafering Blade (8`` x 0.035mm x 0.9 mm), Series 30HC (Max RPM 7640), is used to saw a precise cut along the maximum height, which is the longest axes of the valve, from the ventral margin through the middle of the tooth (Butler et al., 2009a, Schöne, 2013) (Figure 15).

A Phoenix Beta grinding/polishing machine is used for subsequent manual grinding and polishing of the epoxy covered valve section to make the surface as smooth as possible (Ropes, 1987). The grinding is performed using gradually finer BUEHLER Wirtz silicon Carbide grinding paper; P180, P400, P600, P1000, P2500 and P4000, with a constant feed of water to the grinding area, with a speed of between 150-300 rpm, for approximately 2 minutes each. Subsequently, a TexMet coated plate sprayed with BUEHLER MetaDi Supreme Polycrystalline Diamond Suspension & Paste (1F µm) is used for polishing. The polished epoxy block is submerged in a 1 % Hydrogen Chloride solution (HCL) (Scourse et al., 2006) for 2-3 minutes for the valve cross section surface to be adequately etched, thereafter rinsed in a bowl of tap water. It is assumed that the HCl solution becomes weaker after every use and therefore the epoxy block containing the valve sections is submerged for a few more seconds every new round. The block face is left to be completely dry before the acetate peels are made. Drops of Ethyl Acetate (SIGMA-ALDRICH) are placed on the exposed cross section using a pipette. Immediately after this treatment an Agar Scientific Replication acetate sheet (thickness 35 micron) is applied to allow surface tension to pull it down to cover the epoxy block surface, being careful to avoid air bubbles. It is left until completely dry, which usually takes two hours or more. Sometimes the peels where left to dry until the next day. The acetate sheet is then pulled carefully off, revealing a replica of the cross section of the valve. The last step is to

position the completed acetate replica peel between glass slides for examination under a light microscope.

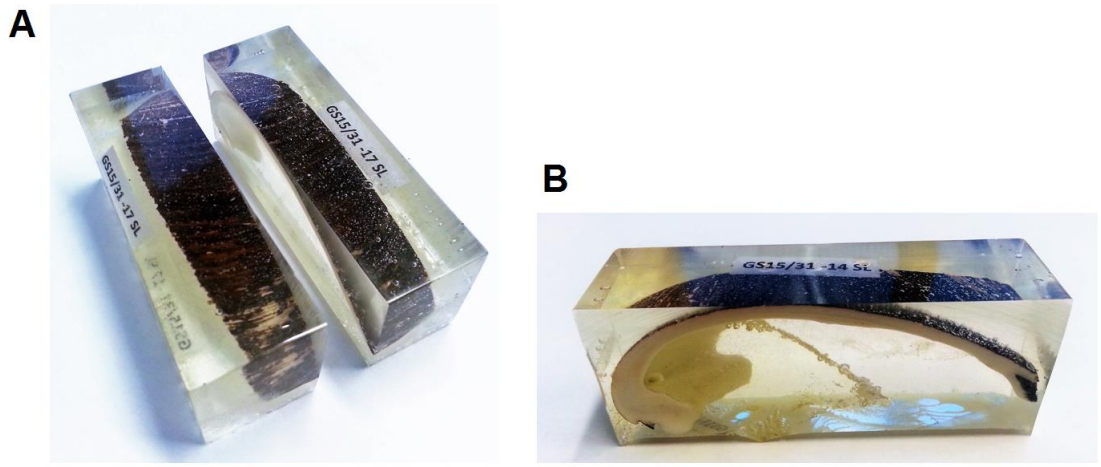

Figure 15: Shell valve embedded in epoxy. (A) Sectioned valve embedded in epoxy and precisely cut through the hinge and the longest axes revealing the (B) Cross section of which acetate replica peels are made.

4.4 Sclerochronological procedures

4.4.1 Increment measurements

Digital images of the cross section of each specimen, which was obtained by producing acetate peels as described above, were taken by an Infinity3 Lumenera microscope camera attached to a light compound microscope lens. All acetate peels were magnified to 5x/0.15 prior to being digitally photographed. The digital images were transferred to an imaging platform, ImagePro Premiere 9.1, which enables onscreen measurements of the annual increment widths (Figure 16). The measuring started with the most recently completed growth increment, in this project the increment representing the year of 2014. The increment of 2015 is not considered as completed since the shells were collected and died in July which is assumed to be prior to the end of the growing season. To ensure a standardized process all measurements were performed in the outer shell layer of the ventral margin, counting backwards in time from the end of the margin towards the umbo. The measurements of each annual growth increment were done perpendicular (Figure 16). Each preliminary measured growth increments series were recorded into a Microsoft Excel spreadsheet, and used to assist he cross-matching of marker years

(Appendix B). All images, with each increment identified with computer generated lines, were stored and sorted in a database file for later re-examination of the increment measurements when performing the cross-matching.

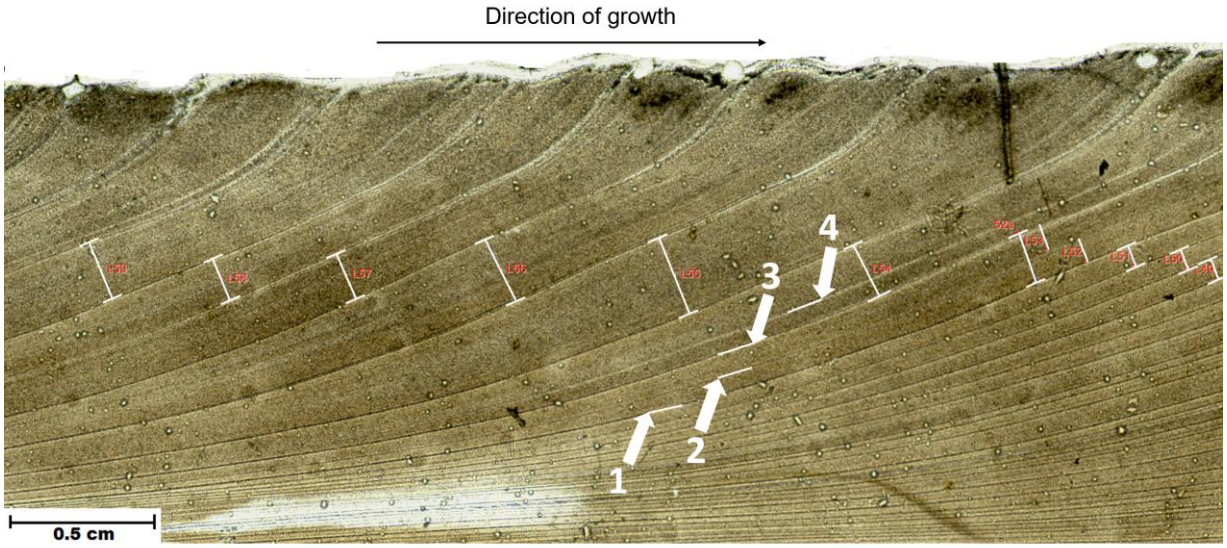

Figure 16: Photomicrographs of acetate replica peel with measurement lines indicating annual increments (white thin lines). It illustrates how some growth lines can be misinterpreted as representing either "fake" lines or actual annual lines (white arrows).

Growth line 1 in Figure 16 is an example of a distinct and easy interpretable annual growth line since it is possible to follow a constant line in both directions. Line 2 however is not as obvious; the line is indistinct and does almost vanish in some areas. Still, it is possible to follow the line and one can argue that this is an actual annual growth line, but in comparison with other specimens this was not interpreted as such. Line 3 is another distinct line and is classified as a growth line, while line 4 is another example of a line interpreted as a "fake" line as it is visible closer to the outer margin but disappears completely further to the left. It is worth mentioning that the acetate replica peel displayed in Figure 16 is a particularly clear peel with distinct growth lines. The peels studied vary between the specimens. The measuring process becomes particularly challenging when the ventral shell margin is damaged. The damaged shell margin will be projected to the acetate replica peel and shown as a substantial incision in the margin and disrupt the continuous series of growth lines. When measuring a damaged section, a measuring error may occur, which needs to be taken into consideration when comparing with the other growth increment series. The measuring is often challenging in the most recently

formed increments as they are much narrower, and it is harder to tell “fake” lines from actual growth lines (Figure 17).

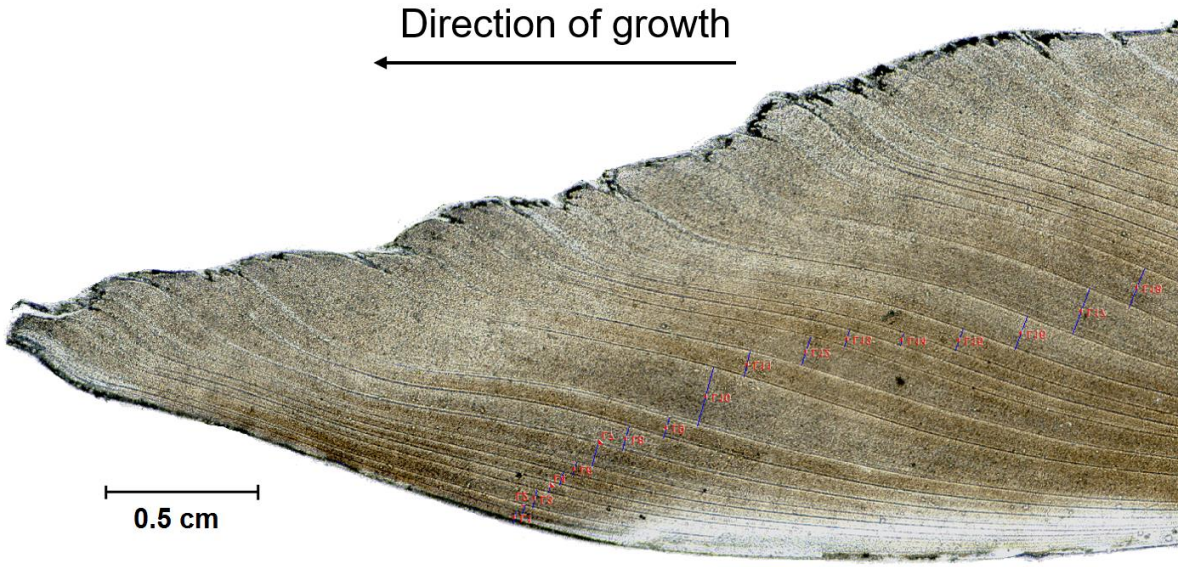

Figure 17: Image of the end piece of the margin with visible annual growth lines. The increments become narrower with age.

Ten additional specimens where processed and visually cross-matched, but not included in the final chronology. One reason for this was their very young age and therefore high ontogenetic growth tendencies along most of their growth increments series. Their inclusion would therefore not have any effect on the length of the chronology or improve the statistics. The shells not included did, however, cross-match nearly perfect with the other specimens in the chronology (data not shown). Ontogenetically juvenile specimens are objects to more metabolic variability along the growth increment series. Including such specimens in the chronology may therefore result in more statistical noise and hence obscure the common environmental signal (Butler et al., 2009a). Another reason to exclude some of the specimens was that they were quite old and therefor particularly challenging to measure due to narrow increments. These specimens can be included in the chronology later and thereby extend the chronology further back in time.

Particularly ontogenetically old shells are challenging to measure due to very narrow increments in the most recent years and the process is made even harder if the acetate peel image is not sufficiently clear and therefore has less distinct increment lines. Sometimes it is

necessary to make new acetate peels due to bubbles that occurs during their construction, or to produce new digital images if parts of the peel are out of focus. The reason for not including all processed specimens (Appendix A) in the chronology is because time became a limiting factor and not because they do not fit the chronology. When time allows, these shells can be analysed and most probably it will be possible to extend the master shell chronology (MSC) even further back in time, e.g. by adding the four oldest specimens of about 200, 250 and 400 years.

4.4.2 Cross-matching

The graphical software SHELLCORR was applied on a few specimens in the early stage of the chronology construction by cross-matching the growth increments series with each other. The output of SHELLCORR shows the Pearson correlation graphically (Figure 18) visualising data from two individual specimens with various lags and within a moving window (Butler et al., 2009b). SHELLCORR assists the visual cross-matching by demonstrating possible lag/lead between two different growth increment series, indicating the location of wrongful increment measurements. Adding or removing increments to make each growth increment series to fit each other is not an option as it is close to fabricating data. Generally, it is sufficient to visually cross-match specimens by comparing digital images of the individual acetate replica peels, supported by the measurements itself with remarks done during the measuring process (see Appendix B for example of notes taken during the measuring and cross-matching process). Nevertheless, SHELLCORR proved to be a valuable tool early on as it was not known if the specimens in this *A. islandica* population had a distinct synchronous growth.

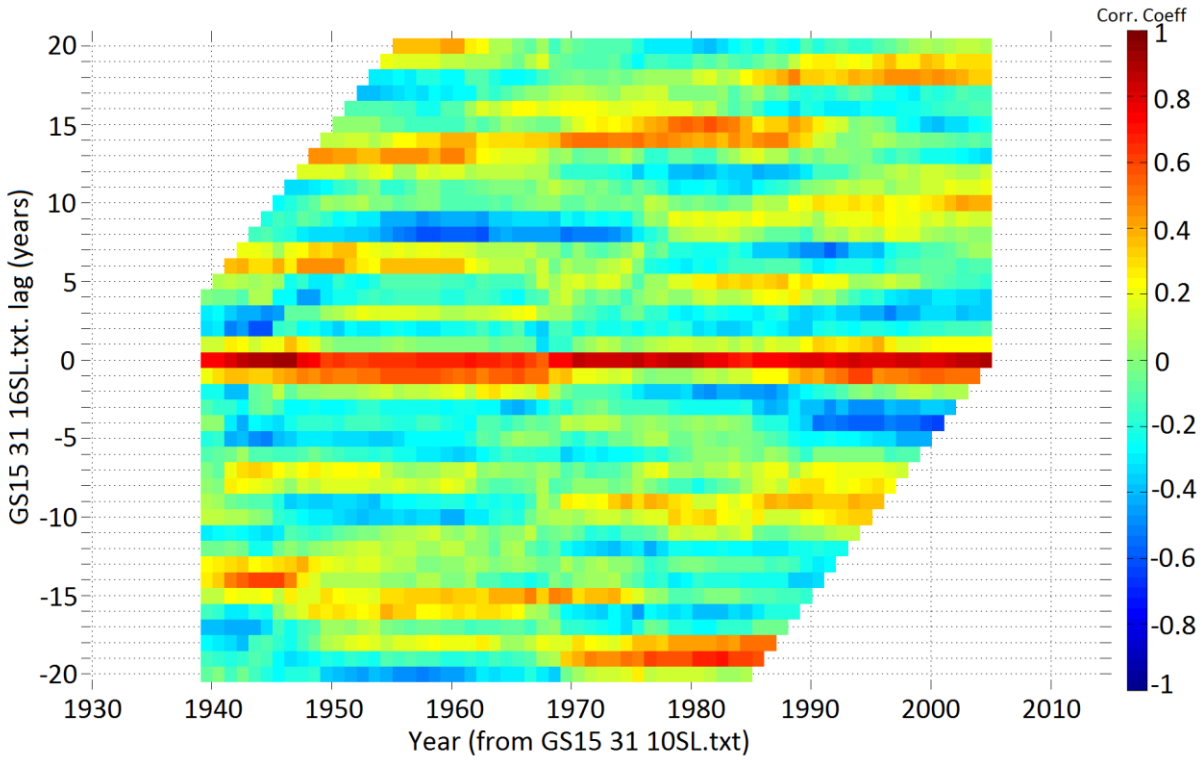

Figure 18: SHELLCORR output showing the correlation coefficients between a pair of growth increment series; GS15/31-16SL and GS15/31-10SL. As shown in the colour bar, positive correlation is red, and negative correlation is blue. This figure is shown with offset equal zero. The distinct red line at 0 indicate an overall significant correlation between the two specimens along the whole of the growth increment series.

COFECHA is another statistical software, originally used to analyse data from dendrochronology measurements. COFECHA is quite similar to the SHELLCORR and by applying segmented time series correlations techniques COFECHA is used to asses measurement accuracy (Grissino-Mayer, 2001).The output is numerical instead of graphical as for SHELLCORR. In contrast to SHELLCORR which compares only two growth increment series per run, COFECHA is used to assess the crossdating quality in all the series at the same time. The COFECHA software detects the distribution of "outlier" increment measurements for all series in any given year (Grissino-Mayer, 2001). This serve as an indication of where in the growth increment series there exists possible lags/leads, and the software suggest what numbers of increments to add or remove at the different locations in order to better make the series correlate with each other. Both SHELLCORR and COFECHA are valuable tools used prior to the chronology composition to assure that the visual increment measurements and cross-matching are done as accurate as possible.

Another method of locating possible increment-measurements that need some sort of modification is to plot all the time-series in a scatter diagram. This method provides an overview picture of the increment width series and makes it possible to compare high and low increment measurement values between different series, and simultaneously comparing with the micrograph acetate peel images when there are "suspicious" offsets in the series.

The specimens used in this chronology were all thoroughly measured individually prior to visually comparing each of them with the others. Visual cross-matching is done by comparing measurements to identify inter-shell marker years in all the microscope pictures of the acetate peels.

4.4.3 Detrending and transformation

The internal growth rate of *A. islandica* vary from year to year as well as throughout the growing season (Weidman et al., 1994, Witbaard et al., 1994). The bivalve grows rapidly in the early years of ontogeny, which cause wider increments and a greater year-to-year variability between increments widths than during the mature years (Butler et al. 2013). The same trend is observed in the growth rings of trees. These age-related trends can be removed with statistical methods, often referred to as detrending, by performing adjustments for the ontogenetic trend in mean and variance of the shell growth. This method is developed by dendrochronologists as tree ring series have similar trends in mean and variance as *A. islandica* increment series (Butler et al., 2009a). The detrending process involves modelling the natural growth curve and then removing it by calculating ratios or residuals between the measured and modelled increment widths (Butler et al. 2013). The challenge caused by the considerable ontogenetically growth trend in the early years can mostly be avoided by simply removing the first years of (juvenile) growth as suggested by Butler et al. (2010) and then work with the remaining chronology. However, these early twenty to forty years are potentially valuable for the chronology. For this project, it was decided to include most of the early years when building the chronology. Taking early years into account is also the usual practice (Scourse et al., 2006, Schöne, 2013, e.g. Helama et al., 2014). Despite the decision to include the first years of the chronology it was decided to leave out 9-21 of the first increments for most of the species because they were not possible to measure perpendicular and consistent with the other measurements. Nevertheless, each individual growth increment series had to be detrended to adjust for the ontogenetic growth

trend. All the growth increment series show a negative exponential trend caused by the rapid growth during the early years and subsequently decreasing growth throughout the bivalve's lifetime. The following equations are derived from (Schöne, 2013, Marali and Schöne, 2015).

The local mean is described as:

$$M = \frac{R_t + R_{t-1}}{2} \textit{ (Equation 1)}$$

The local variation is described as:

$$V = |R_t - R_{t-1}| \textit{ (Equation 2)}$$

where R_t and $R_{t-1}|$ are consecutive increment data. Heteroscedasticity, which means that the local mean (mean of the annual growth) and the local variation (how much the growth measurement values vary) are correlated, is demonstrated by the correlation between log M and log V:

$$logM = logV * b + a \textit{ (Equation 3)}$$

where *a* and *b* are constants, and M and V stands for the local mean and variance, respectively. As such variations influence data detrending, a data-adaptive power transformation (APT) may be used to stabilize the growth increment series and produce homoscedastic chronologies (Cook and Peters, 1997):

$$R_t^* = R_t^{|1-b|} \textit{ (Equation 4)}$$

New exponential trend curves (P_t) can then be generated and the growth indexes (GI) calculated for the growth increment series. The GI are computed by dividing measured growth values (R_t) by the predicted values (P_t) for each year:

$$GI_t^* = R_t^* - P_t \textit{ (Equation 5)}$$

The result of the detrending process is time index series for every individual specimen which shows for each year if the growth rate of this particular specimen was either above or below the expected rate (Witbaard et al., 2003). By mathematically subtracting the average and dividing by the standard deviation of the GI time-series the GI data were standardized.

$$SGI_t = \frac{GI_t - \mu}{\sigma} \quad \textit{(Equation 6)}$$

where μ is the average and σ the standard deviation of all GI values. The relative annual growth or the standardized growth index (SGI) is "*a dimensionless measure of how growth deviates from the predicted trend, where the difference is given in standard deviation units*" (Schöne, 2013). Positive values represent faster than average growth, negative values the opposite. The average SGI value of a chronology equals zero. Subsequently, the arithmetic mean of the SGI values at every single year is calculated and then each SGI series are combined to form a composite master chronology (Lohmann and Schöne, 2013).

4.4.4 Chronology construction

Preliminary measurements of all the growth increments in every individual *A. islandica* specimen were done before proceeding with the chronology building. Each individual time series was thereafter cross-matched, and adjusted if, and only if, examination of the acetate peels could demonstrate a measurement error in the preliminary measurement data. Before precise temporal alignment of the incremental time-series (crossdating), the ontogenetic trend was adjusted for in all the individual time series (Scourse et al., 2006, Schöne, 2013, Helama et al., 2014). The statistical (standard dendrochronology) software ARSTAN, which originally was designed to perform autoregressive time series standardization on tree-ring data was used to crossdate and to build the MSC in this project. Standardization by detrending and transforming the increment widths into dimensionless indices was done to balance the growth variations between the crossdated increment series of all shells regardless of age or size (Cook and Peters, 1997). The measurements were plotted and converted to mathematical indices, e.g. compiling a master chronology by computing yearly averages of these indices (Schöne, 2013). When ARSTAN is run in interactive mode, it performs detrending of the growth widths by plotting all increment width measurements of each time series, fitting a negative exponential curve to the measurements and dividing each increment width by the corresponding value of the curve (Bradley, 2014, p. 464). Detrending by an exponential curve-fitting is considered as the optimal technique to remove the growth trend, and at the same time retain medium to low frequency variability that have an environmental origin, compared to other techniques such as cubic smoothed spline and regional curve standardization (Butler et al., 2010). In ARSTAN it is possible to adjust the curve fit during the visual inspections by changing curve fit method if

considered necessary. An adaptive power transformation is then used to stabilize the variance (Butler et al., 2009a). A robust (biweighted) mean is used when constructing the MSC to reduce the influence of increment width outliers among the time series (Mette et al., 2015) (see appendix H for ARSTAN output). The climatic signal-to-noise ratio is thereby amplified when averaging the growth indices, because variance related to climate is saved, while the non-climatic "noise" from shell to shell variations are partially cancelled (Bradley, 2014, p. 465). Among the various ARSTAN outputs there are a few chronologies offered which differ slightly due to small variations in their calculations. One of these, the 'standard' chronology which is the one presented in this project, is an average of the index values that are standardized. Another version of the chronology, the so called 'residual' chronology has had all autocorrelations removed in all series used in the chronology construction (Butler et al., 2010). The 'residual' chronology is used when comparing the shell growth with environmental factors as it is slightly better at showing high-frequency variability (Butler et al., 2010), although it is quite similar to the standard chronology. The MATLAB (R2015b) software was also used to process the data independent of ARSTAN. The MATLAB curve fit module was used to plot the increment measurement data, and bisquare robust fitting was chosen in the software to fit curves to the data. The relationship between the local variance and local mean was also calculated and used to transform each individual growth curve by using an Excel spreadsheet (Equation 4). The spreadsheet was further used to calculate each individual SGI and the whole chronology.

4.4.5 Assessment of the strength and robustness of the chronology

To examine the signal strength throughout the chronology, the statistics of the series intercorrelation, also called the running r-bar was used. The ARSTAN software was used to calculate the average correlation between all series in a 30-year window with a 29-year overlap throughout the chronology. The output value is dependent upon the sample depth (sample size) and is a good measure of the common signal strength through time, because it is a running correlation between all the series (Schöne, 2013). The strength or robustness of the master chronology is usually assessed by the Expressed Population Signal (EPS) (Schöne, 2013). The EPS is a measure of the common variability in a chronology and is computed as a function of sample size (sample depth) and the mean series intercorrelation (r-bar). The EPS is calculated using the following equation:

$$EPS = \frac{n \cdot R_{bar}}{(n \cdot R_{bar} + (1 - R_{bar}))} \text{ (Equation 7)}$$

Where the R_{bar} is the average of the correlations between two and two GI chronologies, and *n* is the sample size used to compose the master chronology. An EPS threshold of 0.85 have been recommended by Wigley et al. (1984), where high values at or above this threshold indicate a strong common population signal. Values dropping below this threshold means that signals from individual time series is more prominent in certain time periods, interfering with the common signal and affecting the robustness of the chronology (Butler et al., 2010).

4.5 Stable oxygen isotope analysis

4.5.1 Stable oxygen isotope ratio

Oxygen has three naturally occurring isotopes: ^{16}O, ^{17}O, and ^{18}O, where the most abundant is ^{16}O, with a small percentage of ^{18}O and an even smaller percentage of ^{17}O. Cycles in the oxygen isotope ratio in aragonite shell materials are used to mirror climate changes in geologic history, as variations in the ratio of the abundance of ^{16}O with ^{18}O is linked to water temperature of the ancient ocean (Bradley, 2014, p. 201). By calculating the ratio of the two masses present in the sample and compare it to a standard, the temperature at which the sample was formed can be estimated. Due to the difference in mass and bond strength between isotopes, less energy is required to vaporize ^{16}O and it is more disposed to diffuse to the surface and disappear from the sample. The residual material will therefore be enriched in ^{18}O and the isotope ratio is therefore directly linked to the surrounding temperature during the formation of the shell.

Samples of aragonite calcium carbonate from shells of *A. islandica* specimens are produced by micro-drilling, intended for seasonally stable oxygen isotope analysis. The sampled material was sent to the Earth System Science Research Center, Institute of Geosciences, University of Mainz (JGU), Germany, for analysis by a Finnigan MAT 253 continuous flow-isotope ratio mass spectrometer (IRMS). IRMS application details are described by Cooke and Rohling (1999). The IRMS in Mainz has a precision uncertainty of ± 0.09 ‰ for $\delta^{18}O$. The $\delta^{18}O$ aragonite values are processed at 72°C which can require a correction of -0.02 to -0.04 ‰ when used to compute temperature estimates. However, since the difference is smaller than the

precision uncertainty of the IRMS, it is acceptable to refrain from adjusting the data. The analysis of aragonite $\delta^{18}O$ is specified in per mille difference from Vienna Pee Dee Belemnite (VPDB) which is related to the Vienna Standard Mean Ocean Water (VSMOW). To convert VPDB to VSMOW, $\delta^{18}O_{VSMOW} = 1.03092\ \delta^{18}O_{VPDB} + 30.92$ is used (Cooke and Rohling, 1999).

4.5.2 Seasonally resolved oxygen isotope analysis

Micro-drilling was performed to retrieve material for stable isotope composite analysis. Three live-collected juvenile, thereby relatively small, specimens of *A. islandica* were selected. The micro-drilling was done manually using a Minimo One Series Ver.2 drill under a LEICA MZ6 stereo microscope, with a 300 µm wide carbide drill bit. The drilled samples weighed between 40-120 µg which is the mass range required for analysis by the IRMS in Mainz, Germany. Prior to the micro-drilling the selected specimens were processed according to the method used for preparation of the chronology samples (section 4.3). Acetate replica peels were made and the specimens were cross-matched and compared with the master chronology to locate the overlapping years in the chronology. Two of the specimens used for isotope sampling were collected during the cruise GS16-204 in 2016 and did successfully cross-match with the specimens collected in 2015. Prior to the micro-drilling the epoxy covered shell cross-sections is grinded for ca. 2 minutes using BUEHLER Wirtz Silicon Carbide grinding paper P1000, P2500 and last P4000 to remove the remnants of diamond paste and acetyl acetate from previous processing, and afterwards the surface was cleaned with demineralized water. This was done as a precaution to avoid possible contamination of the samples which could potentially influence the isotope analysis. The digital images of the acetate peels were used to identify the lines and to plan the drilling-locations.

The specimens used is approximately of the same age and thereby similar increment widths were formed in the ontogenetically young period. This allows for the same sample-resolution in the increments representing the same years in all the specimens. The specimens used for micro sampling has an ontogenetic age of 15-19 years, and a maximum height of 45-61 mm. The increments need to be wide enough to enable several drill holes along each increment (Figure 19). Hence, when analysing the $\delta^{18}O$ from the sample material, they will represent the various stages of the growing season imprinted in the aragonite calcium carbonate of the increment. The increments selected for sampling in all three specimens are from the years

between 2005 and 2009. Additional samples were also taken directly from the growth lines, providing a mixture of material from the adjacent year on both sides of the increment, an indicator of the start and end-point of each increment. Furthermore, one sample was also taken from the end of the increment representing the year 2004 and one sample from the beginning of year 2010, in order to provide more reference points on the time scale. The widths of the increments sampled are minimum 2800 µm and maximum 8000 µm, where the latter represents year 2006 which is a remarkable year, with exceptionally wide increments seen in all three specimens. The same was seen in all the other specimens studied in this project. To ensure that results from each sample represents one separate drill hole, precautions was taken against contamination by epoxy particles and sample material that origin from other areas of the margin. The drill holes should be as closely drilled as possible, still avoiding the walls between drill holes to collapse which may lead to contamination, or that bits that cannot be used for analysis, break off.

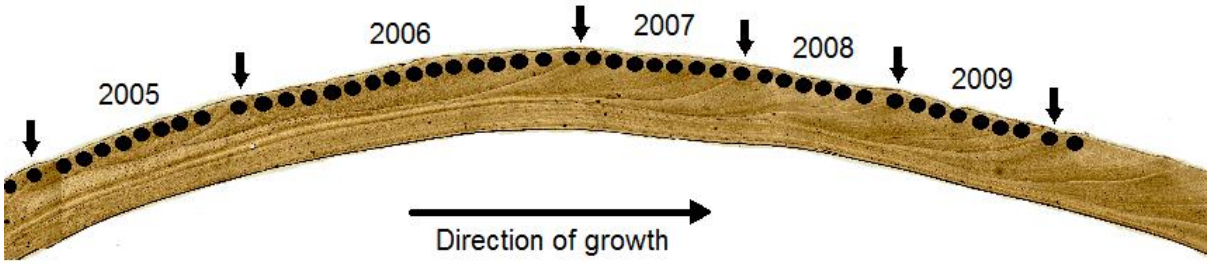

Figure 19: Illustration of the intra-incremental micro-drilling in the shell margin along the ventral shell margin. Each black dot indicates one sample for the seasonally resolved oxygen isotope analysis. The vertical black arrow points to the growth lines which is the border between two subsequent increments.

4.5.3 Temperature reconstructions from $\delta^{18}O_{shell}$

Stable oxygen isotope ratio ($\delta^{18}O$) analysis of multiple samples taken along transects of a growth increment from *A. islandica* shells has been shown in several studies to document a seasonal signal which indicate that the shell growth is related to sea temperatures (Weidman et al., 1994, Witbaard et al., 1994, Schöne et al., 2005a, Butler et al., 2009b). The isotopic oxygen composition of the adjacent seawater ($\delta^{18}O_{water}$) and the ambient temperature during the shell formation is determining the $\delta^{18}O_{shell}$ composition of the aragonite (Weidman et al., 1994, Foster et al., 2009). Hence, by studying the geochemistry of the shells, and producing seasonal $\delta^{18}O$ time-series, this can be used as an environmental correlation tool (Cooke and Rohling,

1999). In contrast to planktonic foraminiferal carbonate that deviate to a certain degree from simple equilibrium (Cooke and Rohling, 1999) (which suggests the influence of biological control), bivalves are assumed to accumulate their aragonite in close isotopic equilibrium, with respect to oxygen, with the surrounding water (Foster et al., 2009). Sea water temperatures estimates ($T_{\delta 18O}$) can be calculated using the aragonite $\delta^{18}O_{shell}$ values in the equation of Grossman and Ku (1986), which is derived from bivalve mollusc data only (Weidman et al., 1994). The following equation was used in this study and is the result of a modification done by Dettman et al. (1999) due to a difference of the $\delta^{18}O_{water}$ values in SMOW–0.27% (Schöne, 2013, Mette et al., 2015).

$$T_{\delta^{18}O}(°C) = 20.60 - 4.34 \cdot (\delta^{18}O_{shell} - (\delta^{18}O_{water} - 0.27)) \quad \textit{(Equation 8)}$$

The $\delta^{18}O_{water}$ is the oxygen isotope composition of the ambient water and the $\delta^{18}O_{shell}$ is the oxygen isotope composition incorporated in the aragonite during a period with a certain temperature (Weidman et al., 1994). Using this equation is based on the assumption that the $\delta^{18}O_{water}$ has remained unchanged over time. Carbonates precipitated in equilibrium with the surrounding water will result in low $\delta^{18}O_{shell}$ values corresponding to high water temperatures in the surrounding environment, which means that $\delta^{18}O_{shell}$ values are inversely related to water temperature (Witbaard et al., 1994).

Due to the lack of available accurate measurements of $\delta^{18}O_{water}$ from the study site it is necessary to use $\delta^{18}O_{water}$ provided from an area nearby. The $\delta^{18}O_{water}$ is related to salinity and this value is therefore possible to derive by using the averaged salinity around the material collection site and then plot it in a salinity-isotope mixing-line diagram (e.g. Mette et al., 2015). Using the North Atlantic mixing-line (Craig and Gordon, 1965) to determine the $\delta^{18}O_{water}$ value of the water surrounding the bivalve population indicates a $\delta^{18}O_{water}$ value of about 0.25 ‰ (using average salinity of 35.09 for Faxaflói station FX3 at 100 m depth). The North Atlantic mixing-line is however not very region-specific as it is an estimate for the whole North Atlantic, and there is much uncertainty involved. $\delta^{18}O_{water}$ values for different depths at a station (IS1: 64° 17.99 N, 24° 13.84 W) located on the west Icelandic shelf area, about 54 km from the material collection site, is reported by Azetsu-Scott and Tan (1997). The measurements at station IS1 show an average value $\delta^{18}O_{water}$ of 0 ‰ and a uniform salinity at about 35 ‰ (Azetsu-Scott and Tan, 1997). However, different $\delta^{18}O_{water}$ occurred at various depths, ranging

from 0.11 ‰ at a depth of 58 meter to -0.03 ‰ at 248 meter. At 108 meter depth the mean salinity was measured 35.113 ‰ and the $\delta^{18}O_{water}$ (‰ vs. SMOW) = 0.1 ‰. This $\delta^{18}O_{water}$ value of 0.1 ‰ was used together with the resulting $\delta^{18}O_{shell}$ from the inter-annual sampling when calculating ambient temperatures ($T_{\delta 18O}$) in this study.

5 Results

5.1 Individual growth increment series

Individual series of growth measurements from ten live-collected specimens, selected for the development of the chronology, are shown in Figure 20, with the oldest specimen reaching back to the 1870s (see Appendix F for raw increment width data). In the first years of ontogeny the increment widths of the specimens are above 1 mm and decreases to less than 400 µm as the organisms reach higher age. All the specimens are of different age, and they lived through their juvenile stage forming the ontogenetically young shell portion at different time periods. The ontogenetically growth does to some extent overshadow the common population signal and this influences how well the synchronicity is between the different specimens. A synchronous growth pattern is easily seen during the most recent years for all specimens where all specimens has grown out of their juvenile period (Figure 20B).

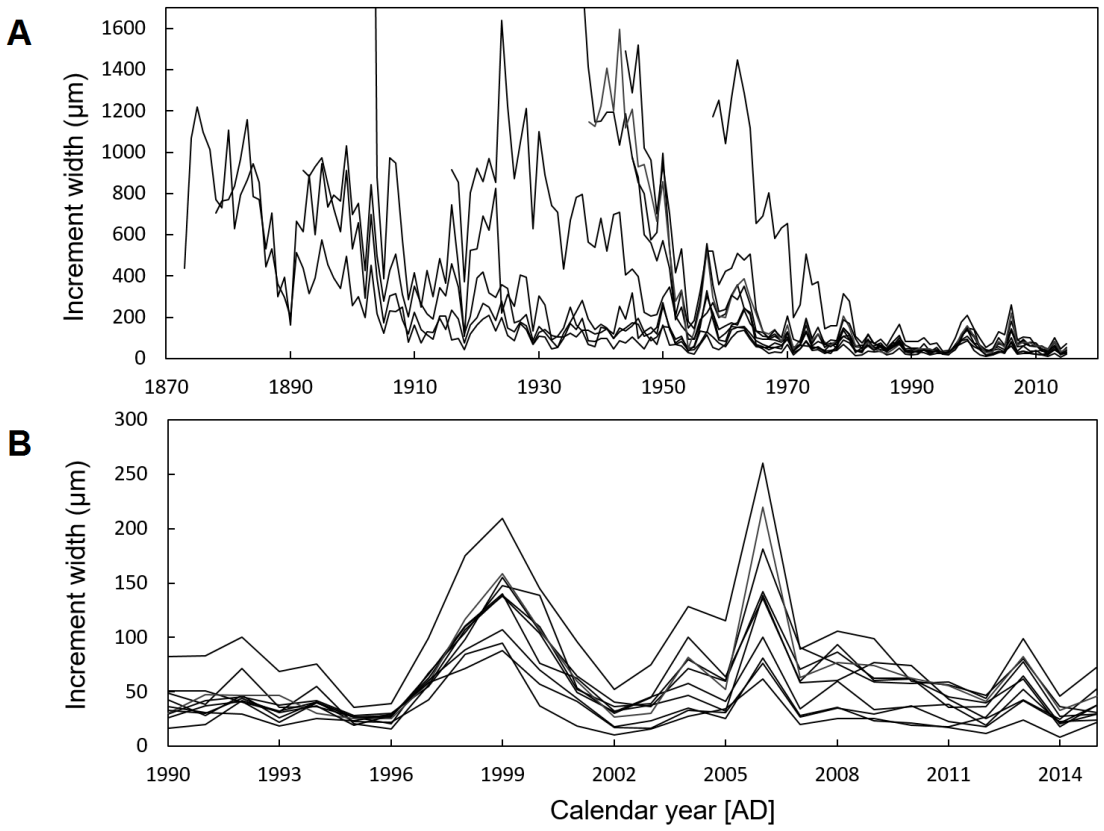

Figure 20: Individual series of growth increment measurements from live-collected specimens**.** A) Growth increment width time series used to construct the master chronology. B) Illustration of synchronous growth of all specimens during the most recent past.

All specimens analysed in this work are listed in Table 4 and includes a total of 13 live collected specimens. Ten of the specimens were selected, based on their ontogenetic age, the quality of the acetate replica peels and the absence of growth disturbances along the margin, for further chronology analysis. Three of the specimens were used for seasonal isotope analysis. The youngest and oldest specimen used for the chronology construction is found to be 72 years and 156 years old, respectively. Mean longevity of all the included specimens is 111 years (Table 4). It is almost always a positive relationship between higher age and shell thickness and weight.

Table 4: Overview of live-collected specimens of *A. islandica* used in this study for the chronology construction and/or isotope analysis.

		Calendar Date					*Sample Dimensions*	
Count	*Shell ID*	*Min (First year)*	*Start year of time series*	*Max (Last year)*	*Age (Longevity)*	*Usage*	*Max. Height [mm]*	*Mass of a single valve [g]*
1	GS15 / 31-59SL	1943	1958	2015	72	Chronology	70	37.44
2	GS15 / 31-17SL	1926	1944	2015	89	Chronology	78	46.30
3	GS15 / 31-10SL	1929	1938	2015	86	Chronology	78	45.00
4	GS15 / 31-4SL	1925	1937	2015	90	Chronology	80	47.56
5	GS15 /31-16SL	1924	1945	2015	91	Chronology	78	40.35
6	GS15 /31-13SL	1906	1916	2015	109	Chronology	82	55.98
7	GS15 / 23-1SL	1891	1891	2015	124	Chronology	88	60.63
8	GS15 / 31-8SL	1873	1892	2015	142	Chronology	83	63.86
9	GS15 /31-9SL	1864	1878	2015	151	Chronology	88	68.58
10	GS15 / 23-6SL	1859	1873	2015	156	Chronology	86	69.66
11	GS15 / 31-68SL	2002	-	2015	14	Seasonal isotope analysis	45	9.16
12	GS16 / 10-10SL	1998	-	2016	19	Seasonal isotope analysis	56	17.86
13	GS16 / 10-11SL	1998	-	2016	19	Seasonal isotope analysis	61	22.16

5.2 Chronology construction

Two software programs, ARSTAN and MATLAB, were used to construct the master shell chronology using the same increment measurement data and calculation steps. The ARSTAN software was initially used with the raw increment data, from each individual specimen, as input which produced both individual growth indexes (GI) per specimen, and by combining all these and calculating the robust (biweighted) mean, the software produced the master shell chronology (mean GI). The chronology is also provided in slightly different versions; two of which are the 'standard' and 'residual' chronologies.

The MATLAB software was used for a more stepwise examination of the chronology construction and enabled comparisons of the results between the two programs (Figure 22). To develop a complete master chronology using the same steps as ARSTAN using the MATLAB software, the raw increment measurement data of each specimen was first fitted an exponential curve function (Figure 21A, data on other specimens are shown in Appendix E). The fitted increment width curve as a function of time, *t*, was:

$$f(x) = a * exp(-b(t-d)) + c \quad \text{(Equation 9)}$$

where *a*, *b* and *c* are fitted constants and *d* is the start year of the chronology. Clearly the fitted curves follow the data well with a mean correlation coefficient of 0.94 (r^2) for all specimens. The exponential trend curve and larger increment variations in the ontogenetically young period of the shell for all specimens, demonstrated heteroscedastic data. The data was further processed by making trend curves between local means against local variances (Equation 1 and 2) (Figure 21B, see Appendix E for all specimens). Using the fitted trend data, a data-adaptive power transformation (APT) of the raw data (Equation 4) was performed to generate homoscedastic data (Figure 21C and Appendix E for all specimens). New exponential trend curves were then generated and used to calculate individual growth indexes (Equation 5) and standardized growth indexes (SGI) (Equation 6) (Figure 21D, see Appendix E for all specimens). Individual GI data was also obtained from ARSTAN, and after calculating the standardized growth index (SGI), this enabled comparison of the two individual SGI-curves, which resulted in a high degree of correlation for all specimens ($r^2 = 0.98$ and $p < 0.001$ for the specimen in Figure 21D).

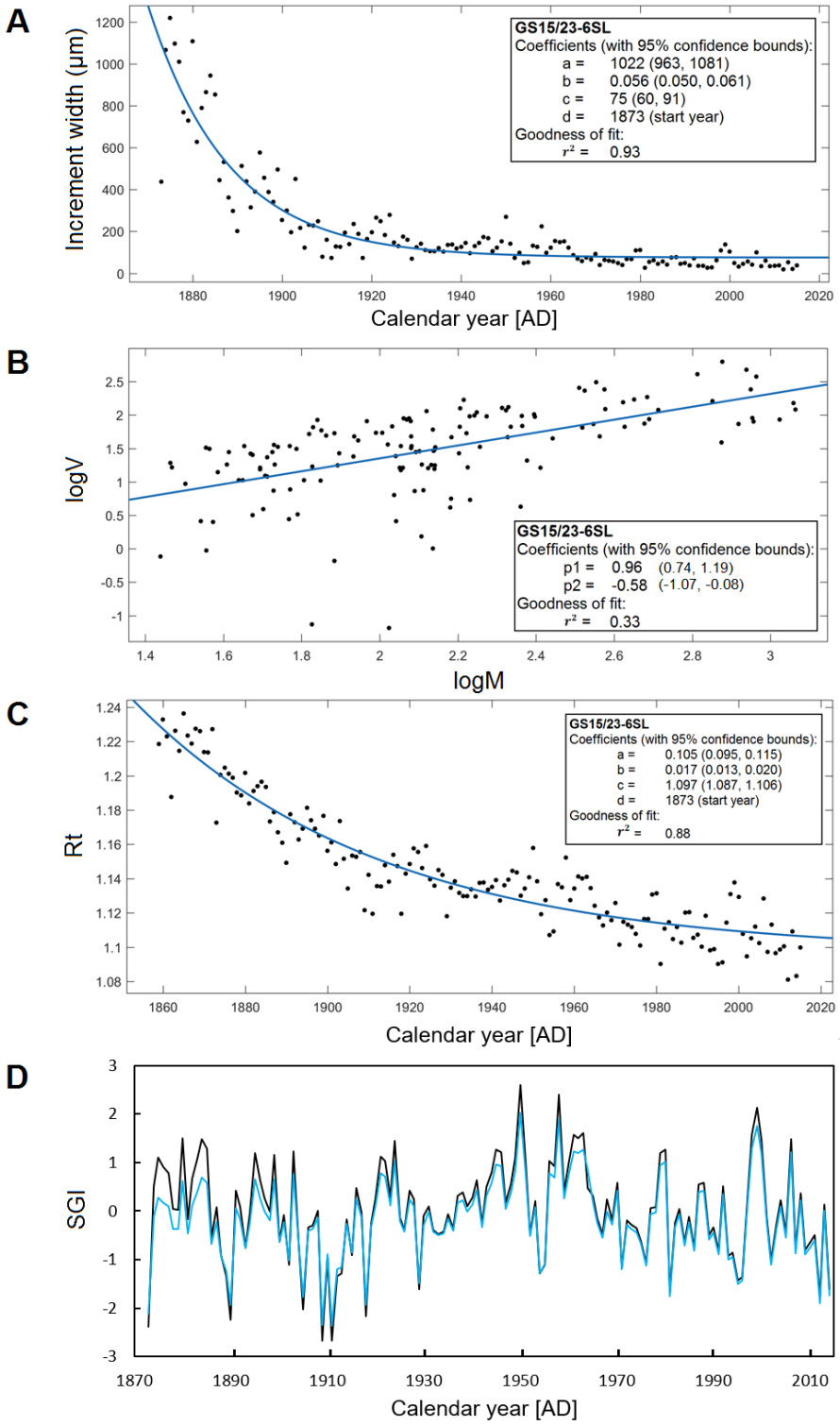

Figure 21: Curve fitting, transformation and generated growth indices of an individual specimen (GS15/23-6SL) using MATLAB (for other specimens see Appendix E). A) Raw increment measurement data with a fitted exponential curve; B) Local mean versus local variance with fitted trend line; C) Data-adaptive power transformed (APT) data with fitted exponential curve calculated from raw data and linear fit in C; D) Standardized growth index curve calculated from the curve and data in C (blue line) and similar obtained growth data using the ARSTAN software (black line).

The standard growth indexes (SGI) were calculated from the individual GI data obtained by ARSTAN (Appendix E), and allowed calculation of mean SGI growth curves, and comparison between the chronology (mean SGI i.e. master shell chronologies (MSC) produced in both programs **(**Figure 22A). Clearly there is a high degree of correspondence between the SGIs produced by the two software programs, and the Pearson's correlation coefficient (r) is calculated to 0.96 (r^2 = 0.93, p < 0.001) **(**Figure 21B). The differences in the chronology calculations may likely be explained by some minor differences in the curve fitting methods.

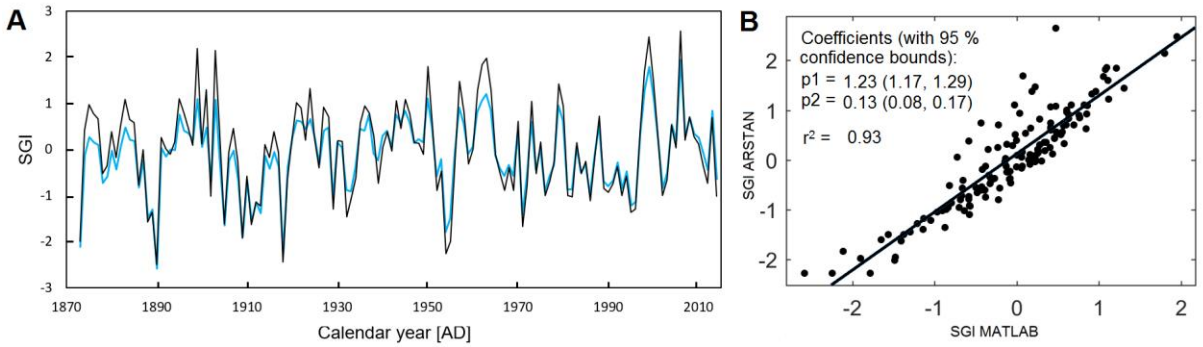

Figure 22: Standardized growth index output and analysis. A) SGI output (master chronologies) derived from ARSTAN (black line) and calculations using MATLAB (blue line). B) Linear regression analysis (*y = p1*x + p2)* of ARSTAN and MATLAB calculated SGI-values (r = 0.96, r^2 = 0.93, p < 0.001).

5.3 Chronology statistics

The sample depth of the chronology varies with a gradual decrease towards the later years of the chronology (Figure 23A). Visual comparison of the individual age-detrended time series (Figure 23B) show highly synchronous growth patterns and several exceptionally wide (e.g. 1950, 1958, 1979, 1999, 2006) and narrow increments (e.g. 1890, 1918, 1954) that helped during the cross-matching process. The master shell chronology (MSC) (Figure 23C) covers the period starting from year AD 2014 and extends back to AD 1873, resulting in a 141-yr long master shell chronology. The first five years of the chronology (1873-1878) were represented by a single specimen (Figure 23).

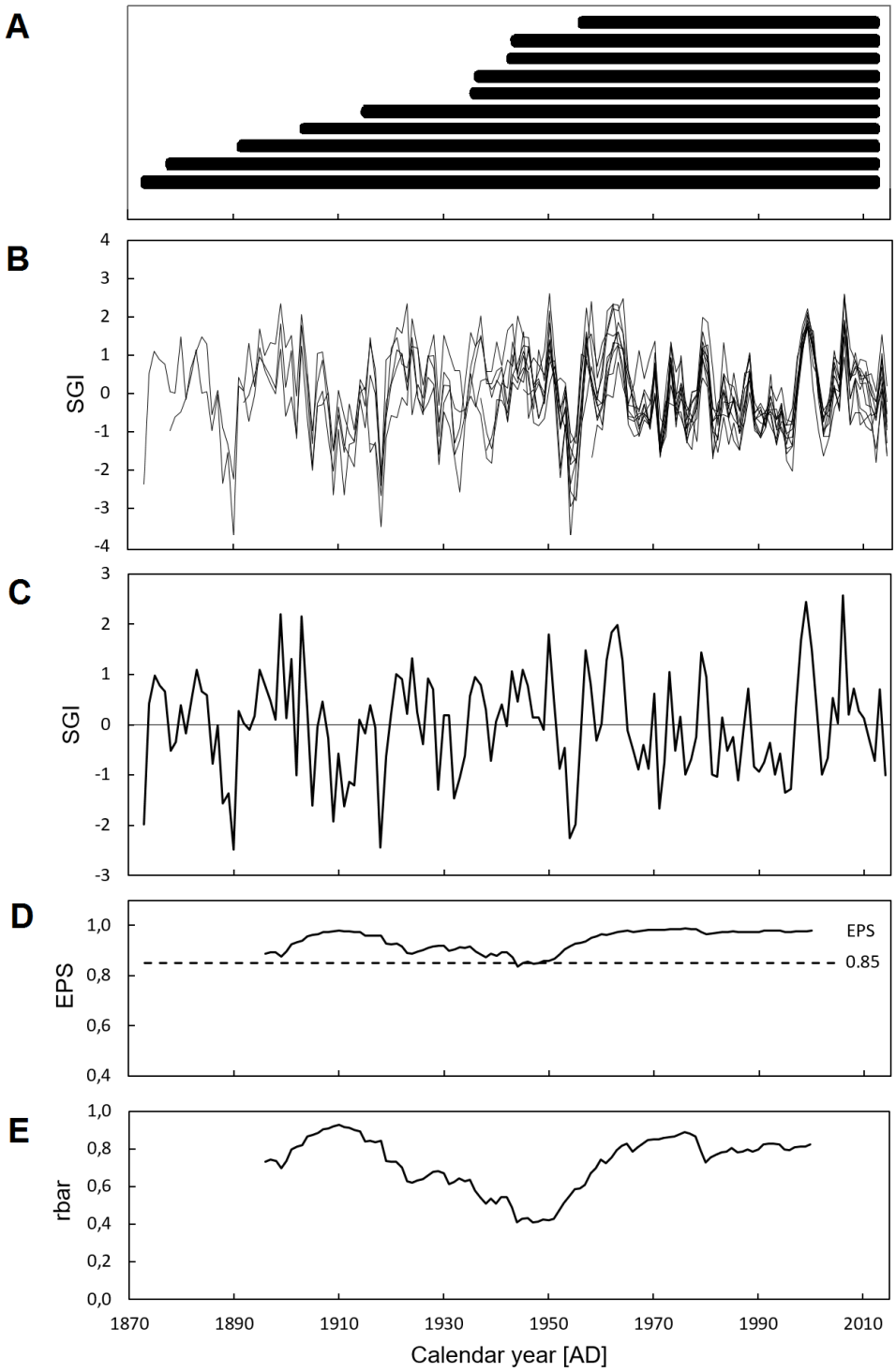

Figure 23: Master shell chronology data. A) Sample depth of the chronology and lifespans of ten *A. islandica* shells determined using crossdating. B) Individual standardized growth indexes of all specimens in the chronology. C) Standardized growth index of the ('standard') master shell chronology calculated by the ARSTAN software. D) Expressed population signal (EPS) (black solid drawn line), EPS threshold of 0.85 (dashed line) E) Mean series intercorrelation (R_{bar}) of the chronology.

The strength and quality of the composite chronology are assessed by first calculating the mean series intercoalition (R_{bar}) of which it is possible to calculate the Expressed Population Signal (EPS) (secion 4 Methods and material, Wigley et al., 1984). The MSC developed in this study is crossdated and statistically robust which is reflected by these two values which both are indicators of the degree of synchronous population growth (Figure 23C and Table 5). The lowest and highest R_{bar} values are 0.41 and 0.89, respectively, and with an average of 0.72. This confirms a strong synchronous growth within the population. The EPS value averaging 0.94 indicate a statistically robust record over the length of the chronology. The r-bar and EPS are calculated when the sample depth consists of two or more specimens. The EPS values are mainly above the EPS threshold of 0.85 throughout the chronology which means that there is a strong synchronous growth in the population. A small depression in the R_{bar} and EPS values the EPS threshold and slightly below it occurs in the period 1943-1951.

Table 5: Overview of chronology characteristics

Study site	*Southwest off Iceland*
Number of crossdated time-series	10
Oldest completed growth increment	1873
Most recent completed growth increment	2014
Average Series Intercorrelation (R_{bar})	0.72
Max EPS	0.99
Min EPS	0.84
Average EPS	0.94

5.4 Seasonally resolved oxygen isotope records

To identify the main growing season of the *A. islandica* population, sub-annually (sub-incremental) resolved $\delta^{18}O_{shell}$ analyses were carried out. In this project, the analysis was performed on shell sample material collected from five increments representing the same five years, 2005-2009, in three individual specimens (Table 6). The samples were produced manually using a micro drill. The increments were micro-drilled from within the first fifteen years of ontogeny, where the increments are widest (Figure 24). The sample resolution per increment varied depending on the increment width (Table 6 and Figure 24). Thus, the widest increment in all three specimens, in year 2006, has the highest sampling resolution of 13-14

samples. The narrowest increments, in year 2009, have the lowest resolution of minimum 5-6 samples. The variation in sampling resolution between the increments may have some influence on the interpretation of the resulting $\delta^{18}O_{shell}$ values. A few of the $\delta^{18}O_{shell}$ values have been excluded from further analysis due to high internal precision (1σ) which indicate low accuracy of the results (see appendix G for $\delta^{18}O_{shell}$ values and internal precision). The average internal precision informs about homogeneity of the sample or reference material, and should be lower than the reproducibility. The accuracy is shown by an external reproducibility 1σ = 0.05 for $\delta^{18}O_{shell}$. The few values with an internal precision exceeding 0.10 have been removed for consistency. A few other values with internal precision between 0.05 and 0.10 were individually evaluated and were found not to deviate much from all the other values (internal precision below 0.05), and it was decided to keep these values in order not to further decrease the sampling resolution.

Table 6: Specimens of *A. islandica* selected for seasonal resolved oxygen isotope analysis with the number of samples collected per increment. Collected samples discarded from the analysis are shown in parenthesis. Increment data are shown in Figure 24.

Count	*Shell ID*	*Calendar Date*		*Age (Longevity)*	*Max. height (mm)*	*Sample resolution per increment*				
		Min (First year)	*Max (Last year)*			*2005*	*2006*	*2007*	*2008*	*2009*
11	GS15 / 31-68SL	2002	2015	14	45	7	13	6	6	5
12	GS16 / 10-10SL	1998	2016	19	56	10	14	8 (-2)	8	6
13	GS16 / 10-11SL	1998	2016	19	61	11	12 (-2)	8 (-2)	6	5

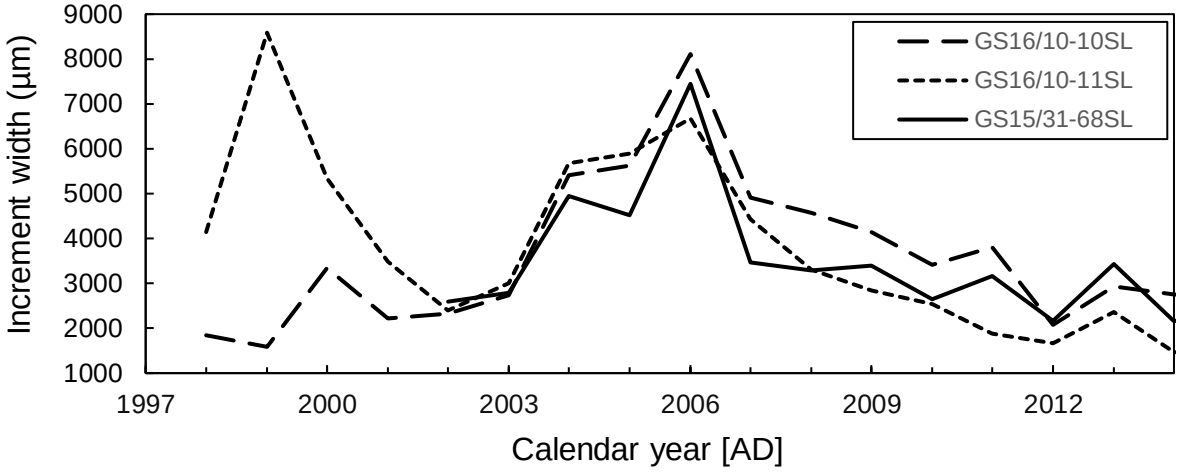

Figure 24: Increment widths of the three juvenile specimens selected for isotope analysis were cross-matched with each other and demonstrate synchronous growth. Five increments, representing year 2005-2009, were used for the isotope sampling.

The oxygen isotope analysis, performed in Mainz, resulted in $\delta^{18}O_{shell}$ values which vary between 2.92 ‰ and 2.02 ‰, where lower values will reflect higher $T_{\delta 18O}$ and vice versa. For all specimens, the data indicate yearly variations of $\delta^{18}O$ values within each increment (Figure 25). For samples drilled directly at the growth lines, i.e. at the border between two increments, materials from both years will most likely be present. The obtained measurements are therefore usually intermediates between the two years. However, although some variations occurred, for the majority of the sample data a yearly decreasing trend for the $\delta^{18}O_{shell}$ values throughout the increment for all three specimens is demonstrated (Figure 25).

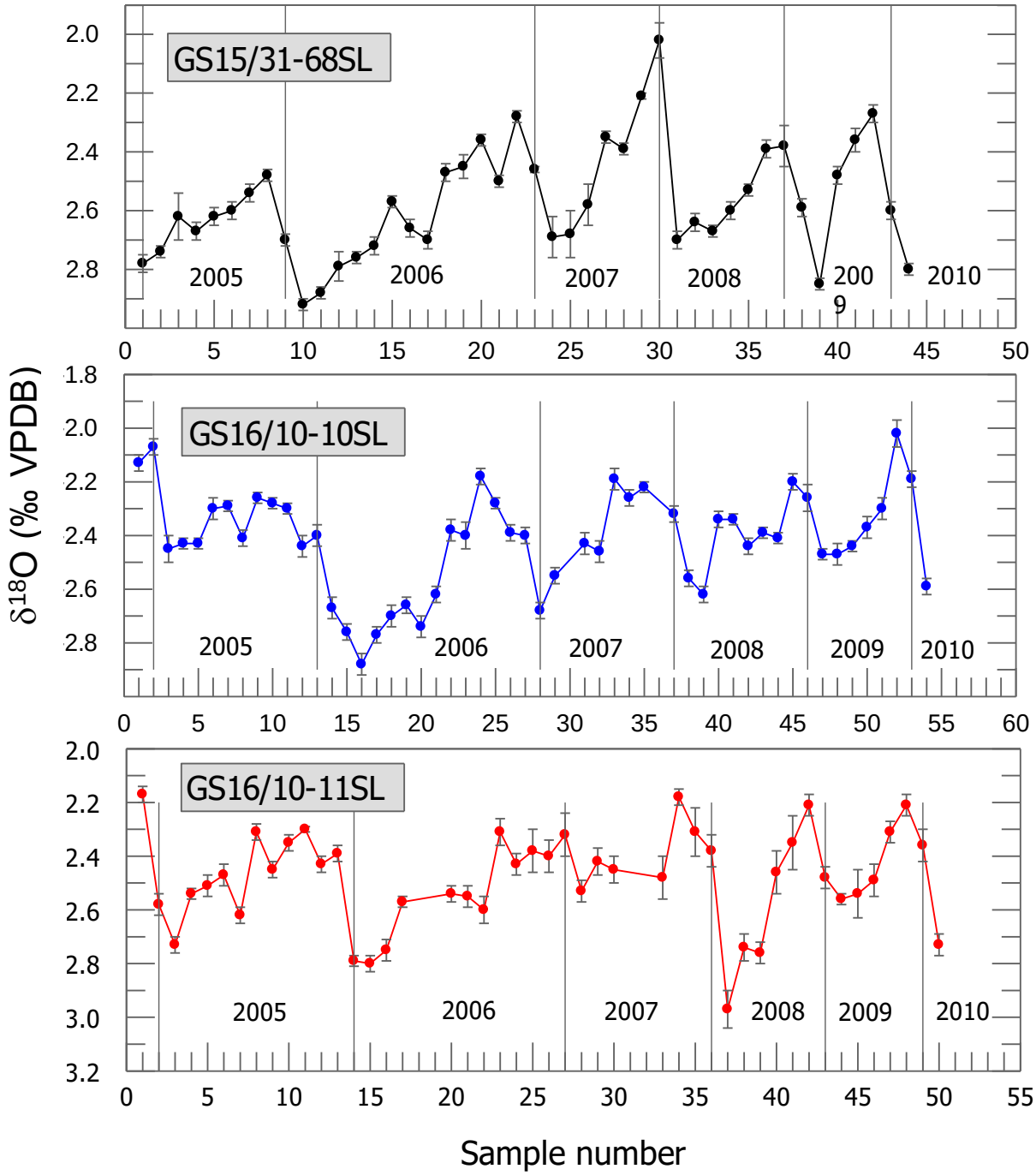

Figure 25: $\delta^{18}O_{shell}$ values derived from inter-annual samples of the three juvenile specimens. Data points shown between the years were from samples collected directly on the growth lines. Error bars show internal precision values (1σ) of each data point. Note: The y-axes are reversed to better illustrate the increasing trend of the corresponding temperature estimates ($T_{\delta 18O}$).

The measured $\delta^{18}O_{shell}$ values and an estimated value for the constant $\delta^{18}O_{water}$ allowed calculation of temperature estimates ($T_{\delta 18O}$). The linear relationship between $\delta^{18}O_{shell}$ values and the calculated ambient water temperatures using Equation 8 results in the same ratio between each value as the raw $\delta^{18}O_{shell}$ values, although inverted. The $\delta^{18}O_{shell}$ data was used to calculate $T_{\delta 18O}$ for the samples and the data was compared with instrumental bottom water temperature (BWT) data recorded at 100 m depth at the Faxaflói station FX4 (Figure 26). The instrumental measurements of BWTs were compared and aligned with $T_{\delta 18O}$ calculated by applying equation 8, using $\delta^{18}O_{shell}$ values and value 0.1 ‰ for $\delta^{18}O_{water}$ (Azetsu-Scott and Tan, 1997) (Figure 26). The resulting $T_{\delta 18O}$ varied from 7.2°C to 11.8°C. The comparison between actual instrumental recorded temperatures and calculated $T_{\delta 18O}$ indicate a mean temperature offset of 0.68°C in these sampled years. The mean temperature difference between the highest instrumental recorded temperature and the highest calculated $T_{\delta 18O}$ from the same year was 1.4°C in this five year period. Assuming the bivalve is forming its aragonite calcium carbonate shell in equilibrium with the ambient ($\delta^{18}O_{water}$) sea water, it is reasonable to expect that the highest and lowest $\delta^{18}O_{shell}$ calculated $T_{\delta 18O}$ values would be within the range of the instrumental values. Some of the values fit with the range of the instrumental measured temperatures and can easily be shifted to match these temperatures. Nevertheless, this would leave the highest $T_{\delta 18O}$ values, meaning the lowest $\delta^{18}O_{shell}$ values, outside this range.

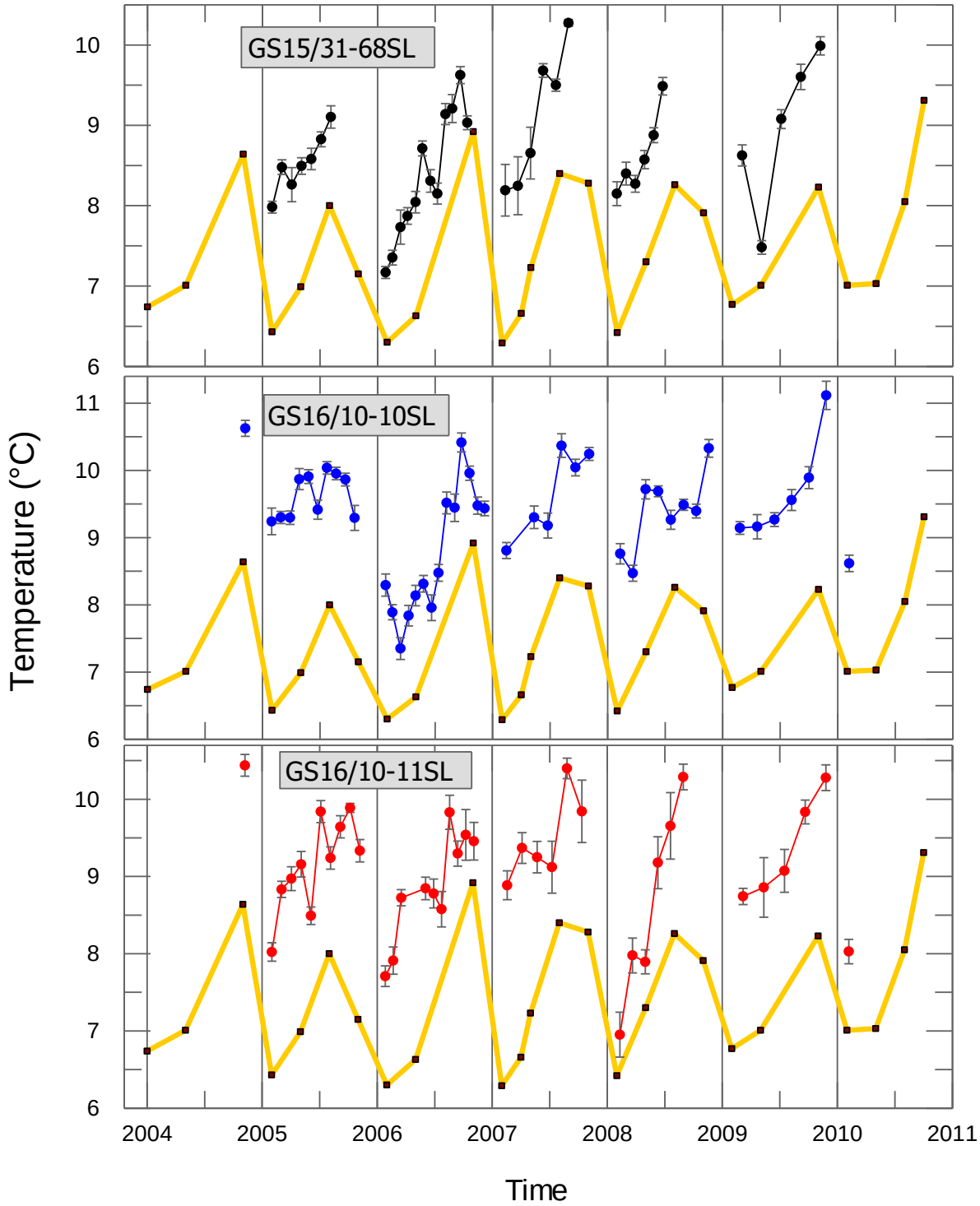

Figure 26: $\delta 18O_{shell}$-derived temperatures using $\delta^{18}O_{water}$= 0.1 ‰ compared with instrumental temperature measurements . BWT at 100 m depth collected from the nearby Faxaflói MRI Oceanographic Monitoring Station, FX4 (yellow lines and black dots) compared with calculated $T_{\delta 18O}$ estimates of the three selected specimens (black, blue and red). The isotope data was placed in time by visually adapting a factor to match the measured rise in temperature each year. Error bars for each value were calculated from the internal precision of the isotope analysis. An offset is apparent between $T_{\delta 18O}$ estimated using $\delta 18O_{water}$ value of 0.1 ‰ and instrumental temperature measurements.

A way of handling the obstacle presented above is to reverse *Equation 8.* This is done by calculating the $\delta^{18}O_{shell}$ which is expected to have been incorporated in the shell during periods with certain measured temperatures. By varying the value of $\delta^{18}O_{water}$ in the equation it is possible to deduce a $\delta^{18}O$ values which are in the same range as the actual results from the $\delta^{18}O_{shell}$ analysis of the shell samples. By doing this it allows to compare $\delta^{18}O_{shell}$ values directly, instead of comparing estimated $T_{\delta 18O}$ with instrumental temperature measurements. The $\delta^{18}O_{shell}$ value is left as unknown and is calculated by using the accurate instrumental temperature data available from FX4 and adjusting the $\delta^{18}O_{water}$ value based on how well the $\delta^{18}O_{shell}$ values correspond with the $\delta^{18}O_{shell}$ extracted from the actual samples extracted from the shells. This procedure results in an $\delta^{18}O_{water}$ value of -0.25 ‰ as the approximate value which should be the result if we took water samples and got the isotope composition of the water in this area. It is assumed that the $\delta^{18}O_{shell}$ values of the shell samples are correctly analysed and that it is a valid assumption that the aragonite is formed in close equilibrium with the ambient water. In temperature reconstructions using $\delta^{18}O$ for calculations in the paleotermometry equation it is also assumed that the $\delta^{18}O_{water}$ has remained somewhat stable in the same area over time. Rationale for this assumption is supported by data from Marali and Schöne (2015) indicating there are very small seasonal $\delta^{18}O_{water}$ variability from measurements of monthly water samples taken from the coast near Reykjavik.

For the new calculations of $T_{\delta 18O}$ the $\delta^{18}O_{water}$ value of -0.25 ‰ was used. Using this value, it is possible to calculate $T_{\delta 18O}$ which are in the same range as the instrumentally measured BWTs. In Figure 27 the isotope data were placed in time within each year by visually adapting a factor to match the seasonally increase in BWT values each year and the yearly temperature increase thus follows the seesaw pattern of the seasonal BWT data. Temperature estimates calculated using equation 8, using measured $\delta^{18}O_{shell}$ values and $\delta^{18}O_{water}$ = -0.25 ‰, varies from 5.65°C to 9.58°C. The instrumental temperature data recorded during these years vary from 6.29°C to 8.92°C, and have an average range of 1.92°C. The $T_{\delta 18O}$ have an average range of 1.94°C. As the instrumental record lack temperature measurements from several months of the year it is to be expected that the actual range of the real temperatures are somewhat higher than what is calculated here.

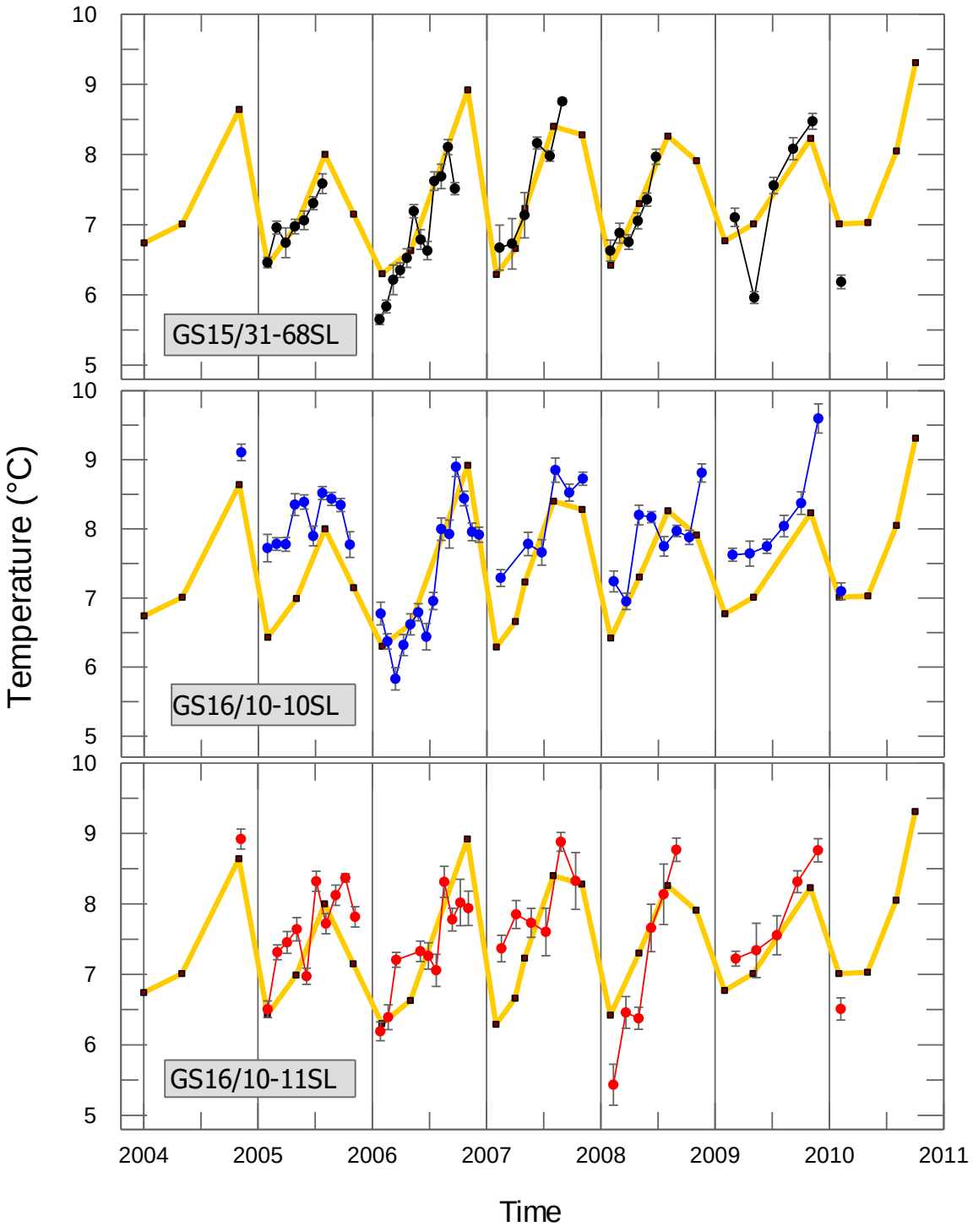

Figure 27: $\delta 18O_{shell}$-derived temperatures using $\delta^{18}O_{water}$ = -0.25 ‰ compared with instrumental temperature measurements. Bottom water temperatures (BWT) at 100 m depth collected from the nearby Faxaflói Marine Research Institute (MRI) Oceanographic Monitoring Station, FX4 (yellow lines and black dots) compared with calculated $T_{\delta 18O}$ estimates of the three selected specimens (black, blue and red). The isotope data was placed in time by visually adapting a factor to match the measured temperature increase each year. Error bars for each value were calculated from the internal precision of the isotope analysis.

6 Discussion

6.1 Master shell chronology

The data from this study confirm conclusions from earlier observations (e.g. Butler et al., 2009a, Butler et al., 2010, Marali and Schöne, 2015), that the relative variability in annual growth in specimens of *A. islandica* compare well, provided they are from the same area and with overlapping lifespans (Figure 23). This high degree of running correlation within a population is reflected in the standardized growth index (SGI) time series. This supports the assumption that common external environmental drivers and combinations of these impact the annual shell growth (Schöne, 2013, Butler et al., 2013). The purpose of constructing a master chronology is therefore to develop a robust reconstruction of some climatic parameter(s) that regardless of sample size or standardization procedure preserves a consistent climate signal (Schöne, 2013). The shell growth of *A. islandica* specimens from the population studied are shown to be highly correlated. The statistical significance in all visually crossdated series was assessed in the ARSTAN software. The synchronous growth of the *A. islandica* population is reflected by the high series intercorrelation (r-bar) and expressed population signal (EPS) (averaging at > 0.94) of the 141-year long master chronology. A statistically robust master chronology enable assignment of calendar dates to all individual increments with a high level of certainty. Furthermore, given that the chronology is well constructed, it is then possible to identify the population response to a common environmental signal.

The EPS values (Figure 23C) are lower during periods of the chronology, decreasing to about 0.85 between 1943-1951, and just below the threshold to 0.84 in 1944. The small decrease in the EPS values signifies that the growth increment series in some sections of the chronology is less synchronized. There are several possible explanations for this observation of which one can be that there is a false signal caused by errors that occurred during the measuring and cross-matching process. Incorrect preliminary interpretations and measurements of the increment width series, by either including or excluding growth lines as actual annual lines, will cause an offset in the time series from that point and back in time (Black et al., 2016). Uncertainties in the crossdating can also consequently affect correlations between the chronology and instrumental records (Butler et al., 2010). However, the high EPS values for most part of the chronology, both before and after this decrease in EPS values, indicate that it is unlikely that a

measuring error is the cause. This does not, however, exclude the possibility that some errors have occurred during the measuring and cross-matching process. By adding more time series to the chronology, this uncertainty can be reduced (Butler et al., 2010).

Another explanation of the lower EPS values, as suggested in a study by Epplé et al. (2006), can be that the common growth signal of the population became disturbed by extreme variations in surrounding temperature, salinity and/or water turbidity. Environments with more local variability in the area where the population is situated can possibly lead to a growth response to different environmental properties and a strengthened individual growth signal. Some of the specimens in the population may also have been affected by stress-factors, e.g. pollution, disease or bottom disturbances (Ropes et al., 1984, Witbaard and Klein, 1994, Marali and Schöne, 2015), which can amplify the individual growth variability. The last and probably most important explanation of the lower EPS values is the age differences, which is between 72 and 156 years for the ten specimens in this master chronology (Table 4). The dip in the EPS values coincide with a period in the chronology when five of the specimens were in their ontogenetically young period of their life because they will have much wider increments relative to the ontogenetically older part of the shell (Figure 20A). The increments in the ontogenetically young part does not necessarily display a strong common growth signal with other older members of the population, hence there are dissimilarities during this period where marker years are not as evident in the young portion of the shell. The decreasing EPS values towards the very end of the chronology is most likely due to the low sample depth (Figure 23A), and because the wider increments in the ontogenetically young part of the shell of the oldest specimens in the chronology cause more variability.

When comparing the ARSTAN-SGI and the numerical fitting performed by MATLAB there are some small variations, demonstrated by higher values in the ARSTAN-SGI (Figure 22). This illustrates the differences in the numerical fitting of the two software programs. Small variations in the numerical detrending using negative exponential fittings in the different software programs are probably the reason for the SGI outputs not to be identical. Such variations in the master chronology will, however, most likely have minor to no influence on its use because it is the mean relative growth variability which is compared with other environmental records. Small differences also occur between the different ARSTAN chronology outputs such as the ‘standard’ and the ‘residual’ chronology (see appendix C for

comparison of all versions of the master shell chronology referred to in this thesis). Other curve fitting techniques would also result in variations in the resulting SGI-values, as discussed by Butler et al. (2013) assessing the sensitivity of the chronology to different detrending techniques. ARSTAN is the software commonly used by dendrochronologists and sclerochronologists, and the difference between the ARSTAN and MATLAB output seems to be insignificant. Potential future comparisons of other shell based records with this master shell chronology (MSC) will be more consistently executed if both records are derived from the same software. The chronology ('standard' and 'residual') produced using the ARSTAN software is therefore used for further analysis in this project.

6.2 Seasonal shell growth

In order to compare shell growth with different environmental parameters of potential interest it is important to know the growing season of the population studied (Schöne et al., 2005a), due to the fact that the environmental variability can be recorded by growing bivalves only. To investigate in which months the *A. islandica* population grows, stable oxygen isotope ratios ($\delta^{18}O_{shell}$) derived from several inter-annual samples taken along selected increments were analysed and used to estimate temperatures ($T_{\delta 18O}$). The $T_{\delta 18O}$ demonstrates an annual cyclicity, with a trend of lower temperature values in the beginning of each increment and higher at the end (Figure 26 and 27). The data correspond with the seasonal seesaw pattern of the instrumentally recorded water temperatures indicating that the bivalve population grows in response to seasonal changes in the temperature of the surrounding water. This trend of increasing temperature (decreasing $\delta^{18}O_{shell}$) along each increment indicate that the growth line is formed just after the period with highest temperatures (lowest $\delta^{18}O$) of the surrounding water. The same trend is recognized in several other studies from other locations in the North Atlantic (Schöne et al., 2005a, Weidman et al., 1994, Witbaard et al., 1994). In a few cases, however, the last $\delta^{18}O_{shell}$ value is not the lowest value which indicates that in some year shell growth also occurs after seasonal temperature maximum.

The instrumental IRM temperature record shows an increase in temperature from the coldest month of the year, February, until the period August-November followed by an evident drop in

temperature at station FX4 (100 m depth) by a mean of 1.54°C between October/November and February (depending on available monthly data, in the period 2004-2011). The $T_{\delta 18O}$, when compared with the instrumental temperature record, usually follows the rising pattern throughout each annual growth increment. Based on this it is reasonable to accept that the growing season of the *A. islandica* population is influenced by the water temperature, and that the seasonal temperature drop corresponds to the end of the main growing season. This is probably linked to shortage of food in the autumn, but also perhaps a metabolic response to falling temperatures where the bivalves are in the possession of an internal biological clock, as suggested by Schöne et al. (2002). The growth lines formed in the shells mark the end of the growing season and represent very slow growth and eventually a total halt in the shell growth, usually seen in late autumn/early winter (Jones, 1980, Weidman et al., 1994, Witbaard et al., 1994). The time period between the last $\delta^{18}O_{shell}$ value of an increment and the first in the next increment confirms that the growth in the bivalve population studied is paused for a certain period of the year.

It is recognised by Witbaard et al. (1994) that the start of the growing season of the *A. islandica* is mainly determined by the availability of food particles reaching the seafloor which in turn is controlled by the seasonal cycle of phytoplankton production. Thus the development of the spring bloom of phytoplankton triggers the start of the bivalve's growth (Witbaard et al., 1994, and references therein). The spring bloom of the study location and the timing of food supply to the benthos usually occur in March/April based on instrumental recordings of primary productivity since 1958 (Gudmundsson, 1998). This, combined with the results of the isotope analysis imply that the growing season of the *A. islanidica* population southwest off Iceland starts in February/March.

The $\delta^{18}O_{shell}$ incorporated in the aragonite of the shell is a result of the $\delta^{18}O$ of the surrounding water at the time of the shell formation, and the period of the year when the estimated $T_{\delta 18O}$ are approximately equal to the instrumentally measured temperatures (i.e. mostly at the time of increasing temperature), is likely to represent the growing season of the *A. islandica* population. The temporal variability of the instrumental measurements, with only three to four temperature measurements in a year, cause difficulties when comparing the $T_{\delta 18O}$ with the instrumentally measured temperatures of the surrounding water of the *A. islandica* population. It is therefore necessary to base some of the analysis on the available and much more extensive gridded SST

record to be able to estimate the period presumed to be the main growing season of the bivalve population. The SST and BWT show a similar seasonal trend, but the amplitude differs showing a much higher variation in sea surface summer temperature than the variations seen in summer temperatures at deeper water (Table 2 and Figure 11). The limited BWT recordings give the impression that the highest temperatures at 100 m depth occurs between August-November, varying from year to year. The highest BWT measured throughout the instrumental period (1947-2016) occur in October, but no more than three measurements are done for October during this period, in 1986,1992 and 2010. For numerous years outside the period mentioned there are no measurements recorded for October and for these other years it seems as the highest yearly temperature occur in either August or November. Furthermore, as the SST and BWT seems to follow the same trend, one could argue that August is the month that likely to often hold the highest temperatures also at the sea bottom given sufficient mixing of the water column.

The growing season of the *A. islandica* population probably occur in the time interval where the $T_{\delta 18O}$ data matches instrumental temperature data, although this interpretation will to some extent be influenced by the selection of the $\delta^{18}O_{water}$ value used in the $T_{\delta 18O}$ equation (Equation 8). According to Marali and Schöne (2015) there are indications of only small seasonal $\delta^{18}O_{water}$ variability between monthly measurements for water samples taken from the coast near Reykjavik. Whether these observations apply to the area from where the shells studied in this project are from is not possible to determine due to the lack of $\delta^{18}O_{water}$ measurements of water samples from this particular location. As demonstrated by the offset between instrumentally measured temperatures and the temperature estimates (Figure 26) using $\delta^{18}O_{water}$ value measured by Azetsu-Scott and Tan (1997) at station IS1, the $\delta^{18}O_{water}$ value of 0.1 ‰ seems likely not to be representative for the location of this study. The reason for the offset may possibly be related considerable differences in oceanographic settings due to the distance of over 50 km between IS1 and the site used for collecting shells for this project. The study site is located much closer to the coast and there are, as accounted for earlier, occasional influence of freshwater input in this area. This affects the salinity to some degree, hence also probably the stable oxygen isotope ratio of the water. An adjusted $\delta^{18}O_{water}$ value of -0.25 ‰ was used for the $T_{\delta 18O}$ calculations to fit the actual instrumentally measured temperatures (Figure 27). It should also be noted that several assumptions are made when the isotope data are used to

calculate the surrounding water temperature during the bivalves' growth period. Firstly, it is assumed that the $\delta^{18}O_{water}$ is relatively stable in the same area over time (Mette et al., 2015, Marali and Schöne, 2015). Variability in the salinity at the study area can signify that the $\delta^{18}O_{water}$ might not have been stable through time. Secondly, it is also implicit that the $\delta^{18}O_{shell}$ values are correctly analysed, and thirdly that the aragonite is formed in close equilibrium with the ambient water (Foster et al., 2009, Mette et al., 2015). The fractionation of aragonite in the shells of bivalves seem to occur correspondingly in different areas, although the assumption that all bivalves fractionate in a state of close equilibrium is not conclusive (Lecuyer et al., 2012). If the adapted value of -0.25 ‰ for $\delta^{18}O_{water}$ is not measured in water samples from this area, there is perhaps reason to suspect that the *A. islandica* shells can have been calcified in disequilibrium with the ambient water. Another possibility for the offset between the instrumental temperatures and the calculated isotope based temperatures may also be related to the other constants used in the paleothermometry equation (Equation 8). Further investigation, regarding particularly the $\delta^{18}O_{water}$ of the study area and the possibility of necessary adjustments of the paleothermometry equation, is therefore needed to clarify this. Based on the current knowledge it is not possible to say which of these assumptions is the one which needs to be reassessed to enable calculations $T_{\delta 18O}$ based on $\delta^{18}O_{shell}$ derived from *A. islandica* with greater certainty. Additional investigations are therefore required.

Nevertheless, basing the analysis of the range of the $\delta^{18}O_{shell}$ results it is possible to determine the approximate main growing season of the *A. ilslandica* population. It is also a valuable indicator to look at findings in other studies of populations in other locations in the North Atlantic. The growing season of an *A. islandica* population located close to the Faroe Islands was estimated to be from March to September (Bonitz 2017, personal communication). Similar results were found by Marali and Schöne (2015) for the population of shells collected northeast off Iceland as they estimated the growing season to be from February to September. A population from the northern Norway was found by Mette et al. (2015) to grow almost all year with only a short growth recession in March/April. It has also been suggested that the growth is not necessarily a continuous process during the growing season, but occasionally it may be interrupted during the spawning period (Schöne et al., 2005b). The spawning period of *A. islandica* from north-east Iceland is estimated to occur in June-August (Thorarinsdóttir, 2000), and this could be an indicator of when bivalves southwest off Iceland also spawn and perhaps

leads to a considerable decrease in growth rate for a short period. The short period of very slow growth during the growing season may be an explanation of the occurrence of the so called "false`" growth lines formed in the shell. These are sometimes detected between the annual growth line.

The growth rate of the bivalves has been shown to vary throughout the growing season (Schöne et al., 2005b, Mette et al., 2015, Marali and Schöne, 2015). When performing stable isotope analysis, the single sample taken in the beginning or at the end of an increment can represent more than one month if the bivalve has grown slowly and only produces a small part of the increment. On the other hand, several samples taken in a row can represent the same month if rapid growth and high aragonite production has occurred within the period. Hence, with a higher sampling resolution, it would have been possible to get more $T_{\delta 18O}$ values and possibly detecting smaller temperature variations throughout the increment and then more accurately determine the start and end of the growing season. The highest sampling resolution per increment was in the increments representing the year 2006 in all three specimens and ranged from 13-14 samples. Nonetheless, the resulting temperature derived from the stable oxygen isotope values from the other narrower increments did not result in values which deviated significantly from the samples of year 2006. Hence, it is reasonable to assume that the overall period of which the population is found to grow every year is from February/March to August/September. However, the growing season probably lasts until November in some years when the water temperatures are particularly high and the phytoplankton bloom lasts longer.

6.3 Shell growth and environmental variables

The main intention of composing high-resolution master chronologies is to improve climate reconstructions, which is also the fundamental purpose of the MSC in this project. Climate variability has been shown in different studies to indirectly influence the growth of the *A. islandica* through the changing properties of the ambient water environment (Figure 28, and references therein), such as changes in water temperature, primary productivity, the rate of nutrient precipitation, and the duration of the season of which primary production occur. However, due to the growth characteristics of the bivalves there are not a fixed environmental condition that affect the bivalves in the same manner throughout its lifetime (Weidman et al., 1994). This should be considered when analysing the shell growth in relation to specific environmental factors. The synchronous growth signal of the *A. islandica* population in the current study clearly demonstrates that the master chronology is an expression of some kind of environmental variability. The (age-detrended and standardized) synchronous shell growth (SGI) master chronology is compared with various relevant regional and local environmental records, both instrumental records and other paleo proxy records. The climate response of the chronology can be tested using a simple linear regression. Pearson correlation coefficient (r) and coefficient of determination (r^2) are used when evaluating linear relationships between environmental indices and the SGI of the MSC. The commonly applied standard *p*-values of < 0.05 and < 0.01 are used for determination of the significance of the correlations. Statistics were calculated using the software programs PAST, Microsoft Excel, MATLAB and KNMI Climate Explorer. The 'residual' chronology output from ARSTAN is assumed to be slightly better at showing high-frequency variability than the 'standard' ARSTAN chronology and is therefore used when comparing the shell growth with other environmental parameters (Butler et al., 2010). Comparing the MSC with environmental data, obtained from instrumental, historical and proxy records, it may be possible to decipher the factors that are the primary drivers of growth in the selected *A. islandica* specimens from southwest off Iceland. The intention is to obtain a better understanding of the environmental variability in this area and in the Irminger Current, which in turn is a consequence of the climatic variations in the North Atlantic region in general.

According to a study of *A. islandica* under experimental conditions by Witbaard et al. (1997b), and confirmed in later studies based on investigation of shell growth in natural settings

(Witbaard et al., 1999) the most important driver of *A. islandica* shell growth is food supply. Estimations show that food supply can explain about 55-66 % of the shell growth (Witbaard et al., 2003, Wanamaker et al., 2009b), and that it is food supply which initially triggers the start of the shell growth (Witbaard et al., 1997b, and references therein). Temperature change of the surrounding water is shown to only explain about 10-30 % of the shell growth variability (Schöne et al., 2003, Butler et al., 2010, Butler et al., 2013).

The master shell chronology of this study was compared with existing records on environmental variability which are assumed to directly or indirectly influence the shell growth, with special attention to biological production, both primary and secondary, sea surface temperature and regional- and depth-specific water temperature (Figure 28). These factors are, however, also known to be affected by both changes in sea ice extent, the strength of the Atlantic Meridional Overturning Circulation (AMOC) and the subpolar gyre (Hátún et al., 2005, Hátún et al., 2009), which in turn are assumed to be linked to large scale variability in atmospheric and oceanic forces such as the North Atlantic Oscillation (NAO) and the Atlantic Multidecadal Oscillation (AMO), respectively (Fromentin and Planque, 1996, Nye et al., 2014, Drinkwater et al., 2014).

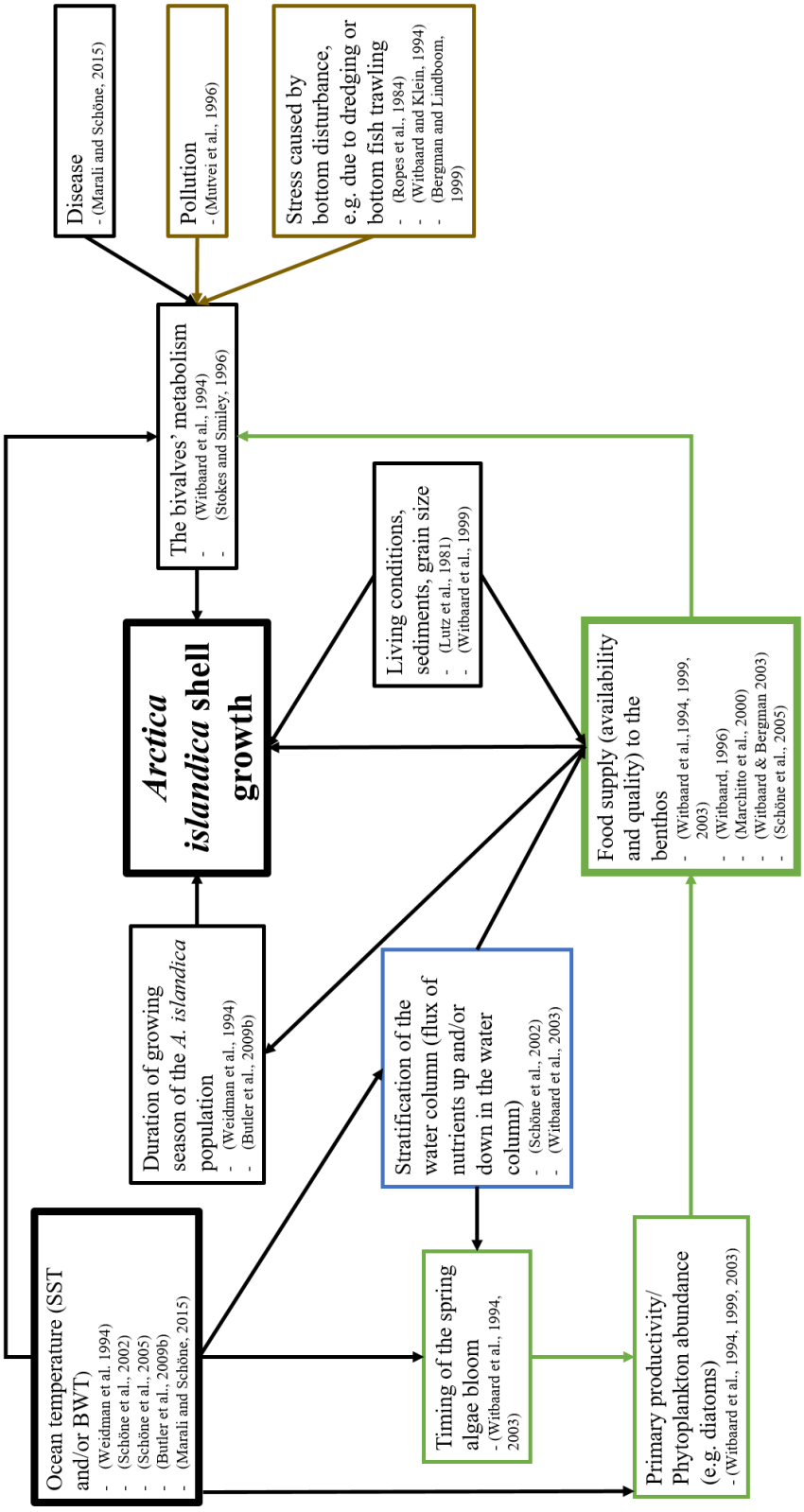

Figure 28: Schematic box diagram showing the direct and indirect links between environmental factors which are assumed, with reference to the literature, to influence shell growth of the *A. islandica*.

6.3.1 Primary productivity

The *A. islandica* has been shown to be affected by changes in both food availability and food quality (Witbaard et al., 1997b, Schöne et al., 2005b). The food of bivalves consists of suspended particles, mostly phytoplankton, but also bacteria, microzooplankton and detritus (Morton, 2011). The bivalves feed by filtration of the water. This process involves the opening of their valves and extension of their siphon in order to filter the water to utilize the available food (Ballesta-Artero et al., 2017, and refernces therein). This filtering process also serve as the shell's respiration (Ballesta-Artero et al., 2017, and refernces therein). The connection, demonstrated in an in situ experiment by Ballesta-Artero et al. (2017), between the activity of valve gaping (i.e. the distance between a valve pair) in the *A. islandica* and the most central processes of the bivalves physiology, which is feeding and respiration, led to the assumption that this also could be an indicator of shell growth. The valve gape activity is not only linked to availability of food in the water but also water temperature and light conditions. The strongest relationship was found between gaping activity and chlorophyll a [Chl-a], which is a measure of primary productivity (Ballesta-Artero et al., 2017). A maximum shell growth can be maintained by increasing the time spent in the filtration, instead of the filtration rate which is observed to decrease with increased cell densities (suspended food particles) in the water (Witbaard et al., 1997b, and reference therein). Hence, the shell growth is not necessarily always increasing during high particle density in the water, whereas a long growing season with continuous supply of nutrients is perhaps more likely to result in wide increments. The start of the growing season of the *A. islandica* population is assumed to be closely related to the start of the phytoplankton bloom and elevated primary production which usually occur in early spring during the timing of increased convection of nutrients upwards in the water column and increased supply of sunlight (Witbaard et al., 1994, Alheit et al., 2014).

An indicator on food availability to the benthic community is Continuous Plankton Recorder (CPR) data (Witbaard et al., 2003), which includes the CPR total Phytoplankton Colour Index (PCI) and CPR total Diatom abundance. PCI is a visual index of chlorophyll, based on the intensity of the green colouration of the CPR filtering silk (Reid et al., 1998), and is a measure of total algal production. CPR Diatom abundance is a relative measure of the spring bloom production. Systematic monthly and yearly CPR measurements started in 1958 in different standard areas in the North Atlantic (see appendix D for map of the standard CPR areas**),** but

has its limitations due to lacking measurements in some months and years. The standard CPR areas A6, B6 and B5 is the areas closest to Iceland and is where CPR data used for comparisons in this study is collected from.

The standardized growth index data of the *A. islandica* population obtained in this thesis was compared with PCI, from standard area A6, B6 and B5, during both individual months and during the main growing season of the bivalve population, but did not result in any significant correlations (data not shown). Similarly, no significant correlations were found between shell growth and CPR total Diatom abundance of standard area A6 and B5. However, comparison of data for CPR Diatom abundance in the area B6, recorded during the period between 1958-2014, with the current SGI-data resulted in some significant positive correlations as listed in Table 7. The sum of the monthly CPR Diatom abundance in the area B6 for the period between 1958-2014 is shown in Figure 29, and shows high abundance during the period May to October. In Table 7, monthly CPR data is compared with the current (annual) SGI-data and show significant values for March and July, but otherwise insignificant values. Average values were also calculated and compared with the SGI-data for the whole year and the periods February-August, March-August and May-August. Due to lacking monthly CPR data it was, however, necessary to exclude several observation years. The average values during the whole year did therefore only include years with four or less lacking monthly measurements. For the monthly periods (February-August), average data with two or less lacking measurement were included. This was done to keep the number of observations as high as possible although it can be argued that it will result in somewhat incorrect values. For all tested periods, positive correlations were found between SGI-data and CPR total Diatom abundance. Visual comparison of the data, however, indicated a stronger relationship between shell growth and Diatom abundance in the years between 1991-2014 (Figure 30). This was tested by comparing only recordings of these years with shell growth to give even more significantly positive correlations, and excluding the data resulted in insignificant correlations (Table 7). The reason for the difference between the two periods is unknown. During the period from 1987 to 1990 no CPR Diatom abundance measurements for standard area B6 were recorded, and the possibility of methodological or other differences between periods before or after this may need further investigations.

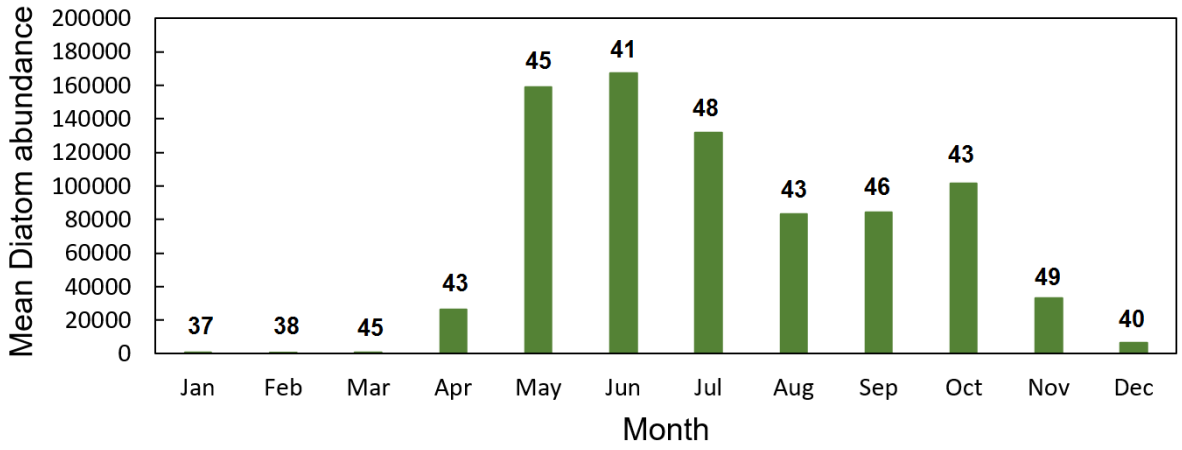

Figure 29: CPR Diatom abundance. Average monthly CPR Diatom abundance during the period between 1958-2014 at standard PCR area B6. The CPR Diatom abundance data was obtained from the Monthly CPR database and requested from The Sir Alister Hardy Foundation for Ocean Science (SAHFOS) (https://www.sahfos.ac.uk/data/data-charts/)

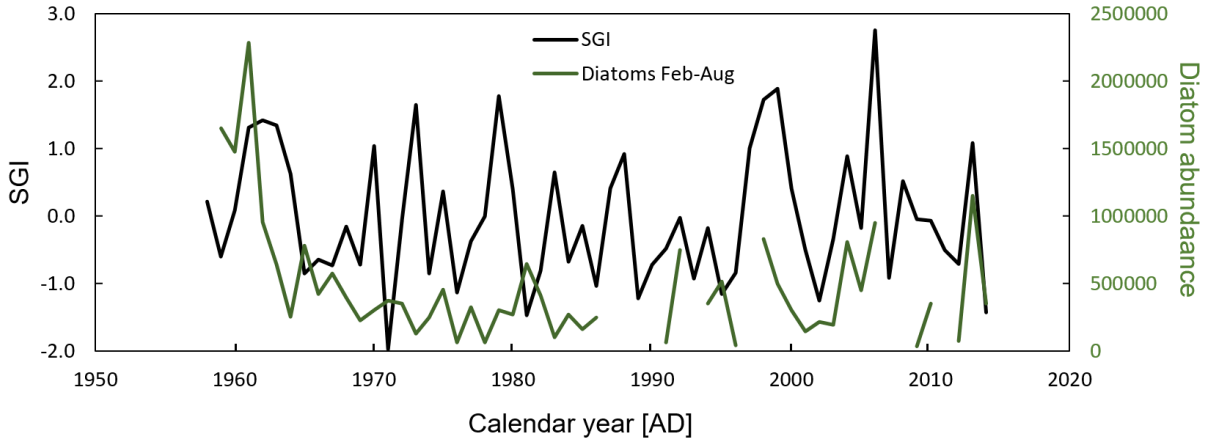

Figure 30: SGI and CPR total Diatom abundance. Mean SGI (black line) and mean CPR Diatom abundance for the months February-August (green line) measured during the period 1959-2014 at standard area B6. The CPR Diatom abundance data was obtained from the Monthly CPR database and requested from The Sir Alister Hardy Foundation for Ocean Science (SAHFOS) (https://www.sahfos.ac.uk/data/data-charts/)

Table 7: Correlation coefficient with *p*-value of SGI compared with CPR total diatom abundance at standard PCR area B6, per month and annual mean, in the period 1958-2014 (shorter periods are shown in parenthesis). *n* is the number of observation years (included years with incomplete monthly observations are shown in parenthesis). Green writing indicates significant correlations.

Time period	*r*	*p-value*	*n (years incomplete)*
January	0.07	0.69	37
February	-0.003	0.98	38
March	**0.38**	**0.01**	45
April	0.20	0.19	43
May	0.01	0.92	45
June	0.21	0.19	41
July	**0.38**	**0.007**	48
August	0.28	0.06	43
September	0.13	0.38	46
October	-0.09	0.55	43
November	0.006	0.97	48
December	0.06	0.72	40
Annual (1959-2014)	0.25	0.09	48 (36)
May-Aug (1959-2014)	0.28	0.051	48 (20)
May-Aug (1991-2014)	**0.67**	**0.0015**	20 (12)
May-Aug (1959-1986)	0.17	0.38	28 (8)
Feb-Aug (1959-2014)	**0.31**	**0.032**	47 (30)
Feb-Aug (1991-2014)	**0.68**	**0.0013**	19 (17)
Feb-Aug (1959-1985)	0.16	0.41	28 (13)
Mar-Aug (1959-2014)	**0.46**	**0.03**	22
Mar-Aug (1991-2014)	**0.71**	**0.003**	15 (13)
Mar-Aug (1959-1985)	0.39	0.11	18

High abundance of diatom phytoplankton in early spring, during March, can be argued to have a positive effect on the shell growth by supplying the bivalves with food which initiate an early growing season. In March, the temperature of the water column is usually homogenized, and the variability in both temperature and salinity is usually low at the study location between sea surface and 100 m depth. The consequence of this is less stratification and an increased downward flux of decaying phytoplankton to the benthic community. Years with an early spring bloom already in March seem to have a positive effect on shell growth: this assumption is supported by the earlier start in shell growth observed in some years as demonstrated in the analysis of $\delta^{18}O_{shell}$ (Figure 27). Marker years of particular wide growth increments, e.g. 1999 and 2006, in the bivalve population correspond with an early phytoplankton bloom combined with a long phytoplankton growing season. For instance, the phytoplankton spring bloom

started already in January in 1999 and the abundance were relatively high during the bivalve growing season and lasted until November. The even wider increment of 2006 correspond with an early phytoplankton spring bloom in March and a particular high Diatom abundance until November.

The abundance of herbivorous zooplankton is also usually low in early spring, which means less competition for the same food source as the bivalves. This may have had a positive effect on the growth of the bivalves in this period. A possible explanation for a positive relationship between elevated diatom abundance in July and increased shell growth is a new 'wave' of increased primary productivity that occasionally occur during this period, June-July, in the Faxaflói area (Stefánsson et al., 1987), combined with less stratification which permits downward flux of nutrients. The positive relationship in this period can also be related to a possible growth recession which may occur around June when the bivalves spawn (Schöne et al., 2005b, Thorarinsdóttir, 2000), and a heightened abundance closely after this growth recession can lead to an evident positive growth effect. A possible explanation for the lack of a positive relationship between shell growth and total Diatom abundance in the other months of the growing season is that other environmental factors may be more prominent which therefore interfere and mask a potential common trend signal with phytoplankton abundance.

Other studies have also found positive correlations between shell growth and primary productivity. In a study by Witbaard et al. (2003) a positive relationship was found between growth of *A. islandica* collected from the Fladen Ground (northern North Sea) and autumn phytoplankton abundance. The relationships found in other studies between primary productivity and shell growth are, however, in general not strong if present at all, due to both the complexity of the local environment at different study sites and the uncertainties caused by the instrumental records used for comparisons (Witbaard, 1996, Marali and Schöne, 2015). A major influencing factor for the availability of food to the benthos, other than the phytoplankton abundance, is the stratification of the water column (Witbaard, 1996, Schöne et al., 2002, Butler et al., 2010). Both seasonal and regional variability in the nutrient flux and vertical stratification of the water column are associated with changing SST (Richardson and Schoeman, 2004). As accounted for, the mean temperature difference between sea surface and 100 m depth at the study location during the summer is higher than 3°C, which signifies a strong stratification of the water column during this period (Figure 11). The greatest change in salinity in the surface

waters due to influence by coastal water occur between August and November (based on MRI instrumental data) and can strengthen the stratification of the water column during this period. This indicates that the bivalve population studied here is living below the thermocline in the summer period. Higher water temperatures during the summer cause stronger stratification, and combined with sunlight and enough nutrients, this results in boosting the production of the phytoplankton which results in increased primary production in the upper layers of the water column (Richardson and Schoeman, 2004, and references therein). Consequently, stratification can both be favourable and a disadvantage for the benthic community. Increased phytoplankton coupled to warmer temperatures leading to increased stratification means more potential food for the bivalves. But increased stratification can also prevent the downward flux of food to the benthos, regardless of the phytoplankton abundance at the surface. Particles are held in suspension above the thermocline which hinder the downward flux of nutrients to the bottom waters significantly, thus limiting the food availability to the benthos (Butler et al., 2010). Although there is a thermocline present, some particles will always reach the seafloor, but the food supply will be severely reduced in the months with particularly high temperature differences between the surface and sub-surface water. However, the stratification is not temporally fixed throughout the summer. The thickness and depth of the thermocline is dependent on temperature variability between day and night, but also weather, wind, and dynamics of currents and tides which greatly influence the mixing of the water column. The near surface water is mixed by waves and surface currents, and events with strong winds and high waves during storms may cause increased mixing of the water column, reducing the stratification (Mahadevan et al., 2012). Weakening of the thermocline will potentially result in an increased downward flux of food particles to the bivalve population. It was also suggested by Stefánsson et al. (1987) that the nutrient distribution of the water in the southern part of the Faxaflói area are affected by the increased turbidity as a result of the IC crossing the Reykjanes Ridge. The strength of the westerly winds in the North Atlantic, associated with the NAO, are also very important for mixing and stratification of the water column, and this affects in turn the primary production (Richardson and Schoeman, 2004).

The lack of a strong relationship between food source and shell growth is probably due to the complexity of the local environment, where a combination of many variable factors eventually result in either above or below average shell growth. It is challenging to estimate the effects the

variability of primary productivity has on shell growth based on the available instrumental data as it is marked by some limitations. It is therefore not possible to infer that there is a direct relationship between primary productivity and shell growth southwest off Iceland based on the CPR data available. The positive correlated CPR data obtained (Table 7) was based on data from the standard area B6 which does not include the shell collection site. However, the Irminger Current is flowing through area B6 on its way to the southwest off Iceland. As accounted for, the inflow of NAW brings nutrients (P and N) to the Icelandic water and contributes to the phytoplankton abundance in the areas where the IC flows (Astthorsson et al., 2007). Based on this it is reasonable to assume that effects seen in years with favourable environmental conditions for phytoplankton at area B6 also is valid for stations in the Faxaflói area which receives the same water masses. Although, the biological production probably is higher closer to the coast (Astthorsson et al., 2007). CPR measurements performed in a more locally confined area around the study site could potentially lead to higher correlations between shell growth and phytoplankton abundance.

6.3.2 Zooplankton abundance

As suggested by Witbaard et al. (2003), the food supply to the benthic fauna is to some degree determined by the abundancy of zooplankton, mainly copepods, which intercept the fluctuation downwards in the water column of potential food particles. Information about long-term variability of the copepod community from southern Icelandic waters are limited, although the taxonomic composition is known to mainly be comprised of a few copepod species (Gislason, 2003, and references therein). Zooplankton abundance is related to both primary productivity and temperature, and changes in zooplankton abundance and taxonomic composition southwest off Iceland has been shown to be influenced by the subpolar gyre (Hátún et al., 2009). Copepod abundance is also associated with the NAO index (Fromentin and Planque, 1996). Records of CPR Copepod abundance, which can be applied as a measure of the zooplankton abundance, from standard areas close to Iceland exist from 1958 until today (Figure 31) and enables comparison with shell growth of the studied *A. islandica* population (see Appendix D for map of the standard CPR areas). The sum of the CPR Copepod abundance for the months March-October was calculated in order to compare with the master shell chronology (MSC) (Figure 32). This period includes the main growing season of the bivalve population. There were fewer

recorded CPR observations in the months outside this period. In order to obtain a useful dataset for the March-October period, it was decided to include data from years with one monthly measurement missing. This resulted in 35 years included in the dataset, of which 20 years had incomplete data. Comparison resulted in a significant negative, but not strong, correlation (r = -0.37; $p > 0.05$) between the SGI and CPR total Copepod abundance in March-October for the standard area B6 (Figure 33).

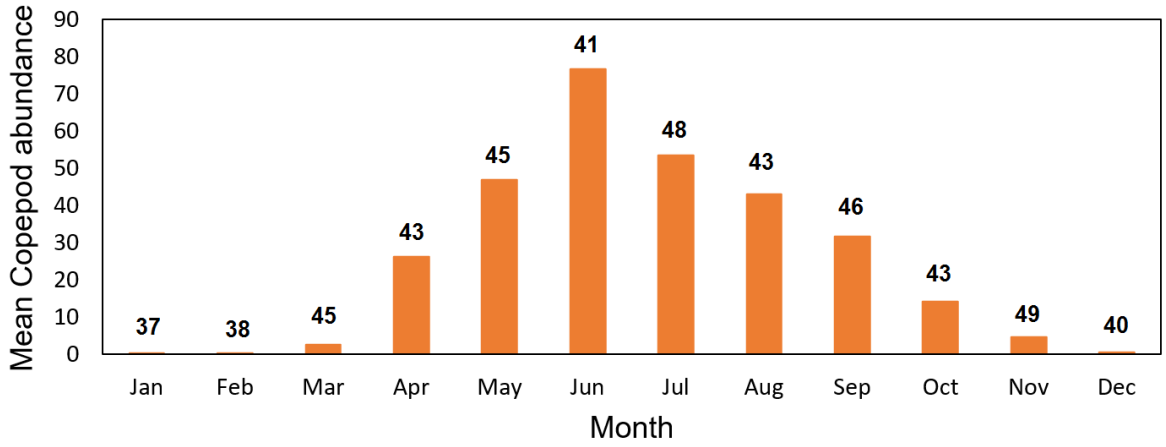

Figure 31: Average monthly CPR Copepod abundance during the period between 1958-2014 at standard area B6. No. of observations are shown above each month. The CPR Copepod abundance data was obtained from the Monthly CPR database and requested from The Sir Alister Hardy Foundation for Ocean Science (SAHFOS) (https://www.sahfos.ac.uk/data/data-charts/)

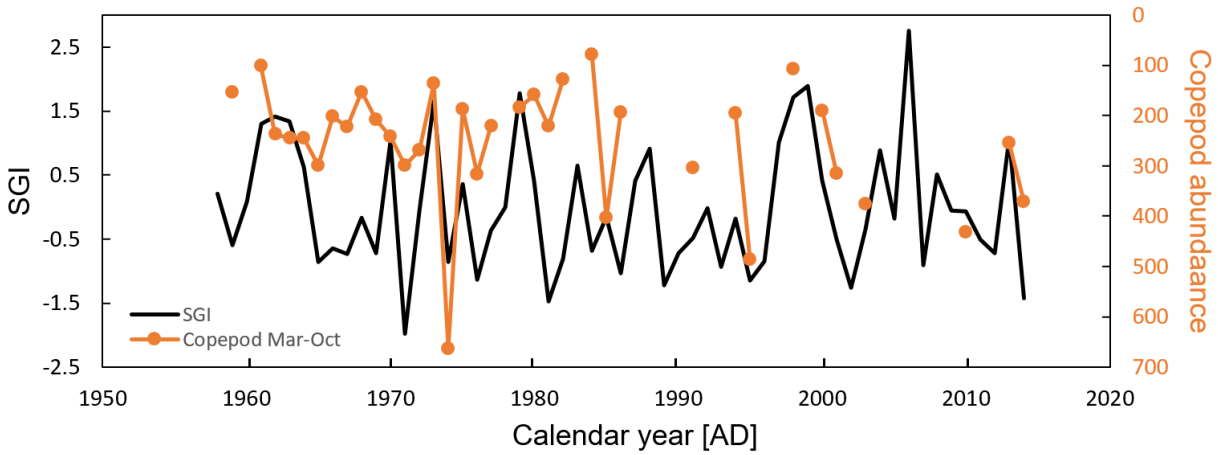

Figure 32: SGI-data obtained in this work (black line) and mean CPR Copepod abundance for March-October (orange line and dots) during the period 1958-2014. Copepod abundance scale (right) is reversed. The CPR Copepod abundance data was obtained from the Monthly CPR database and requested from The Sir Alister Hardy Foundation for Ocean Science (SAHFOS) (https://www.sahfos.ac.uk/data/data-charts/)

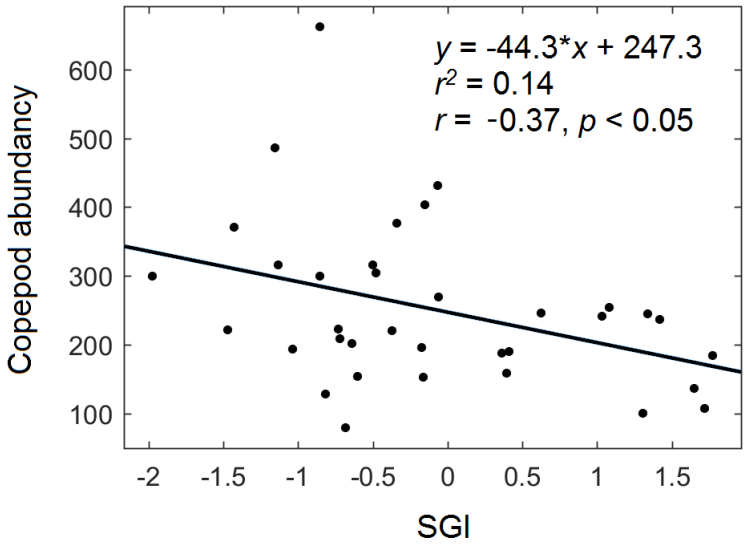

Figure 33: Regression analysis between copepod abundance and SGI during the months March-October in standard area B6, during the period 1958-2014 (n = 35, data from Figure 32).

The negative relationship is possibly related to a decreased food supply to the bivalves, hence lower shell growth, in years with high abundance of herbivorous copepods as a consequence of competition for the phytoplankton. Perhaps in accordance with this, Witbaard et al. (2003) found a significant negative correlation between shell growth of an *A.Isclandica* population from Fladen Ground (northern Norway) and a 6-months lagged copepod abundance. Shell growth in another population from the same area studied by Mette et al. (2015) was found to be inversely related to SST, and a relationship was suggested to the increased abundance of herbivorous zooplankton in periods with higher temperatures at the sea surface. Wanamaker et al. (2009b), however, found a significant positive correlation between relative abundance of the specific copepod *Calanus finmarchicus* and shell growth in an *A. islandica* population from the western Gulf of Maine, USA. This positive relationship was associated with the overall biological productivity in the area, where an increase in zooplankton abundance meant a correspondingly high primary production, hence more potential food for the bivalves. Previous findings by others are therefore ambiguous, although with the negative relationship between shell growth and copepod abundance found in this study which seem to support the findings of Witbaard et al. (2003) it is reasonable to assume that copepods and *A. islandica* are linked to one another in the way mentioned.

Comparison of SGI and CPR total Copepod abundance in May between 1958-2014 in the standard area A6 did result in a significant positive, but weak, correlation ($r = 0.32$, $p < 0.05$). This positive correlation could mean an indirect relationship via the increased phytoplankton abundance in this period which has a positive effect on both copepods and *A. islandica* independent of each other. The positive relationship between shell growth and copepod abundance correspond to the findings of Wanamaker et al. (2009b). These findings indicate that depending on the timing of the year and the relative abundance between phytoplankton and zooplankton, and probably also the dynamics of water mixing, shell growth is either positively or negatively linked to the abundance of copepods. No other significant correlations were found when comparing measurements from standard area A6 with shell growth. The standard area A6 has fewer recorded data in the most recent years compared with B6 which may affect the analysis. Area A6 includes the coastal water around most of Iceland. This area is influenced by different ocean currents and various amounts of freshwater input from land, and occasionally sea ice by the northern and eastern coast. This standard area is therefore not necessarily more representative for the study area than the B6 standard area which is the closest standard area located south off Iceland. Standard area B6 is more likely to be affected by the same North Atlantic water masses as the current study area.

6.3.3 Sea water temperature

Temperature is assumed to influence the growth of *A. islandica* indirectly through primary productivity which is decisive for the food supply, and to a small degree directly affecting the organisms' metabolism (Witbaard et al., 1994). Some previous studies have found significant correlations, usually not strong, between shell growth and water temperature (Schöne et al., 2002, Wanamaker et al., 2009b, Butler et al., 2010, Marali and Schöne, 2015). Other studies, however, found no correlation between shell growth and water temperature (Witbaard, 1996, Marchitto et al., 2000, Schöne et al., 2004). Thus, there are mixed conceptions about the impact of water temperature on shell growth. There are at least three possible ways in which temperature can drive shell growth (Figure 28):

Firstly, it is possible that the shell growth is directly influenced by some sort of thermodynamic effect (Witbaard et al., 1997b). Warmer water can for instance lead to increased metabolic

activity of the bivalves on expense of the growth efficiency (Blicher et al., 2010), thus less growth during periods of particularly high temperatures. However, this is not likely to be the case for the bivalve population of this study as the water temperature difference at 100 m depth is minor. Changing filtration rate, linked to valve gape activity, is shown to be affected first and foremost by the food particle density of the ambient water, but also to some extent by the water temperature (Witbaard et al., 1997b, Ballesta-Artero et al., 2017). Temperature has been shown to be related to valve gaping activity, or filtration rate through siphon extension, and high siphon activity did correspond with faster growth (Witbaard et al., 1997b, Ballesta-Artero et al., 2017). As demonstrated in the tank experiment of Witbaard et al. (1997b) the growth rate of the bivalve changed the most between 1°C and 6°C (the lower temperature range). Furthermore, the shell growth kept on increasing, only to a lesser rate, up to 12°C. Also a higher increase in growth occurred between 9°C and 12°C, compared to less variation in growth between 6°C and 9°C (Witbaard et al., 1997b).

Secondly, shell growth can be linked to sea surface temperature variability indirectly through primary productivity which influence potential food availability to the benthos (Butler et al., 2010). Thirdly, the total yearly phytoplankton growth is also shown to be related to the duration of the growing season of the shell population, which is assumed to be indirectly related to temperature (Weidman et al., 1994, Schöne et al., 2005a, Butler et al., 2009b). These possible influences may also vary both in space and time, which further complicate identification of the overall effect of temperature on shell growth.

Provided the estimated main growing season of the population, from February/March to August/September (Figure 27), it is hypothesised that there may be some sort of relationship between shell growth and local water temperature variations at 100 m depth in these months. The MSC obtained in this project was therefore compared with instrumental temperature measurements at 100 m depth at station FX3 in February, May, August and November, which are the months with the most frequent temperature measurements. However, the instrumental measurements are also here marked by temporal gaps, with lacking data for several years and months (Figure 27). A linear regression was performed for all four months mentioned. The data did not show any significant correlation in February and November, and since the sample resolution of these two months were quite low (n = 10) the plots are not included here. The positive incline of the correlation plots of May and August **(**Figure 34), however, imply a

possible relationship between temperature and annual shell growth southwest off Iceland. The relationship is, however, not significant. The limited instrumental temperature data and the temporal dispersion of the data available does not provide a solid foundation to state that there is or is not a relationship between local sea water temperature at 100 m depth and shell growth. The probability of a direct relationship may, however, not be very high as the mean temperature difference of the water surrounding the population is very small throughout the year (1.92°C, average of 2005-2009), and this is therefore not very likely to have any substantial effect on the organisms' metabolism and siphon activity, thereby no major influence on the total shell growth.

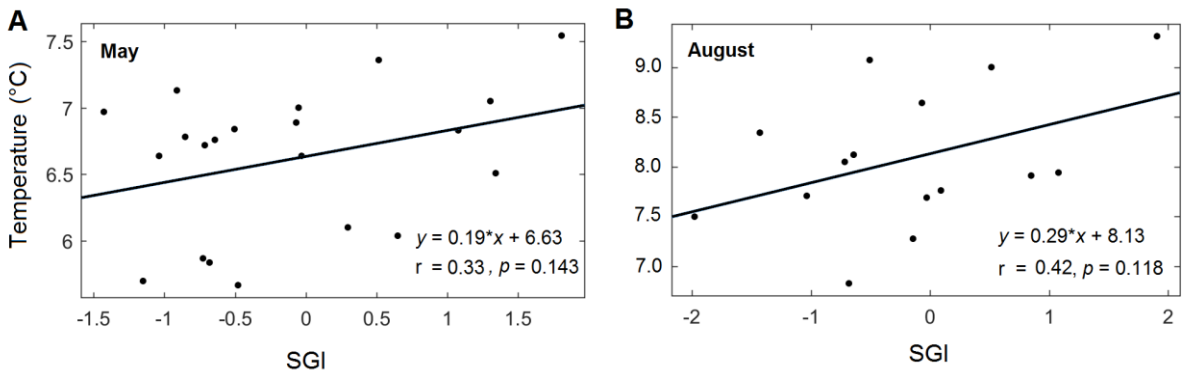

Figure 34: Linear regression analysis between annual shell growth and BWT (100 m depth) at FX3 in A**)** May, n = 21 (1948-2014), and B) August, n = 15 (1949-2014).

The growth of *Arcitca islandica* in this study is assumed not to be directly influenced by sea surface temperature (SST) because the population is located at 100 m depth and the surface waters tend to be more stratified during the summer months, thus decoupling the bottom waters from the surface conditions (Butler et al., 2010). Instead, the shell growth is assumed to be indirectly related to sea surface temperatures via primary production which mainly occur at the sea surface (Mellard et al., 2011). In a study by Richardson and Schoeman (2004) it was established that in the northeast Atlantic, including the area around Iceland, an increase in abundance of phytoplankton is positively related to a warming of the sea surface water, as well as affecting the taxonomic phytoplankton composition. Winter convection of nutrients and increased sunlight is often the factors which initiate the spring phytoplankton bloom, but also elevated SST has been shown to result in stratification of the water column and increased phytoplankton bloom in surface waters during the summer (Ogilvie and Jonsdottir, 2000).

Positive significant correlations between higher SST and phytoplankton abundance were found at both the standard CPR areas A6 and B6 (Richardson and Schoeman, 2004), which is the areas closest to the study site (see appendix D for map of the standard CPR areas**)**.

Compared to instrumental records on primary productivity and records on bottom water temperatures, records on sea surface temperature in the North Atlantic have an extensive sampling resolution, with monthly measurements covering the whole period of the master shell chronology. Both the SST records HadISST1 and ERSST are used for comparison with the MSC, and these records vary to a certain degree due to the differences in spatial distribution of the instrumental stations included in the records. How well these SST records represent the SST at the study location depend on the proximity and number of instrumental stations where temperature measurements have been performed over time. Comparisons of annual shell growth with monthly, seasonal and annual averages of North Atlantic SST did not result in any significant correlations (data not shown). Other studies which did find correlations, whether negative (Mette et al., 2015) or positive (Marali and Schöne, 2015), typically investigated shells from shallower water depths (< 35 m) where stratification seem to not have any major influence on the food availability to the benthos. However, a study by Schöne et al. (2002) of *A. islandica* specimens from 50 and 35 m depths at the Dogger Bank in the central North Sea, discovered a statistically significant negative relationship between annual shell growth and winter SST. Explanations to the nonexciting correlation between shell growth and SST on an annual level is probably due to complexity of the system. As previously discussed, there are several factors which have an effect on the environmental conditions at the study site, including seasonal and yearly variability in stratification of the water column due to temperature differences and varying degree of water mixing by e.g. waves and currents, and the presence of zooplankton creating competition of the food source.

On a lower frequency, the trend in shell growth and mean SST of the main growing season seems to covary, comparing smoothed data (7 year running mean) (Figure 35). The similarity is most prominent in the period of 1950-2000. Interestingly enough, prior to 1950 the two variables seem to share almost the same periodicity, only the shell growth is lagged 5-10 years behind the SST. It is perhaps reasonable to argue that the MSC may have been constructed with an offset, but this offset would in this scenario mean many missing increments in all the specimens, which is not a probable explanation. It is therefore reasonable to assume that the lag

is caused by some delay in the bivalves' response to the climate system. The shell growth seems to be more related to the ERSST record which is also expected as it is derived from a 2° cell (63°N - 65°N; 024°W - 022°W) around the sampling location. The offset between the SST records and shell growth is interesting, and a possible explanation can be that SST measurements prior to 1950 is also marked by more spatial and temporal coverage gaps which increase the uncertainties. Another interesting observation is the decreasing trend in multiyear shell growth in the most recent years as the SST is markedly increasing. This indicate that the link between temperature and shell growth is not the same over time, probably due to the interference of other environmental variables. Increased NAW transport and higher sea surface water temperatures are probably often beneficial for the bivalves as it contributes to the increased primary production and increased potential food supply. However, greater stratification in periods with increased SST and less water mixing will in some periods counteract this effect leading to less total shell growth.

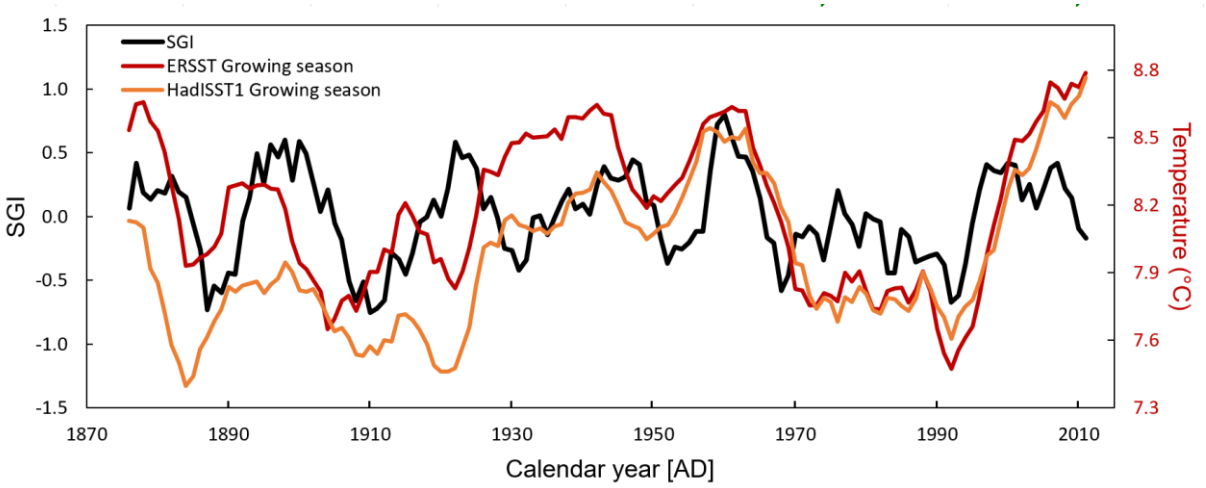

Figure 35: Standardized growth Index of the MSC and sea surface temperature (SST) shown as smoothed (7-year running mean) SGI (black line) of the chronology with equally smoothed mean SST of the main growing season. SST data is derived from Hadley Centre Sea Ice and Sea Surface Temperature (HadISST1) (orange line) and from a 2° cell (63°N - 65°N; 024°W - 022°W) around the sampling location, based on the monthly Extended Reconstructed Sea Surface Temperature (ERSST) v4 (red line) from the International Comprehensive Ocean-Atmosphere Dataset (ICOADS). Both SST datasets is downloaded via the Royal Netherlands Meteorological Institute (KNMI Climate Explorer) website (https://climexp.knmi.nl).

6.3.4 AMO

Instrumental measurements, historical records and marine paleo proxy records all demonstrate temperature variabilities in the northern North Atlantic which coincide with the assumed Atlantic Multidecadal Oscillation (Knight et al., 2006, Drinkwater et al., 2014). Variability of the AMO and NAO has been shown to indirectly influence marine ecosystems, including phytoplankton, zooplankton, pelagic and benthic communities (Drinkwater et al., 2003, Nye et al., 2014). It is therefore also reasonable to expect that such multidecadal variability in North Atlantic SST may be detected in the growth of the *A. islandica* population studied in this project. The study site southwest off Iceland is strategically located in one of the continuations of the NAC and in an area dominated by important oceanic and atmospheric forcing. The hydrographic conditions southwest off Iceland are sensitive to small changes in the strength of the NAC. Increased inflow of NAW to the Iceland area by the IC is associated with a stronger density driven overturning circulation (AMOC) (Mahajan et al., 2011) and weaker subpolar gyre (SPG), which both are shown to be more frequent during positive AMO phases (Nye et al., 2014). As mentioned earlier, an increased transport of the warm, salty and nutrient rich IC has a positive effect on the ecosystem southwest off Iceland by boosting the phytoplankton bloom, hence providing food for copepods and the bivalve population of this study, as well as other organisms higher up in the food chain (Astthorsson et al., 2007). The relationship found in this study on a multiyear time scale between shell growth and SST (Figure 35) indicates that the bivalves are influenced by lower-frequency changes in the temperature of the IC, and a similar relationship can be expected with multidecadal AMO variability.

The master shell chronology span over almost the entire length of the instrumental AMO record (1870 until today). Over this period, the AMO exhibits a 65-80-year cycle with warm phases (AMO+) at about 1860-1880 and 1930-1960 and cold phases (AMO-) during 1905-1925 and 1970-1990. In the mid-1990s the AMO seems to have returned to a warm phase. AMO applies not only to the sea surface but also to sub surface waters (Drinkwater et al., 2014). By studying the variability of sea ice extent and water temperature in the area, Drinkwater (2006) found that the transport of NAW by the IC was above normal between 1920-1940 coinciding with the beginning of the early twentieth century warming period and the AMO+ period (Drinkwater et al., 2014). Observations has shown that the subpolar gyre was weakened in the mid-late 1990s

(Hátún et al., 2009), coinciding with increased SSTs and the beginning of the current AMO+ period, which is associated with increased NAW transport by the IC.

Comparison of shell growth data from this project and the AMO index, on a year-to-year time scale, did not result in any significant correlations (data not shown). The obtained SGI data and different AMO indexes was, however, also calculated on a multidecadal time scale with a 21-year running mean for both records (Figure 36). Visual comparison of the two records in the period 1880-2000 demonstrate a coverability with a 70-year cycle during the same period, between 1910 and 1980. The AMO index calculated based on the ERSST v3b shows an offset from the other indexes, which is not surprising as this index include instrumental stations over a wide area. The standardized growth indices reveal an oscillatory growth signal with a multi-year periodicity, which is positively related to both the Hadley Centre Sea Surface Temperature (HadSST) AMO index and the Kaplan SST AMO index. The HadSST has some temporal and spatial coverage gaps, particularly early in the record, combined with other uncertainties such as individual measurement errors and changes in measurement methods (e.g. bucket measurements or buoy data) (NCAR, Climate Data Guide, 08.05.17).

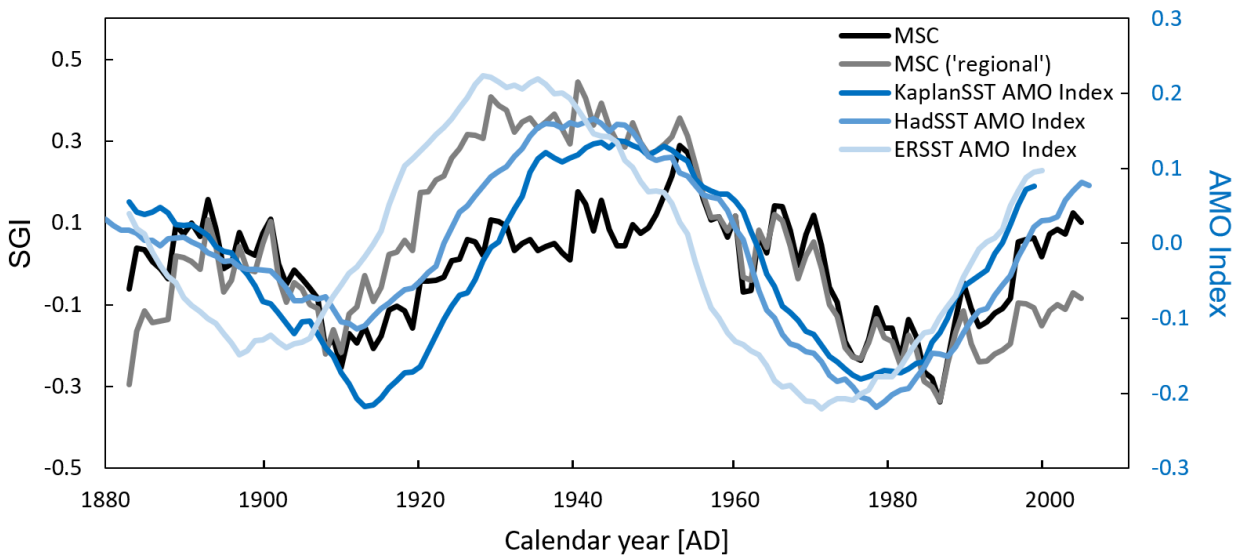

Figure 36: The MSC compared with AMO index. Master shell chronology **(**MSC) and 'regional MSC (21-yr running mean), compared with AMO Index (21-yr running mean) based on Kaplan SST, HadSST and ERSST). Both the HadSST and ERSST AMO index datasets can be downloaded via the Royal Netherlands Meteorological Institute (KNMI Climate Explorer) website (https://climexp.knmi.nl). The AMO index based on Kaplan SST (Kaplan et al., 1998) can be obtained from NOAA website (https://www.esrl.noaa.gov).

Butler et al. (2010) discussed the use of the different output from ARSTAN calculated chronologies and how some of them are better suited for comparisons with certain environmental records. They found that when the aim is to compare multidecadal environmental records, such as the AMO index, it is more appropriate to use 'regional' curve standardization when producing the chronology (RCS chronology), since this method can, in principal, be used to better preserve the low-frequency climate signals in the chronology (Butler et al., 2010). This RCS ARSTAN chronology was computed and compared with both the original chronology and the different AMO indexes. This resulted in a higher amplitude than in the original chronology. This supports the findings of Butler et al. (2010) who found that this alternative RCS chronology is more suitable for this kind of low-frequency multi-decadal record comparisons. However, it is important to be aware of the fact that the chronology constructed in this project has a sample depth of only ten specimens, which is quite low compared to what is normal in dendrochronological studies. This low sample depth, and the difference in biological age, can have an effect on the usefulness of the RCS chronology (Butler et al., 2010). Both the RCS chronology at the originally produced chronology demonstrates a visual co-variability between the smoothed SGI and AMO (Figure 36).

The coverability between smoothed shell growth and SST variability on multidecadal time intervals is supported by similar findings by Lohmann and Schöne (2013) studying an *A. islandica* population from north off Iceland, which was associated with sea ice extent in the same area. Mette et al. (2015), however, found a strong inversed relationship between annual AMO index and shell growth in northern Norway, which was also supported by an annually resolved $\delta^{18}O_{shell}$ record, developed using the same specimens as in the shell growth chronology, which showed even stronger negative correlations.

The findings of the current study support the assumption of a multi-decadal SST variability in the Irminger Current. The master shell chronology from the Faxaflói area may provide valuable insight into the still incomplete understanding of high-latitude AMO variability and its impact in the North Atlantic region (Drinkwater et al., 2014).

6.3.5 NAO

Positive phases of the North Atlantic Oscillation (NAO) are associated with warmer waters which in turn are related to higher biological production, including phytoplankton and zooplankton, which are assumed to affect the growth of *A. islandica* (Witbaard, 1996, Fromentin and Planque, 1996). Schöne et al. (2003), Helama et al. (2007) and Wanamaker et al. (2009b) all suggests a positive link between shell growth variability and winter NAO index. Other studies such as the one by Marali and Schöne (2015) did not find any statistically significant relationship between NAO index and shell growth of specimens from the shallow waters of the north-eastern coast of Iceland. Comparison of annual SGI from the current study with both winter and annual NAO index (Hurrell et al., 2001, Luterbacher et al., 2001) did not result in any significant correlations. Some annual co-variability seem to be present from the mid-1990s, which was as already accounted for a period with above normal transport of NAW into southwest Icelandic waters (Hátún et al., 2009). However, the lack of any evident relationship indicates that the growth signal of the bivalve population south west off Iceland is not forced by the NAO, and that more local environmental variability has caused the ecological response. The comparison between the smoothed NAO-index and MSC (7-year running mean) did show a similar signal in the period 1918-1930 (Figure 37). A possible explanation can be that during this period with mostly positive NAO years a stronger AMOC resulted in increased NAC transport, and therefore increased supply of warm, salty and high-productive NAW to the study site west off Iceland which had a positive effect on the shell growth (Drinkwater, 2006). However, the majority of the shell growth signal of the population did not correspond with the NAO. Neither shell growth and subpolar gyre index (Hátún et al., 2005), nor shell growth and AMOC index (26°N), used due to the lack of long-term AMOC records from higher latitudes, did result in any significant correlations on both year-to-year time scale and multiyear timescale. There was not found any relationship between shell growth and lagged NAO-, subpolar gyre- or AMOC-indexes.

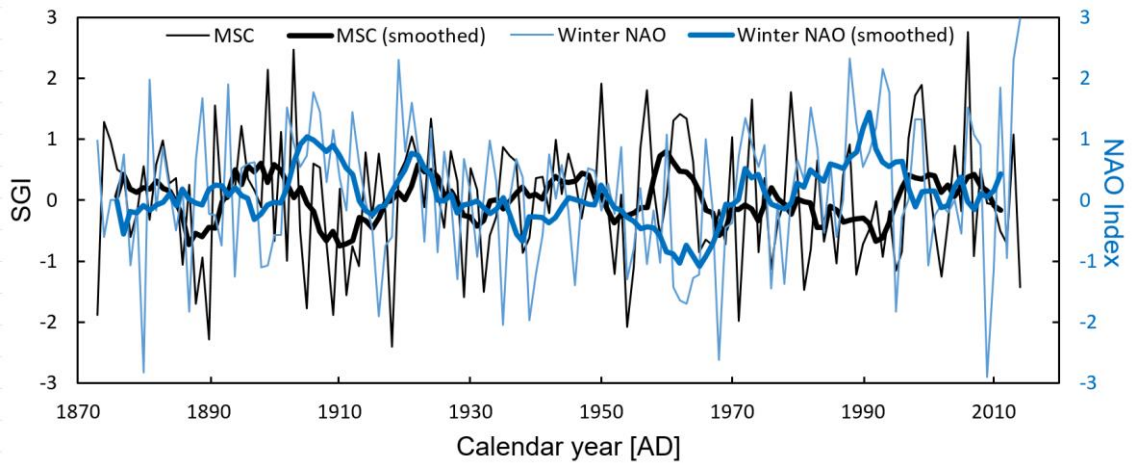

Figure 37: Comparison of SGI of MSC and annual winter North Atlantic Oscillation Index (NAO). The winter NAO index is a mean of December-March. NAO index data is obtained from the NCAR Climate Data Guide webpage (https://climatedataguide.ucar.edu), and the data is described by (Hurrell et al., 2001).

6.3.6 Sea ice extent

The fluctuations of the North Atlantic water (NAW) inflow to the northern North Atlantic are believed to, directly or indirectly, influence the sea ice extent in the area (Miles et al., 2014). The North Icelandic Irminger Current (NIIC) transport NAW to the northern parts of Iceland, and the behaviour of the NAC in general and the properties of the NAW, is assumed to influence the SST and therefore the sea ice extent in this area. A study by Lohmann and Schöne (2013) found a link between growth of *A. islandica* from northeast off Iceland and sea ice extent. The connection between variability of sea ice extent north off Iceland and changes of the NAC could possibly lead to an indirect relationship between shell growth bathed in NAW southwest off Iceland and sea ice extent. However, comparisons of instrumental, historical and proxy records on sea ice extent (Macias Fauria et al., 2010, Wallevik and Sigurjónsson, 1998, Ogilvie, 2005) with the SGI of the SW Iceland *A. islandica* population did not result in any correlations, and there were no indications of any relationship from this study (data not shown). Drifting sea ice most commonly occur along the north-western, northern and eastern coasts of Iceland (Ogilvie and Jonsdottir, 2000). Because of the prevailing direction of ocean currents around Iceland, especially the warm IC, sea ice virtually never occur on the southwest coast (Jennings et al., 2001). In some rare cases during severe sea-ice years, sea ice may reach the southern coast of Iceland due to the clockwise ice drift around the country from the north-eastern coast (Jennings et al., 2001). It is therefore not likely that sea ice has had any local effect southwest

off Iceland during the last century. The colder intervals during the 16th and 18th century, which is linked to a more pronounced climate variability with increased sea ice extent in northern latitudes, spans past the duration of the MSC constructed in this project. Nevertheless, the increased sea ice extent north off Iceland, and decreased salinity in the upper ocean layer (above 500 m), during the Great Salinity Anomaly years from 1968-1982 in the North Atlantic (Dickson et al., 1988), can be argued to coincide with lower than average shell growth in the *A. islandica* population southwest off Iceland. The possibility of a link between shell growth southwest off Iceland and sea ice extent during other periods of the past with more pronounced sea ice occurrence cannot be excluded.

6.4 Comparisons between Icelandic master shell chronologies

The combination of several shell-based chronologies from different areas to create a network is of great interest as it can potentially widen the use of *A. islandica* as a paleo proxy (Butler et al., 2009a). How well this can be done depends on the spatial range of the shared environmental growth signal preserved by the bivalves (Butler et al., 2009a). The use of specimens of *A. islandica* from Icelandic waters as a paleo proxy have been accounted for in several previous studies (Schöne et al., 2005a, Wanamaker et al., 2008, Wanamaker et al., 2012, Butler et al., 2013, Lohmann and Schöne, 2013, Marali and Schöne, 2015), however, almost all of these studies are of specimens collected from north off Iceland. Combined, these studies have resulted in the construction of three separate shell-based chronologies using different *A. islandica* populations situated on the North Icelandic shelf (Butler et al., 2013, Lohmann and Schöne, 2013, Marali and Schöne, 2015). Butler et al. (2013) presents a master chronology consisting of specimens collected from deep-water settings (81-83 m) at a location on the North Icelandic Shelf west off Grimsey Island, and is referred to as the Grimsey chronology. The Grimsey chronology, first worked on by Wanamaker et al. 2008, resulted later in an absolutely-dated, 1357-year long chronology for the marine environment of the North Icelandic shelf (Butler et al., 2013). This chronology is the longest existing master chronology ever constructed using bivalves as proxy, and does also include the ontogenetically oldest *A. islandica* specimen, of 507 years, ever found (Butler et al., 2013). The master shell chronology by Marali and Schöne (2015) is based on shell material collected from shallower waters, i.e. the upper well-mixed portion of the water column (<23 m), northeast off Iceland near Lónafjörður, and is referred to as the NE Iceland chronology. The NE Iceland chronology is based on material collected from the shallow shelf area southeast off Iceland (Schöne et al., 2005a, Lohmann and Schöne, 2013, Marali and Schöne, 2015) and is therefore considerably affected by surface and coastal water properties. The third chronology, presented by Lohmann and Schöne (2013), is based on a few live-collected shells from Northeast Iceland at about 30 m depth. This chronology has not been compared further here as it is from almost the same location as the chronology by Marali and Schöne (2015), and since the last mentioned chronology demonstrates a higher degree of synchronous growth, indicated by higher average EPS value, than the chronology of Lohmann and Schöne (2013).

If there is a correlation between the chronologies north and northeast off Iceland, respectively, one could also look for a common growth signal between the north/northeast and southwest *A. islandica* populations (Figure 38A). Comparisons of the smoothed SGIs (7-year running mean) of the Grimsey chronology and the NE Iceland chronology indicate a shared growth signal between 1905-1945. However, other periods seem to be mostly governed by different environmental growth signals both on annual and multiannual time scale (Figure 38A). One could also argue that the two chronologies outside the mentioned period show a similar variability but with some offsets in time.

As previously accounted for, both the southwestern and the north/north-eastern Icelandic shelf seas are affected by NAW carried by the IC and the NIIC, respectively. The influence of NAW in both regions could possibly result in growth similarities between these spatially separated *A. islandica* populations. One could suspect that the Grimsey chronology (ca. 80 m depth), which include material collected from similar depths as the material used in the current study (ca. 100 m depth), could share a common growth signal. Comparison of instrumental Marine Research Institute (MRI) data at 100 m depth between stations FX3/FX4 and the closest MRI station close to the Grimsey chronology location, the Siglunes transect station SI3 (66° 32´ N, 18° 50´ W) (Figure 5**),** demonstrate a similar seasonal temperature fluctuation throughout the year. Although the water temperature in the north is generally a couple of degrees lower than southwest off Iceland.

However, the master shell chronology (MSC) from southwest off Iceland (SW Iceland MSC) obtained in this work and the Grimsey chronology did not correlate on a year-to-year basis in the period compared (1873-2005), which indicate that the shell growth in the populations are controlled by different local changes in their surrounding environment (Figure 38B). Visual examination of the smoothed SGI's of the SW Iceland MSC and both of the other two Icelandic chronologies also show that the MSC obtained in the current work do not share any obvious common growth signal (Figure 38B and 38C). There are some indications, however, that the currently obtained SW Iceland MSC and the Grimsey chronology are inversely related on a multiyear timescale, when visually comparing the 7-yr running mean of both chronologies. For the smoothed MSC of SW Iceland and NE Iceland there is perhaps a positive relationship between 1918-1930, although not at an annual timescale. This period is associated with NAO+ years with increased IC transport and consequently increased supply of high productive,

relatively warm and saline water to the southwest and northeast Icelandic coast (Drinkwater, 2006).

The spatial extent of the common growth signal of an *A. islandica* population is likely to be confined by the variability in the patterns of water mass mixing, i.e. changes in temperature and salinity, in the marine environment (Butler et al., 2009a). These patterns are forced by wind fields (Witbaard et al., 2003), stratification dynamics in the water column (Schöne et al., 2002, Butler et al., 2010) and ocean bottom topography (Mork and Blindheim, 2000). The Icelandic marine ecosystem and physical oceanographic characteristics of the southern and western areas differ from those in the north and east (Astthorsson et al., 2007). The main reason is that NAW is governing the south and west, while the north and east are influenced by a combination of Atlantic, Arctic and Polar water masses which leads to greater seasonal variability (Astthorsson et al., 2007). NAW reaching the North Atlantic Shelf carried by the North Icelandic Irminger Current (NIIC) constitute only 5-10 % of the IC (Vilhjálmsson, 2002). The temperature and salinity of the NIIC decrease with the direction of the flow because of the mixing that occurs along the way with colder less-saline polar water and freshwater runoff from land (Astthorsson et al., 2007). Due to the greater influence of NAW on the southwestern self the spring phytoplankton bloom will typically start earlier in the spring compared to the shelf area north-east off Iceland (Gudmundsson, 1998), and the mean primary production is in general higher in the southwest off Iceland (Astthorsson et al., 2007). Such differences, in the mechanisms controlling the NAW influence, which are present in the shell sample areas discussed here, and combined with local differences in freshwater runoff, coastal currents, degree of stratification and possibly also sea ice occurrence, likely causes considerable differences between the bivalve populations' living environments. Hence, the *A. islandica* in these areas record very dissimilar environmental variability.

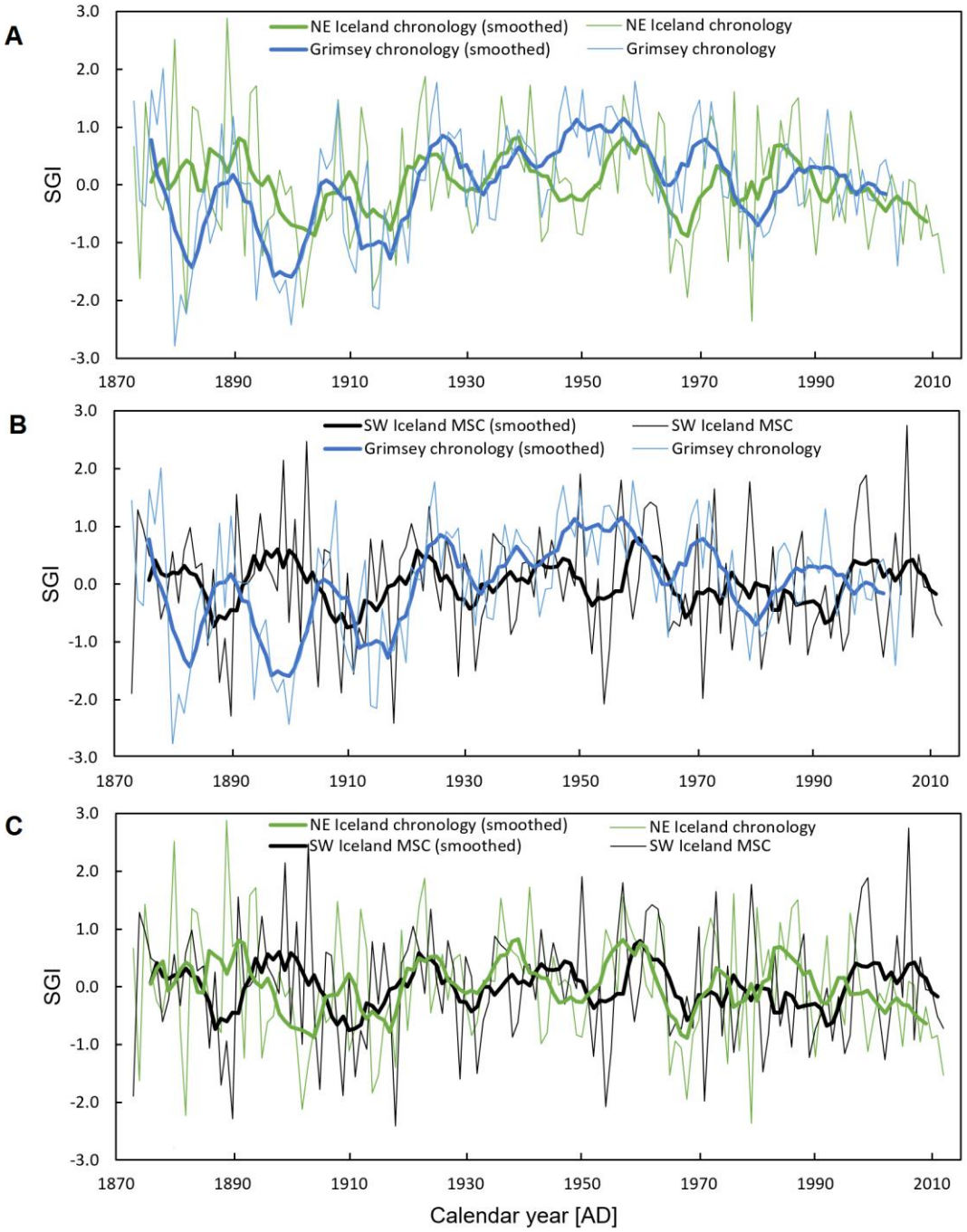

Figure 38: Icelandic master shell chronologies compared with included annually resolved chronologies and 7 year running means. A) Standardized growth index (SGI) of the Grimsey chronology (blue lines) compared with the SGI of the NE Iceland chronology (green lines). B) SGI of the Grimsey chronology (blue lines) compared with SGI of the SW Iceland current work chronology (black lines). C) SGI of the NE Iceland chronology (green lines) compared with SGI of the SW Iceland current work chronology (black lines). The original record and data used by Butler et al. (2013) to construct the 1357-year chronology, is retrieved from the National Climate Data Centre, (National Oceanic and Atmospheric Administration, NOAA). Data on the NE Iceland chronology is retrieved from corresponding author of Marali and Schöne (2015).

7 Conclusions

- Annual growth increments in specimens of the long-lived bivalve *A. islandica* was successfully crossdated and combined to form an absolutely dated, annually resolved master shell chronology from southwest off the coast of Iceland in the Faxaflói area.
- The statistics of the master shell chronology show a strong shared growth signal within the *A. islandica* population of this study, which demonstrate that the specimens sampled in the area function as recorders of environmental changes.
- The main growing season of the bivalve population, estimated from the seasonal oxygen isotope composition within the increments, reflects the seasonal variability of water temperature at the study site. Furthermore, the data supports that the main growing season occurs during the period of mainly increasing water temperatures, between February/March and August/September. In some years, growth outside this period also seems to occur.
- The growth of the bivalve population shows a large year-to-year variability, which is likely mostly a result of the local food availability and quality throughout the growing season. This has been shown to vary greatly between different areas and seems to depend on a combination of multiple factors: 1: SST which influence the spring phytoplankton bloom and the overall primary production in the area, 2) copepod abundance, depending on the SST and the primary production, which interfere by competing of the same food source, 3) the SST, wind and the properties of the IC which influence the stratification and the convection of nutrients both upwards and downwards in the water column.
- Comparison with the growth data from this thesis indicate that the bivalves are positively linked to the abundance of phytoplankton, and negatively with the abundance of herbivorous copepods. The links are, however, probably weakened by the influence of other interfering environmental variables at the study location as mentioned above, particularly changes in stratification of the water column.
- On a lower-frequency, the standardized growth index (SGI) of the population was found to covary with the multiannual variability of the SST in the North Atlantic and indicated a positive relationship between the shell growth and SST for the period 1950-2010.

- The data seems to support a relationship on a multidecadal time scale between smoothed shell SGI data obtained in this study and AMO index in the period 1883-2004.

7.1 Potential future research

The obtained master chronology of this study form a reference to which new increment series may be compared and dated, using additional live-collected and sub-fossil specimens from the same area. Materials available for future research include, among other specimens, a live-collected specimen preliminarily dated to be about 400 years of age (Appendix A, Figure A2), and several AMS ^{14}C dated sub-fossil specimens that have a wide range of geological age. One of the sub-fossil specimens were found to be around 10 000 years old. Furthermore, stable oxygen isotope analyses from each year of the master chronology can potentially be used as a paleothermometer on the variability in mean annual temperature of the Irminger Current through time. For this, annual $\delta^{18}O_{shell}$ sampling has already been performed and are awaiting analysis. For more reliable temperature estimates, and to more accurately determine the growing season of the bivalve population, it is necessary to collect water samples from the study area for measurements of the $\delta^{18}O_{water}$ value. It would also be of interest to study, in more detail, the effects of variations that occur in the chronology even when using the same detrending technique, but with small variations in the fitting of the negative exponential curve to the data, which occur when using a different statistical software. This small variation can possibly be notable when the chronology is used for climate reconstructions. Future work may also involve additional comparison with data from other paleo proxy archives, for example highly resolved sediment cores, which are now being worked on within the EU Ice2ice project at Uni Research Climate and the University of Bergen.

References

ALHEIT, J., DRINKWATER, K. F. & NYE, J. A. 2014. Introduction to Special Issue: Atlantic Multidecadal Oscillation-mechanism and impact on marine ecosystems.

ANDERSSON, C., PAUSATA, F. S. R., JANSEN, E., RISEBROBAKKEN, B. & TELFORD, R. J. 2010. Holocene trends in the foraminifer record from the Norwegian Sea and the North Atlantic Ocean. *Climate of the Past***,** 179-193.

ANDERSSON, C., RISEBROBAKKEN, B., JANSEN, E. & DAHL, S. O. 2003. Late Holocene surface ocean conditions of the Norwegian Sea (Vøring Plateau). *Paleoceanography,* 18**,** 1044.

ASTTHORSSON, O. S., GISLASON, A. & JONSSON, S. 2007. Climate variability and the Icelandic marine ecosystem. *Deep-Sea Res. II,* 54**,** 2456-2477.

AZETSU-SCOTT, K. & TAN, F. C. 1997. Oxygen isotope studies from Iceland to an East Greenland Fjord: behaviour of glacial meltwater plume. *Marine Chemistry,* 56**,** 239-251.

BA, J., KEENLYSIDE, N., LATIF, M., PARK, W., DING, H., LOHMANN, K., MIGNOT, J., MENARY, M., OTTERÅ, O., WOUTERS, B., SALAS Y MELIA, D., OKA, A., BELLUCCI, A. & VOLODIN, E. 2014. A multi-model comparison of Atlantic multidecadal variability. *Observational, Theoretical and Computational Research on the Climate System,* 43**,** 2333-2348.

BALLESTA-ARTERO, I., WITBAARD, R., CARROLL, M. L. & VAN DER MEER, J. 2017. Environmental factors regulating gaping activity of the bivalve Arctica islandica in Northern Norway. *Marine Biology*.

BLACK, B. A., GRIFFIN, D., VAN DER SLEEN, P., WANAMAKER JR., A. D., SPEER, J. H., FRANK, D. C., STAHLE, D. W., PEDERSON, N., COPENHEAVER, C. A., TROUET, V., GRIFFIN, S. & GILLANDERS, B. M. 2016. The value of crossdating to retain high-frequency variability, climate signals, and extreme events in environmental proxies. *Global Change Biology,* 22**,** 2582-2595.

BLICHER, M. E., RYSGAARD, S. & SEJR, M. 2010. Seasonal growth variation in Chlamys islandica (Bivalvia) from sub-Arctic Greenland is linked to food availability and temperature. *Marine Ecology Progress Series,* 407**,** 71-86.

BRADLEY, R. S. 2014. Marine Sediments (Chp. 6) & Tree Rings (Chp. 13). *Paleoclimatology: reconstructing climates of the quaternary 3rd Edition.* Third edition. ed. Oxford, U. K.: Elsevier Inc.

BRYSON, R. A. 1974. A Perspective on Climatic Change. *Science,* 184**,** 753-760.

BUTLER, P. G., RICHARDSON, C. A., SCOURSE, J. D., WANAMAKER, A. D., SHAMMON, T. M. & BENNELL, J. D. 2010. Marine climate in the Irish Sea: analysis of a 489-year marine master chronology derived from growth increments in the shell of the clam Arctica islandica. *Quaternary Science Reviews,* 29**,** 1614-1632.

BUTLER, P. G., RICHARDSON, C. A., SCOURSE, J. D., WITBAARD, R., SCHÖNE, B. R., FRASER, N. M., WANAMAKER, A. D., BRYANT, C. L., HARRIS, I. & ROBERTSON, I. 2009a. Accurate increment identification and the spatial extent of the common signal in five Arctica islandica chronologies from the Fladen Ground, northern North Sea. *Paleoceanography,* 24**,** n/a-n/a.

BUTLER, P. G., SCOURSE, J. D., RICHARDSON, C. A., WANAMAKER, A. D., BRYANT, C. L. & BENNELL, J. D. 2009b. Continuous marine radiocarbon reservoir calibration and the 13C Suess effect in the Irish Sea: Results from the first multi-centennial shell-based marine master chronology. *Earth and Planetary Science Letters,* 279**,** 230-241.

BUTLER, P. G., WANAMAKER, A. D., SCOURSE, J. D. & RICHARDSON, C. A. 2013. Variability of marine climate on the North Icelandic Shelf in a 1357-year proxy archive based on growth increments in the bivalve Arctica islandica. *Palaeogeography, Palaeoclimatology, Palaeoecology,* 373**,** 141-151.

COOK, E. R. & PETERS, K. 1997. Calculating unbiased tree-ring indices for the study of climatic and environmental change. *The Holocene,* 7**,** 361-370.

COOKE, S. & ROHLING, E. J. 1999. Stable Isotopes in Foraminiferal Carbonate

CRAIG, H. & GORDON, L. I. 1965. Deuterium and oxygen-18 variations in the ocean and the marine atmosphere. *Stable Isotopes in the Oceanographic Studies and Paleotemperatures***,** 9-130.

DAHLGREN, T. G., WEINBERG, J. R. & HALANYCH, K. M. 2000. Phylogeography of the ocean quahog (Arctica islandica): influences of paleoclimate on genetic diversity and species range. *International Journal on Life in Oceans and Coastal Waters,* 137**,** 487-495.

DETTMAN, D. L., REISCHE, A. K. & LOHMANN, K. C. 1999. Controls on the stable isotope composition of seasonal growth bands in aragonitic fresh-water bivalves (unionidae). *Geochimica et Cosmochimica Acta,* 63**,** 1049-1057.

DICKSON, R. R., MEINCKE, J., MALMBERG, S.-A. & LEE, A. J. 1988. The "great salinity anomaly" in the Northern North Atlantic 1968–1982. *Progress in Oceanography,* 20**,** 103-151.

DRINKWATER, K. F. 2006. The regime shift of the 1920s and 1930s in the North Atlantic. *Progress in Oceanography,* 68**,** 134-151.

DRINKWATER, K. F., BELGRANO, A., BORJA, A., CONVERSI, A., EDWARDS, M., GREENE, C. H., OTTERSEN, G., PERSHING, A. J. & WALKER, H. A. 2003. The response of marine ecosystems to climate variability associated with the North Atlantic Oscillation. Chapter 10. *In:* AL., H. E. (ed.) *The North Atlantic Oscillation: Climate Significance and Environmental Impact.* . American Geophysical Union, Washington, DC,: Geophysical Monograph.

DRINKWATER, K. F., MILES, M., MEDHAUG, I., OTTERÅ, O. H., KRISTIANSEN, T., SUNDBY, S. & GAO, Y. 2014. The Atlantic Multidecadal Oscillation: Its manifestations and impacts with special emphasis on the Atlantic region north of 60°N. *Journal of Marine Systems,* 133**,** 117-130.

EPPLÉ, V., BREY, T., WITBAARD, R., KUHNERT, H. & PÄTZOLD, J. 2006. Sclerochronological records of Arctica islandica from the inner German Bight. *The Holocene,* 16**,** 763-769.

FIELD, C. B., BEHRENFELD, M. J., RANDERSON, J. T. & FALKOWSKI, P. 1998. Primary Production of the Biosphere: Integrating Terrestrial and Oceanic Components. *Science,* 281**,** 237-240.

FOSTER, L. C., ALLISON, N., FINCH, A. A., C., A. & U.S., N. 2009. Controls on δ18O and δ13C profiles within the aragonite bivalve Arctica islandica. *The Holocene,* 19**,** 549-558.

FROMENTIN, J.-M. & PLANQUE, B. 1996. Calanus and environment in the eastern North Atlantic. II. Influence of the North Atlantic Oscillation on C. finmarchicus and C. helgolandicus. *Marine Ecology Progress Series,* 134**,** 111-118.

GISLASON, A. 2003. Life-cycle strategies and seasonal migrations of oceanic copepods in the Irminger Sea. *The International Journal of Aquatic Sciences,* 503**,** 195-209.

GISLASON, A. & SILVA, T. 2012. Abundance, composition, and development of zooplankton in the Subarctic Iceland Sea in 2006, 2007, and 2008. *ICES Journal of Marine Science,* 69**,** 1263-1276.

GRAY, S. T., GRAUMLICH, L. J., BETANCOURT, J. L. & PEDERSON, G. T. 2004. A tree-ring based reconstruction of the Atlantic Multidecadal Oscillation since 1567 A.D. *Geophysical Research Letters,* 31**,** 1-4.

GRISSINO-MAYER, H. D. 2001. Evaluating Crossdating Accuracy: A manual and tutoral for the computer prgram COFECHA. *Tree-ring Research.* Knoxville, USA: Institute of Geography, the University of Tennessee

GROSSMAN, E. L. & KU, T.-L. 1986. Oxygen and carbon isotope fractination in biogenic aragonite: temperature effects *Chemical Geology,* 59**,** 59-74.

GUDMUNDSSON, K. 1998. Long-term variation in phytoplankton productivity during spring in Icelandic waters. 55**,** 635-643.

HANSEN, B. & ØSTERHUS, S. 2000. North Atlantic–Nordic Seas exchanges. *Progress in Oceanography,* 45**,** 109-208.

HANSEN, B., ØSTERHUS, S., TURRELL, W. R., JÓNSSON, S., VALDIMARSSON, H., HÁTÚN, H. & MALSKÆR, S. O. 2008. The Inflow of Atlantic Water, Heat, and Salt to the Nordic Seas Across the Greenland–Scotland Ridg *In:* DICKSON, R. R., MEINCKE, J. & RHINES, P. (eds.) *Arctic–Subarctic Ocean Fluxes: Defining the Role of the Northern Seas in Climate.* Springer Netherlands.

HÁTÚN, H., PAYNE, M. R., BEAUGRAND, G., REID, P. C., SANDØ, A. B., DRANGE, H., HANSEN, B., JACOBSEN, J. A. & BLOCH, D. 2009. Large bio-geographical shifts in the north-eastern Atlantic Ocean: From the subpolar gyre, via plankton, to blue whiting and pilot whales. *Progress in Oceanography,* 80**,** 149-162.

HÁTÚN, H., SANDØ, A. B., DRANGE, H., HANSEN, B. & VALDIMARSSON, H. 2005. Influence of the Atlantic subpolar gyre on the thermohaline circulation. *Science,* 309**,** 1841-1844.

HELAMA, S., NIELSEN, J. K., NIELSEN, J. K., HANKEN, N.-M. & EVISON, K. 2014. Preboreal oscillations inferred from Arctica islandica sclerochronology. *Geobios,* 47**,** 305-313.

HELAMA, S., SCHÖNE, B. R., KIRCHHEFER, A. J., NIELSEN, J. K., RODLAND, D. L. & JANSSEN, R. 2007. Compound response of marine and terrestrial ecosystems to varying climate: Pre-anthropogenic perspective from bivalve shell growth increments and tree-rings. *Marine Environmental Research,* 63**,** 185-199.

HOLLAND, H. A., SCHÖNE, B. R., LIPOWSKY, C. & ESPER, J. 2014. Decadal climate variability of the North Sea during the last millennium reconstructed from bivalve shells (Arctica islandica). *The Holocene,* 24**,** 771-786.

HOPKINS, T. S. 1991. The GIN Sea - A synthesis of its physical oceanography and literature review 1972–1985. *Earth Science Reviews,* 30**,** 175-318.

HURRELL, J. W. 1995. Decadal trends in the North Atlantic Oscillation: Regional temperatures and precipitation. *Science,* 269**,** 676-679.

HURRELL, J. W., KUSHNIR, Y. & VISBECK, M. 2001. The North Atlantic Oscillation. *Science,* 291**,** 603-605.

HURRELL, J. W. J. 2001. The North Atlantic Oscillation. *Science,* 291**,** 603-605.

JENNINGS, A. E., HAGEN, S., HARÐARDÓTTIR, J., STEIN, R., OGILVIE, A. E. J. & JÓNSDÓTTIR, I. 2001. Oceanographic Change and Terrestrial Human Impacts in a Post A.D. 1400 Sediment Record from the Southwest Iceland Shelf. *Climatic Change,* 48**,** 83-100.

JONES, D. S. 1980. Annual Cycle of Shell Growth Increment Formation in Two Continental Shelf Bivalves and its Paleoecologic Significance. *Paleobiology,* 6**,** 331-340.

JONES, P. D., BRIFFA, K. R., OSBORN, T. J., LOUGH, J. M., VAN OMMEN, T. D., VINTHER, B. M., LUTERBACHER, J., WAHL, E. R., ZWIERS, F. W., MANN, M.

E., SCHMIDT, G. A., AMMANN, C. M., BUCKLEY, B. M., COBB, K. M., ESPER, J., GOOSSE, H., GRAHAM, N., JANSEN, E., KIEFER, T., KULL, C., KÜTTEL, M., MOSLEY-THOMPSON, E., OVERPECK, J. T., RIEDWYL, N., SCHULZ, M., TUDHOPE, A. W., VILLALBA, R., WANNER, H., WOLFF, E. & XOPLAKI, E. 2009. High-resolution palaeoclimatology of the last millennium: a review of current status and future prospects. *The Holocene,* 19**,** 3-49.

JUSTWAN, A., KOC, N. & JENNINGS, A. E. 2008. Evolution of the Irminger and East Icelandic Current systems through the Holocene, revealed by diatom-based sea surface temperature reconstructions. *Quaternary Science Reviews,* 27**,** 1571-1582.

KAPLAN, A., CANE, M. A., KUSHNIR, Y., CLEMENT, A. C., BLUMENTHAL, M. B. & RAJAGOPALAN, B. 1998. Analyses of global sea surface temperature 1856–1991. *Journal of Geophysical Research: Oceans,* 103**,** 18567-18589.

KERR, R. A., ROWAN, L. R. & SMITH, H. J. 2000. A North Atlantic climate pacemaker for the centuries. *Science,* 288**,** 1984-1986.

KNIGHT, J. R., FOLLAND, C. K. & SCAIFE, A. A. 2006. Climate impacts of the Atlantic Multidecadal Oscillation. *Geophysical Research Letters,* 33**,** 1-4.

KNUDSEN, K. L., EIRÍKSSON, J., JANSEN, E., JIANG, H., RYTTER, F. & RUTH GUDMUNDSDÓTTIR, E. 2004. Palaeoceanographic changes off North Iceland through the last 1200 years: foraminifera, stable isotopes, diatoms and ice rafted debris. *Quaternary Science Reviews,* 23**,** 2231-2246.

LECUYER, C., HUTZLER, A., AMIOT, R., DAUX, V., GROSHENY, D., OTERO, O., MARTINEAU, F., FOUREL, F., BALTER, V. & REYNARD, B. 2012. Carbon and oxygen isotope fractionations between aragonite and calcite of shells from modern molluscs. *Chem. Geol.,* 332**,** 92-101.

LOGEMANN, K., ÓLAFSSON, J., SNORRASON, Á., H., V. & MARTEINSDÓTTIR, G. 2013. The circulation of Icelandic waters – a modelling study. *Ocean Science Discussions (OSD),* 10**,** 763-824.

LOHMANN, G. & SCHÖNE, B. R. 2013. Climate signatures on decadal to interdecadal time scales as obtained from mollusk shells (Arctica islandica) from Iceland. *Palaeogeography, Palaeoclimatology, Palaeoecology,* 373**,** 152-162.

LOHMANN, K., DRANGE, H. & BENTSEN, M. 2009. A possible mechanism for the strong weakening of the North Atlantic subpolar gyre in the mid-1990s. *Geophysical Research Letters,* 36**,** n/a-n/a.

LUTERBACHER, J., XOPLAKI, E., DIETRICH, D., JONES, P. D., DAVIES, T. D., PORTIS, D., GONZALEZ-ROUCO, J. F., VON STORCH, H., GYALISTRAS, D., CASTY, C. & WANNER, H. 2001. Extending North Atlantic oscillation reconstructions back to 1500. *Atmospheric Science Letters,* 2**,** 114-124.

MACIAS FAURIA, M., GRINSTED, A., HELAMA, S., MOORE, J., TIMONEN, M., MARTMA, T., ISAKSSON, E. & ERONEN, M. 2010. Unprecedented low twentieth century winter sea ice extent in the Western Nordic Seas since A.D. 1200. *Climate Dynamics,* 34**,** 781-795.

MAHADEVAN, A., D'ASARO, E., LEE, C. & PERRY, M. J. 2012. Eddy-driven stratification initiates North Atlantic spring phytoplankton blooms. *Science,* 337**,** 54.

MAHAJAN, S., ZHANG, R. & DELWORTH, T. 2011. Impact of the Atlantic Meridional Overturning Circulation (AMOC) on Arctic Surface Air Temperature and Sea Ice Variability. *Journal of Climate,* 24**,** 6573-6581.

MANN, M. E., ZHANG, Z., RUTHERFORD, S., BRADLEY, R. S., HUGHES, M. K., SHINDELL, D., AMMANN, C., FALUVEGI, G. & NI, F. 2009. Global signatures

and dynamical origins of the Little Ice Age and Medieval Climate Anomaly. *Science,* 326**,** 1256.

MARALI, S. & SCHÖNE, B. R. 2015. Oceanographic control on shell growth of Arctica islandica (Bivalvia) in surface waters of Northeast Iceland — Implications for paleoclimate reconstructions. *Palaeogeography, Palaeoclimatology, Palaeoecology,* 420**,** 138-149.

MARCHITTO, T. M., JONES, G. A., GOODFRIEND, G. A. & WEIDMAN, C. R. 2000. Precise Temporal Correlation of Holocene Mollusk Shells Using Sclerochronology. *Quaternary Research,* 53**,** 236-246.

MARSHALL, J., KUSHNIR, Y., BATTISTI, D., CHANG, P., CZAJA, A., DICKSON, R., HURRELL, J., MCCARTNEY, M., SARAVANAN, R. & VISBECK, M. 2001. North Atlantic climate variability: phenomena, impacts and mechanisms. *International Journal of Climatology,* 21**,** 1863-1898.

MAURITZEN, C. 1996. Production of dense overflow waters feeding the North Atlantic across the Greenland-Scotland Ridge. Part 1: Evidence for a revised circulation scheme. *Deep-Sea Research Part I,* 43**,** 769-806.

MELLARD, J. P., YOSHIYAMA, K., LITCHMAN, E. & KLAUSMEIER, C. A. 2011. The vertical distribution of phytoplankton in stratified water columns. *Journal of Theoretical Biology,* 269**,** 16-30.

METTE, M. J., WANAMAKER, A. D., CARROLL, M. L., AMBROSE, W. G. & RETELLE, M. J. 2015. Linking large-scale climate variability with Arctica islandica shell growth and geochemistry in northern Norway. *Limnology and Oceanography,* 61**,** 748-764.

MILES, M. W., DIVINE, D. V., FUREVIK, T., JANSEN, E., MOROS, M. & OGILVIE, A. E. J. 2014. A signal of persistent Atlantic multidecadal variability in Arctic sea ice. *Geophysical Research Letters,* 41**,** 463-469.

MORK, K. A. & BLINDHEIM, J. 2000. Variations in the Atlantic inflow to the Nordic Seas, 1955–1996. *Deep-Sea Research Part I,* 47**,** 1035-1057.

MORTON, B. 2011. The biology and functional morphology of Arctica islandica (Bivalvia: Arcticidae): A gerontophilic living fossil. *Marine Biology Research,* 7**,** 540-553.

NYE, J. A., BAKER, M. R., BELL, R., KENNY, A., KILBOURNE, K. H., FRIEDLAND, K. D., MARTINO, E., STACHURA, M. M., VAN HOUTAN, K. S. & WOOD, R. 2014. Ecosystem effects of the Atlantic Multidecadal Oscillation. *Journal of Marine Systems,* 133**,** 103-116.

OESCHGER, R. & STOREY, K. B. 1993. Impact of anoxia and hydrogen sulphide on the metabolism of Arctica islandica L. (Bivalvia). *Journal of Experimental Marine Biology and Ecology,* 170**,** 213-226.

OGILVIE, A. E. J. 1983. The past climate and sea-ice record from Iceland, Part 1: Data to A.D. 1780. *Climatic Change,* 6**,** 131-152.

OGILVIE, A. E. J. 2005. *Local knowledge and travellers' tales: a selection of climatic observations in Iceland, In Iceland – Modern Processes and Past Environments* Elsevier, Amsterdam.

OGILVIE, A. E. J. & JONSDOTTIR, J. 2000. Sea ice, climate, and Icelandic fisheries in the eighteenth and nineteenth century. *Arctic,* 53**,** 383-94.

OSCHMANN, W. 2009. Sclerochronology: editorial. *International Journal of Earth Sciences,* 98**,** 1-2.

REID, P., C., EDWARDS, M., HUNT, H., G. & WARNER, A., J. 1998. Phytoplankton change in the North Atlantic. *Nature,* 391**,** 546.

REYNOLDS, D. J., SCOURSE, J. D., HALLORAN, P. R., NEDERBRAGT, A. J., WANAMAKER, A. D., BUTLER, P. G., RICHARDSON, C. A., HEINEMEIER, J., EIR1′, K. J., KNUDSEN, K. L. & HALL, I. R. 2016. Annually resolved North Atlantic marine climate over the last millennium. *Nature Communication,* 7.

RICHARDSON, A. J. & SCHOEMAN, D. S. 2004. Climate impact on plankton ecosystems in the Northeast Atlantic. *Science,* 305**,** 1609-1612.

ROPES, J. W. 1987. Preparation of Acetate Peels of Valves from the Ocean Quahog, *Arctica islandica*, for Age Determinations. *NOAA Technical Report NMFS 50.* U. S.: Department of Commerce.

ROPES, J. W., MURAWSKI, S. A. & SERSCHUK, F. M. 1984. Size, age, sexual maturity, and sex ratio in ocean quahogs, Arctica islandica Linné, off Long Island, New York *Fishery Bull,* 82**,** 253-268.

SCHÖNE, B. R. 2013. Arctica islandica (Bivalvia): A unique paleoenvironmental archive of the northern North Atlantic Ocean. *Global and Planetary Change,* 111**,** 199-225.

SCHÖNE, B. R., FIEBIG, J., PFEIFFER, M., GLEB, R., HICKSON, J., JOHNSON, A. L. A., DREYER, W. & OSCHMANN, W. 2005a. Climate records from a bivalved Methuselah (Arctica islandica, Mollusca; Iceland). *Palaeogeography, Palaeoclimatology, Palaeoecology,* 228**,** 130-148.

SCHÖNE, B. R., FREYRE CASTRO, A. D., FIEBIG, J., HOUK, S. D., OSCHMANN, W. & KRÖNCKE, I. 2004. Sea surface water temperatures over the period 1884–1983 reconstructed from oxygen isotope ratios of a bivalve mollusk shell (Arctica islandica, southern North Sea). *Palaeogeography, Palaeoclimatology, Palaeoecology,* 212**,** 215-232.

SCHÖNE, B. R. & GILLIKIN, D. P. 2013. Unraveling environmental histories from skeletal diaries. Advances in sclerochronology. *Palaeogeography, Palaeoclimatology, Palaeoecology,* 373**,** 1-5.

SCHÖNE, B. R., HOUK, S. D., FREYRE CASTRO, A. D., FIEBIG, J., OSCHMANN, W., KRÖNCKE, I., DREYER, W. & GOSSELCK, F. 2005b. Daily Growth Rates in Shells of Arctica islandica : Assessing Sub-seasonal Environmental Controls on a Long-lived Bivalve Mollusk. *PALAIOS,* 20**,** 78-92.

SCHÖNE, B. R., KRÖNCKE, I., HOUK, S. D., CASTRO, A. D. F. & OSCHMANN, W. 2002. The cornucopia of chilly winters: Ocean quahog (Arctica islandica L., Mollusca) master chronology reveals bottom water nutrient enrichment during colder winters (North Sea). *Senckenbergiana maritima,* 32**,** 165-175.

SCHÖNE, B. R., OSCHMANN, W., ROESSLER, J., CASTRO, A. D. F., HOUK, S. D., KROENCKE, I., DREYER, W., JANSSEN, R., RUMOHR, H. & DUNCA, E. 2003. North Atlantic Oscillation dynamics recorded in shells of a long-lived bivalve mollusk. *Geology,* 31**,** 1037-1040.

SCOURSE, J. D., RICHARDSON, C., FORSYTHE, G., HARRIS, I., HEINEMEIER, J., FRASER, N., BRIFFA, K. R., JONES, P. D. & SCOURSE, J. D. 2006. First cross-matched floating chronology from the marine fossil record; data from growth lines of the long-lived bivalve mollusc Arctica islandica. *The Holocene,* 16**,** 967-974.

SICRE, M.-A., JACOB, J., EZAT, U., ROUSSE, S., KISSEL, C., YIOU, P., EIRÍKSSON, J., KNUDSEN, K. L., JANSEN, E. & TURON, J.-L. 2008. Decadal variability of sea surface temperatures off North Iceland over the last 2000 years. *Earth and Planetary Science Letters,* 268**,** 137-142.

SMITH, T., REYNOLDS, R. & SMITH, T. 2003. Extended Reconstruction of Global Sea Surface Temperatures Based on COADS Data (1854-1997). *Journal of Climate,* 16**,** 1495-1510.

STEFÁNSSON, U. & GUÐMUNDSSON, G. 1976. The freshwater regime of Faxaflói, Southwest Iceland, and its relationship to meteorological variables. *Estuarine and Coastal Marine Science,* 6**,** 535-551.

STEFÁNSSON, U., THÓRDARDÓTTIR, T. & ÓLAFSSON, J. 1987. Comparison of seasonal oxygen cycles and primary production in the Faxaflói region, southwest Iceland. *Deep Sea Research Part A, Oceanographic Research Papers,* 34**,** 725-739.

STEMMER, K., NEHRKE, G., BREY, T. & STEPANOVA, A. 2013. Elevated CO2 Levels do not Affect the Shell Structure of the Bivalve Arctica islandica from the Western Baltic. *PLoS ONE,* 8.

STOKES, M. A. & SMILEY, T. L. 1996. Principles of tree-ring dating (Chp. 1). *An Introduction to Tree-ring Dating.* Chicago, Illinois University of Chicago Press.

THOMPSON, I. & JONES, D. S. 1977. The ocean quahog, Arctica islandica, "tree" of the north Atlantic shelf. . Annu. Meet. Geol. Soc. Amer. Abstr. 9, 1199.

THOMPSON, I., JONES, D. S. & DREIBELBIS, D. 1980. Annual internal growth banding and life history of the ocean quahog Arctica islandica (Mollusca: Bivalvia). *Marine Biology,* 57**,** 25-34.

THORARINSDÓTTIR, G. G. 2000. Annual gametogenic cycle in ocean quahog, Arctica islandica from north-western Iceland. *Journal of the Marine Biological Association of the U. K.,* 80**,** 661-666.

VALDIMARSSON, H. & MALMBERG, S.-A. 1999. Near-surface circulation in Icelandic waters derived from satellite tracked drifters. *Rit Fiskideildar* 16**,** 23-39.

VILHJÁLMSSON, H. 2002. Capelin (Mallotus villosus) in the Iceland–East Greenland–Jan Mayen ecosystem. *ICES Journal of Marine Science,* 59**,** 870-883.

VÅGE, K., PICKART, R. S., SARAFANOV, A., KNUTSEN, Ø., MERCIER, H., LHERMINIER, P., VAN AKEN, H. M., MEINCKE, J., QUADFASEL, D. & BACON, S. 2011. The Irminger Gyre: Circulation, convection, and interannual variability. *Deep-Sea Research Part I,* 58**,** 590-614.

WALLEVIK, J. E. & SIGURJÓNSSON, H. 1998. The Koch index: formulation, corrections and extensions. *Vedurstofa Íslands Report, VÍ-G98035-ÚR28.* Reykjavik, Iceland.

WANAMAKER, J. A. D., BUTLER, P., G. , SCOURSE, J., D. , HEINEMEIER, J., EIRÍKSSON, J., KNUDSEN, K. L. & RICHARDSON, C., A. 2012. Surface changes in the North Atlantic meridional overturning circulation during the last millennium. *Nature Communications,* 3**,** 899.

WANAMAKER, J. A. D., BUTLER, P. G., SCOURSE, J. D., RICHARDSON, C. A. & HEINEMEIER, J. 2009a. A near millennium-long record of annual summer seawater temperature changes from the North Icelandic Shelf; climate perspectives from a continuous, multi-century, master shell chronology. *GSA Annual Meeting.* Boulder, CO, United States: : Geological Society of America (GSA).

WANAMAKER, J. A. D., HEINEMEIER, J., SCOURSE, J. D., RICHARDSON, C. A., BUTLER, P. G., EIRÍKSSON, J. & KNUDSEN, K. L. 2008. Very Long-Lived Mollusks Confirm 17th Century AD Tephra-Based Radiocarbon Reservoir Ages for North Icelandic Shelf Waters. *Radiocarbon,* 50**,** 399-412.

WANAMAKER, J. A. D., HETZINGER, S. & HALFAR, J. 2011. Reconstructing mid- to high-latitude marine climate and ocean variability using bivalves, coralline algae, and marine sediment cores from the Northern Hemisphere. *Palaeogeography, Palaeoclimatology, Palaeoecology,* 302**,** 1-9.

WANAMAKER, J. A. D., KREUTZ, K., SCHÖNE, B., MAASCH, K., PERSHING, A., BORNS, H., INTRONE, D. & FEINDEL, S. 2009b. A late Holocene paleo-productivity record in the western Gulf of Maine, USA, inferred from growth histories

of the long-lived ocean quahog (Arctica islandica). *International Journal of Earth Science (Geologische Rundschau)*, 98**,** 19-29.
WEIDMAN, C. R., JONES, G. A. & LOHMANN, K. C. 1994. The long-lived mollusc Arctica islandica; a new paleoceanographic tool for the reconstruction of bottom temperatures for the continental shelves of the northern North Atlantic Ocean. *Journal of Geophysical Research,* 99**,** 18305-18311.
WIGLEY, T. M. L., BRIFFA, K. R. & JONES, P. D. 1984. On the average value of correlated time series, with applications in dendroclimatology and hydrometeorology. *Journal of Climate and Applied Meteorology,* 23**,** 201-213.
WITBAARD, R. 1996. Growth variations in Arctica islandica L. (Mollusca): a reflection of hydrography-related food supply. *ICES Journal of Marine Science,* 53**,** 981-987.
WITBAARD, R., DUINEVELD, G. C. A. & DE WILDE, P. A. W. J. 1999. Geographical differences in growth rates of Arctica islandica (Mollusca: Bivalvia) from the North Sea and adjacent waters. *Journal of Marine Biological Association of the U. K.,* 79**,** 907-915.
WITBAARD, R., DUINEVELD, G. C. A. & DEWILDE, P. A. W. J. 1997a. A long-term growth record derived from *Arctica ilandica* (Mollusca, Bivalvia) from the Fladen Ground (Northern North Sea). . *Journal of Marine Biological Association of the U. K.* , 77**,** 801-816.
WITBAARD, R., FRANKEN, R. & VISSER, B. 1997b. Growth of juvenile Arctica islandica under experimental conditions. *Helgoländer Meeresuntersuchungen,* 51**,** 417-431.
WITBAARD, R., JANSMA, E. & SASS KLAASSEN, U. 2003. Copepods link quahog growth to climate. *Journal of Sea Research,* 50**,** 77-83.
WITBAARD, R., JENNESS, M. I., VAN DER BORG, K. & GANSSEN, G. 1994. Verification of annual growth increments in Arctica islandica L. from the North Sea by means of oxygen and carbon isotopes. *Netherlands Journal of Sea Research,* 33**,** 91-101.
WITBAARD, R. & KLEIN, R. 1994. Long-term trends on the effects of the southern North Sea beamtrawl fishery on the bivalve mollusc Arctica islandica L. (Mollusca, Bivalvia). *ICES Journal of Marine Science,* 51**,** 99-105.

Online references

HURREL, J. & National Center for Atmospheric Research Staff (Eds.) (2017) *The Climate Data Guide: Hurrell North Atlantic Oscillation (NAO) Index (stationed based)* [Internet]
Available from: https://climatedataguide.ucar.edu/climate-data/hurrell-north-atlantic-oscillation-nao-index-station-based [Date accessed: 08.02.17]
National Center for Atmospheric Research Staff (Eds.) (2017) *Data Guide: SST data: HadiSST v1.1*. [Internet]
Available from: https://climatedataguide.ucar.edu/climate-data/sst-data-hadisst-v11 [Date accessed: 08.02.17]
National Oceanic and Atmospheric Administration (2013) *North Icelandic Shelf Arctica islandica Shell Measurement 1357 Year Record* [Internet]
Available from:
https://www.ncdc.noaa.gov/cdo/f?p=519:1:0::::P1_STUDY_ID:14609 [Date accessed: 01.01.2017]

SAHFOS – The Sir Alister Hardy Foundation for Ocean Science (2017) *Monthly Mean Graphs for CPR standard areas*. Plymouth [Internet]
Available from: https://www.sahfos.ac.uk/data/data-charts/ [Date accesses: 25.01.2017]

VALDIMARSSON, H. & DANIALSEN, M. (2017) Icelandic Marine Research Group. Reykjavik [Internet]
Available from: http://www.hafro.is/Sjora/ [Date accessed: 12.05.17]

VAN OLDENBORGH, G. J. (2017) Royal Netherlands Meteorological Institute, KNMI Climate Explorer [Internet]
Available from: https://climexp.knmi.nl [Date accessed: 23.10.16]

Appendices

Appendix A – Samples not included in the chronology

Table A1: Samples of *A. islandica* specimens which were processed, measured and studied, but not included in the chronology construction. All specimens were collected live in 2015.

Count	*Shell ID*	*Calendar Date*		*Sample Dimensions*	
		First increment formed (year)	*Age (Longevity)*	*Max. Height [mm]*	*Mass of a single valve [g]*
14	GS15 / 31-5SL	Ca. 1600	Ca. 400	94	89.69
15	GS15 / 31-2L	Ca. 1760	Ca.250	85	78.50
16	GS15 / 31-1SL	Ca. 1800	Ca.200	86	79.32
17	GS15 / 31-14SL	Ca. 1800	Ca. 200	80	47.56
18	GS15 /31-13SL	Ca. 1900	Ca. 110	82	55.98
19	GS15 / 31-20SL	Ca. 1950	Ca. 60	74	41.22
20	GS15 / 31-41SL	Ca. 1950	Ca. 60	77	40.85
21	GS15 / 31-37SL	Ca. 1960	Ca. 50	70	28.84
22	GS15 / 31-39SL	2002	14	44	8.13
23	GS15 / 31-34SL	2003	13	39	6.83

Figure A2: The oldest live collected *A. islandica* specimen examined in this study. Preliminary measurements and counting of the increments indicate an age of approximately 400 years.

Appendix B – Excel spreadsheet with increment width measurements compared during the visual cross-matching process

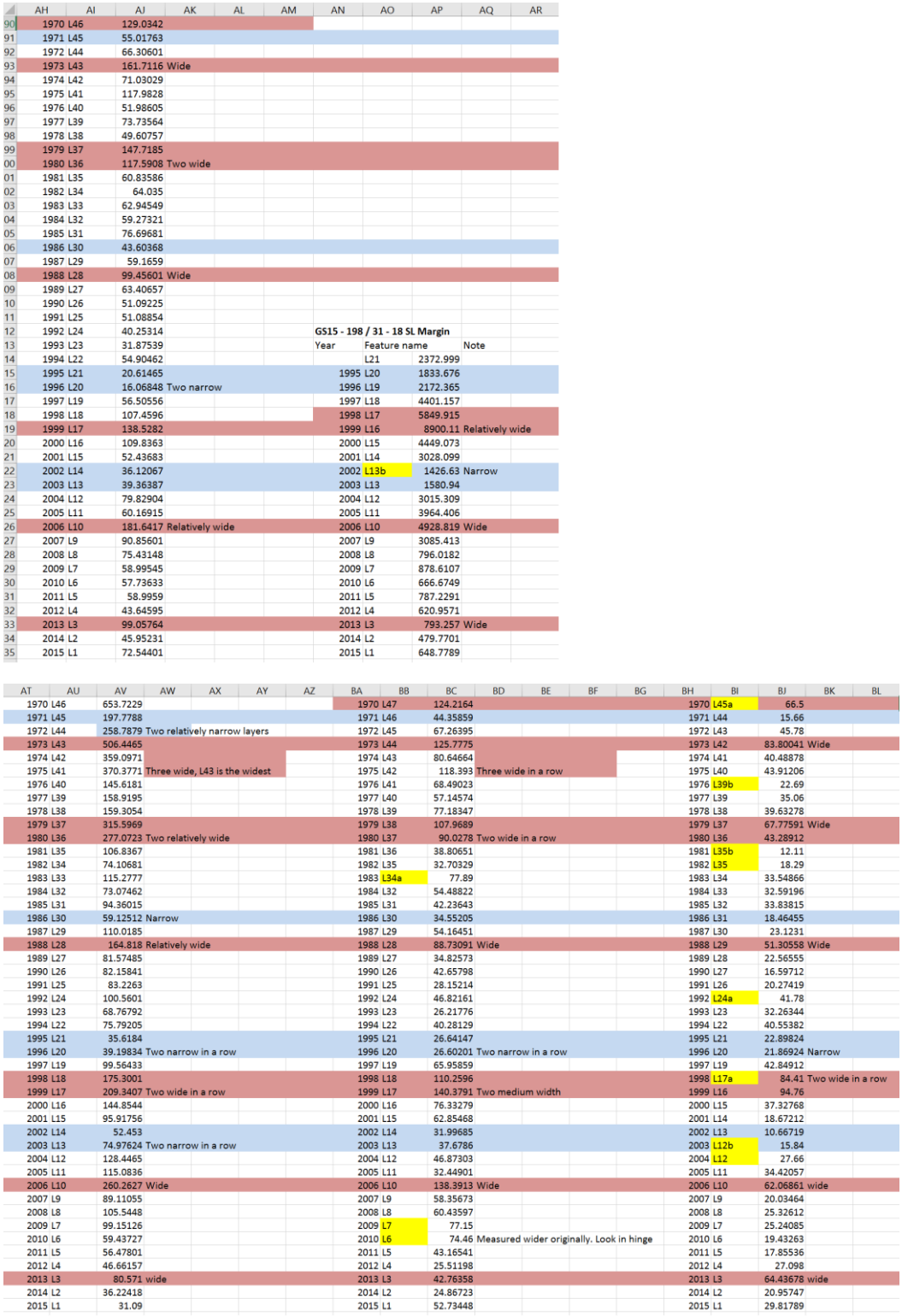

	AH	AI	AJ	AK	AL	AM	AN	AO	AP	AQ	AR
90	1970	L46	129.0342								
91	1971	L45	55.01763								
92	1972	L44	66.30601								
93	1973	L43	161.7116	Wide							
94	1974	L42	71.03029								
95	1975	L41	117.9828								
96	1976	L40	51.98605								
97	1977	L39	73.73564								
98	1978	L38	49.60757								
99	1979	L37	147.7185								
00	1980	L36	117.5908	Two wide							
01	1981	L35	60.83586								
02	1982	L34	64.035								
03	1983	L33	62.94549								
04	1984	L32	59.27321								
05	1985	L31	76.69681								
06	1986	L30	43.60368								
07	1987	L29	59.1659								
08	1988	L28	99.45601	Wide							
09	1989	L27	63.40657								
10	1990	L26	51.09225								
11	1991	L25	51.08854								
12	1992	L24	40.25314				GS15 - 198 / 31 - 18 SL Margin				
13	1993	L23	31.87539				Year		Feature name		Note
14	1994	L22	54.90462					L21	2372.999		
15	1995	L21	20.61465				1995	L20	1833.676		
16	1996	L20	16.06848	Two narrow			1996	L19	2172.365		
17	1997	L19	56.50556				1997	L18	4401.157		
18	1998	L18	107.4596				1998	L17	5849.915		
19	1999	L17	138.5282				1999	L16	8900.11	Relatively wide	
20	2000	L16	109.8363				2000	L15	4449.073		
21	2001	L15	52.43683				2001	L14	3028.099		
22	2002	L14	36.12067				2002	L13b	1426.63	Narrow	
23	2003	L13	39.36387				2003	L13	1580.94		
24	2004	L12	79.82904				2004	L12	3015.309		
25	2005	L11	60.16915				2005	L11	3964.406		
26	2006	L10	181.6417	Relatively wide			2006	L10	4928.819	Wide	
27	2007	L9	90.85601				2007	L9	3085.413		
28	2008	L8	75.43148				2008	L8	796.0182		
29	2009	L7	58.99545				2009	L7	878.6107		
30	2010	L6	57.73633				2010	L6	666.6749		
31	2011	L5	58.9959				2011	L5	787.2291		
32	2012	L4	43.64595				2012	L4	620.9571		
33	2013	L3	99.05764				2013	L3	793.257	Wide	
34	2014	L2	45.95231				2014	L2	479.7701		
35	2015	L1	72.54401				2015	L1	648.7789		

	AT	AU	AV	AW	AX	AY	AZ	BA	BB	BC	BD	BE	BF	BG	BH	BI	BJ	BK	BL
	1970	L46	653.7229					1970	L47	124.2164					1970	L45a	66.5		
	1971	L45	197.7788					1971	L46	44.35859					1971	L44	15.66		
	1972	L44	258.7879	Two relatively narrow layers				1972	L45	67.26395					1972	L43	45.78		
	1973	L43	506.4465					1973	L44	125.7775					1973	L42	83.80041	Wide	
	1974	L42	359.0971					1974	L43	80.64664					1974	L41	40.48878		
	1975	L41	370.3771	Three wide, L43 is the widest				1975	L42	118.393	Three wide in a row				1975	L40	43.91206		
	1976	L40	145.6181					1976	L41	68.49023					1976	L39b	22.69		
	1977	L39	158.9195					1977	L40	57.14574					1977	L39	35.06		
	1978	L38	159.3054					1978	L39	77.18347					1978	L38	39.63278		
	1979	L37	315.5969					1979	L38	107.9689					1979	L37	67.77591	Wide	
	1980	L36	277.0723	Two relatively wide				1980	L37	90.0278	Two wide in a row				1980	L36	43.28912		
	1981	L35	106.8367					1981	L36	38.80651					1981	L35b	12.11		
	1982	L34	74.10681					1982	L35	32.70329					1982	L35	18.29		
	1983	L33	115.2777					1983	L34a	77.89					1983	L34	33.54866		
	1984	L32	73.07462					1984	L32	54.48822					1984	L33	32.59196		
	1985	L31	94.36015					1985	L31	42.23643					1985	L32	33.83815		
	1986	L30	59.12512	Narrow				1986	L30	34.55205					1986	L31	18.46455		
	1987	L29	110.0185					1987	L29	54.16451					1987	L30	23.1231		
	1988	L28	164.818	Relatively wide				1988	L28	88.73091	Wide				1988	L29	51.30558	Wide	
	1989	L27	81.57485					1989	L27	34.82573					1989	L28	22.56555		
	1990	L26	82.15841					1990	L26	42.65798					1990	L27	16.59712		
	1991	L25	83.2263					1991	L25	28.15214					1991	L26	20.27419		
	1992	L24	100.5601					1992	L24	46.82161					1992	L24a	41.78		
	1993	L23	68.76792					1993	L23	26.21776					1993	L23	32.26344		
	1994	L22	75.79205					1994	L22	40.28129					1994	L22	40.55382		
	1995	L21	35.6184					1995	L21	26.64147					1995	L21	22.89824		
	1996	L20	39.19834	Two narrow in a row				1996	L20	26.60201	Two narrow in a row				1996	L20	21.86924	Narrow	
	1997	L19	99.56433					1997	L19	65.95859					1997	L19	42.84912		
	1998	L18	175.3001					1998	L18	110.2596					1998	L17a	84.41	Two wide in a row	
	1999	L17	209.3407	Two wide in a row				1999	L17	140.3791	Two medium width				1999	L16	94.76		
	2000	L16	144.8544					2000	L16	76.33279					2000	L15	37.32768		
	2001	L15	95.91756					2001	L15	62.85468					2001	L14	18.67212		
	2002	L14	52.453					2002	L14	31.99685					2002	L13	10.66719		
	2003	L13	74.97624	Two narrow in a row				2003	L13	37.6786					2003	L12b	15.84		
	2004	L12	128.4465					2004	L12	46.87303					2004	L12	27.66		
	2005	L11	115.0836					2005	L11	32.44901					2005	L11	34.42057		
	2006	L10	260.2627	Wide				2006	L10	138.3913	Wide				2006	L10	62.06861	wide	
	2007	L9	89.11055					2007	L9	58.35673					2007	L9	20.03464		
	2008	L8	105.5448					2008	L8	60.43597					2008	L8	25.32612		
	2009	L7	99.15126					2009	L7	77.15					2009	L7	25.24085		
	2010	L6	59.43727					2010	L6	74.46	Measured wider originally. Look in hinge				2010	L6	19.43263		
	2011	L5	56.47801					2011	L5	43.16541					2011	L5	17.85536		
	2012	L4	46.66157					2012	L4	25.51198					2012	L4	27.098		
	2013	L3	80.571	wide				2013	L3	42.76358					2013	L3	64.43678	wide	
	2014	L2	36.22418					2014	L2	24.86723					2014	L2	20.95747		
	2015	L1	31.09					2015	L1	52.73448					2015	L1	29.81789		

Figure B1: Example of how increment width measurements were compared in an Excel spreadsheet during the visual cross-matching process, with notes and colour coding for ‘marker years’. Yellow squares indicate increments which needed modification after visual inspection of Acetate peel images.

Appendix C – Master shell chronology versions

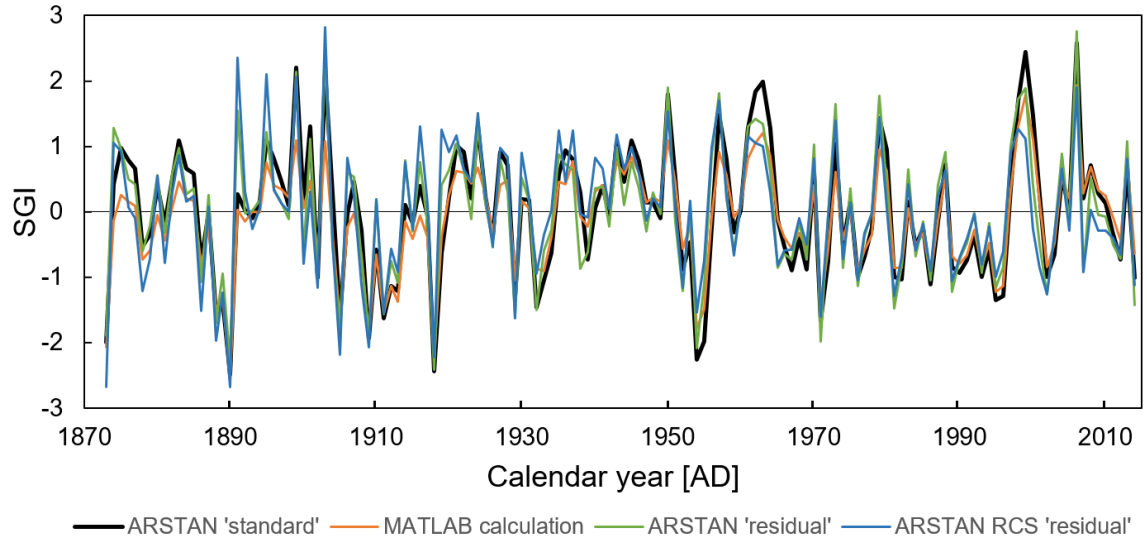

Figure D1: Mean Standard Growth Index (SGI) results from the 10 selected specimens as calculated by MATLAB/Excel and ARSTAN.

Appendix D – Continuous Plankton Recorder areas

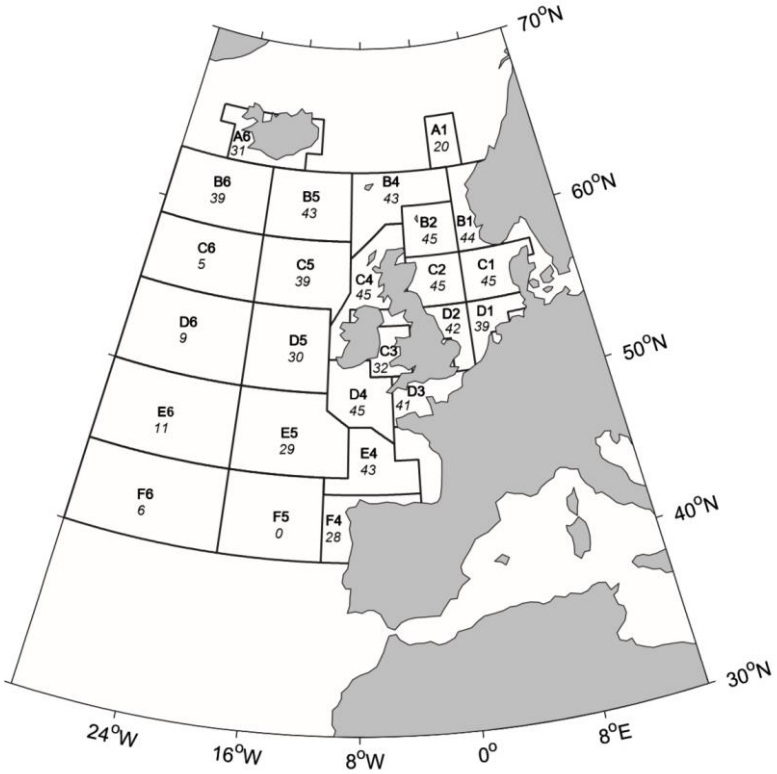

Figure F1: Map of the Northeast Atlantic Ocean showing standard CPR areas (bold) and the number of years (from 1958 to 2002) that eight or more months were sampled within each box (italics) (Richardson and Schoeman, 2004).

Appendix E – Individual chronology calculations

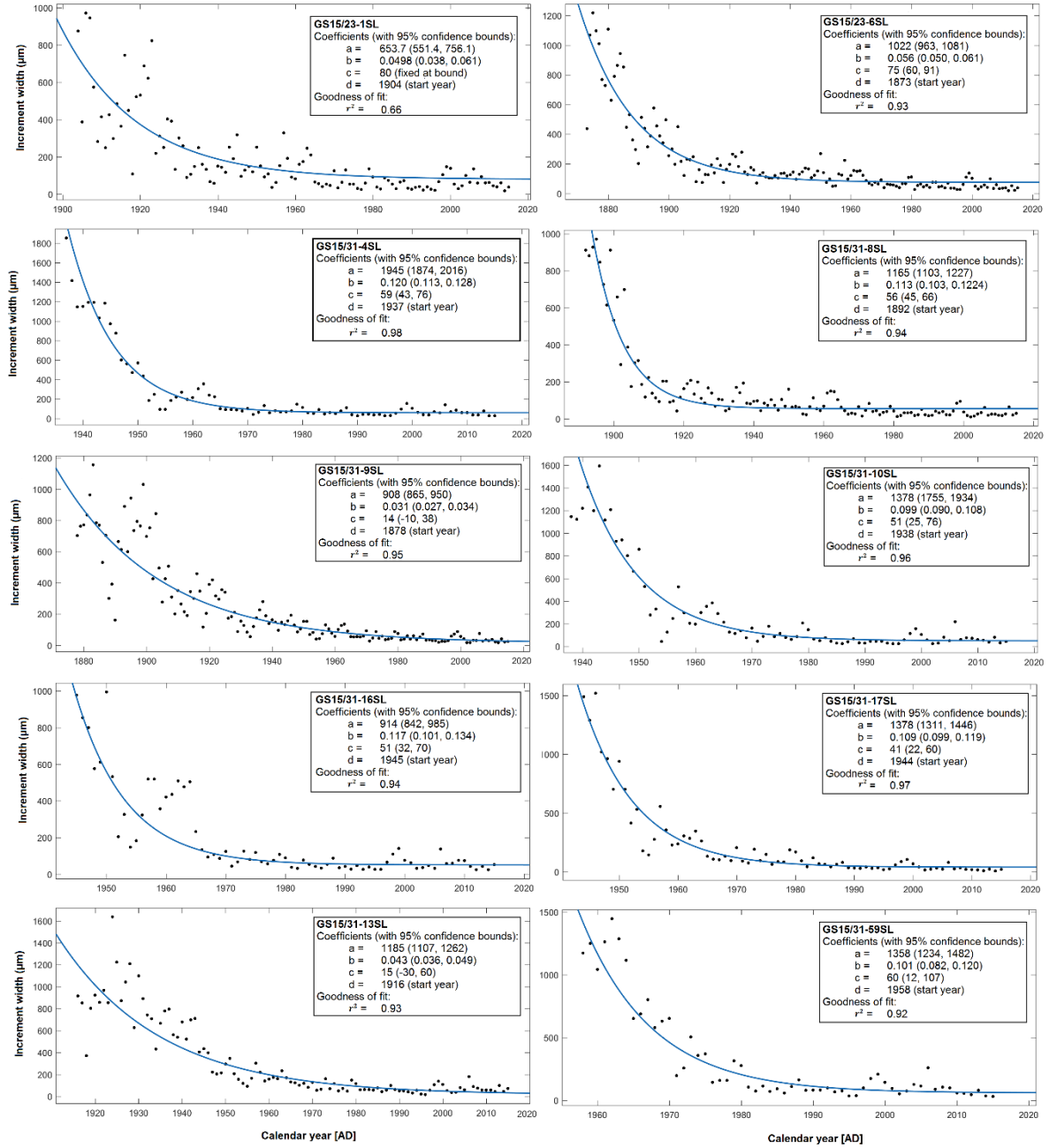

Figure E1**:** Raw increment measurement data with fitted exponential curves of the ten individual specimens calculated using MATLAB. The fitted curve was: f(x) = a *exp(-b *(x - d) + c

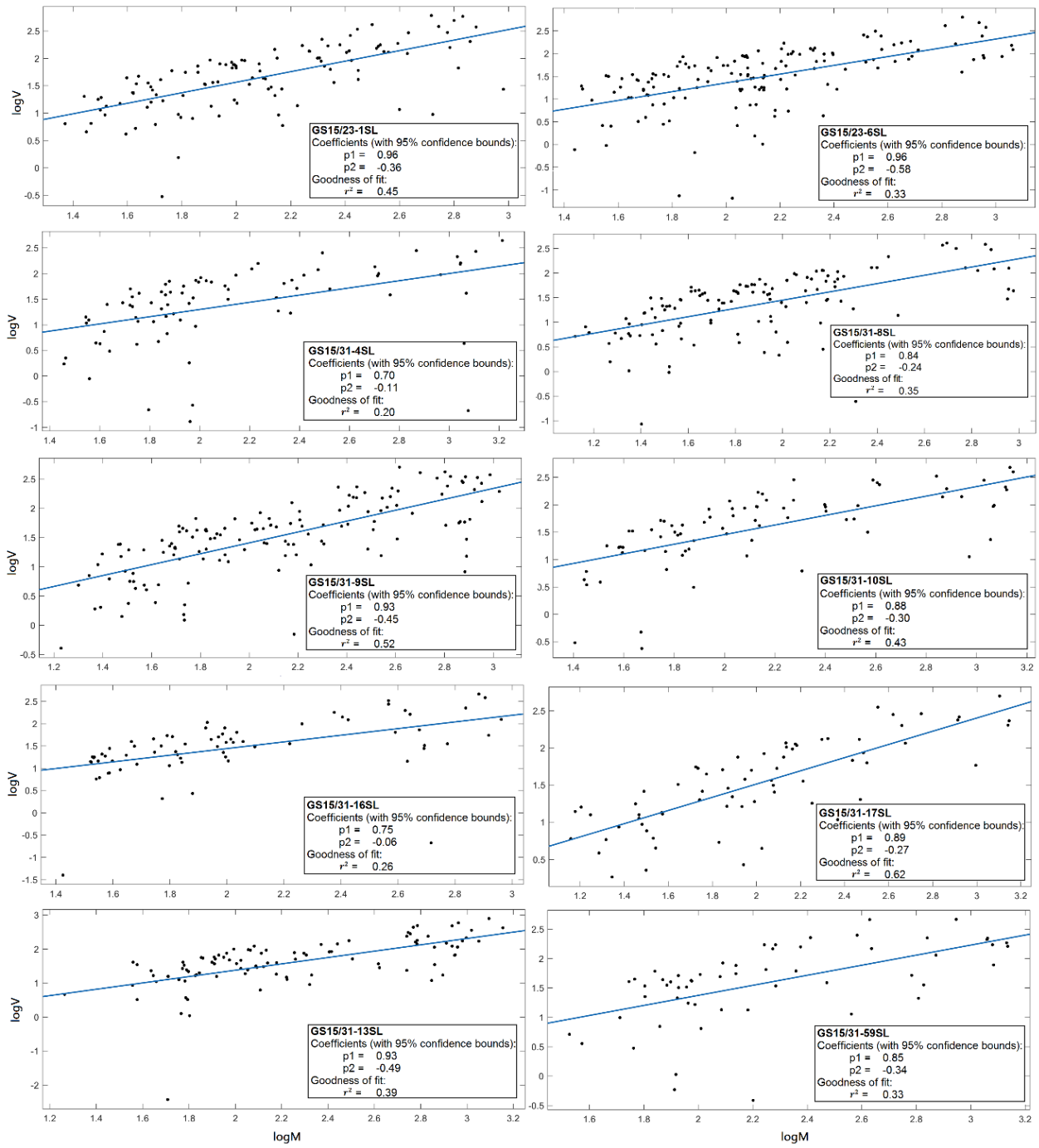

Figure E2: Local mean versus local variance with fitted trend line of the ten individual specimens calculated using MATLAB. The fitted curve was: *f(x) = p1*x + p2*.

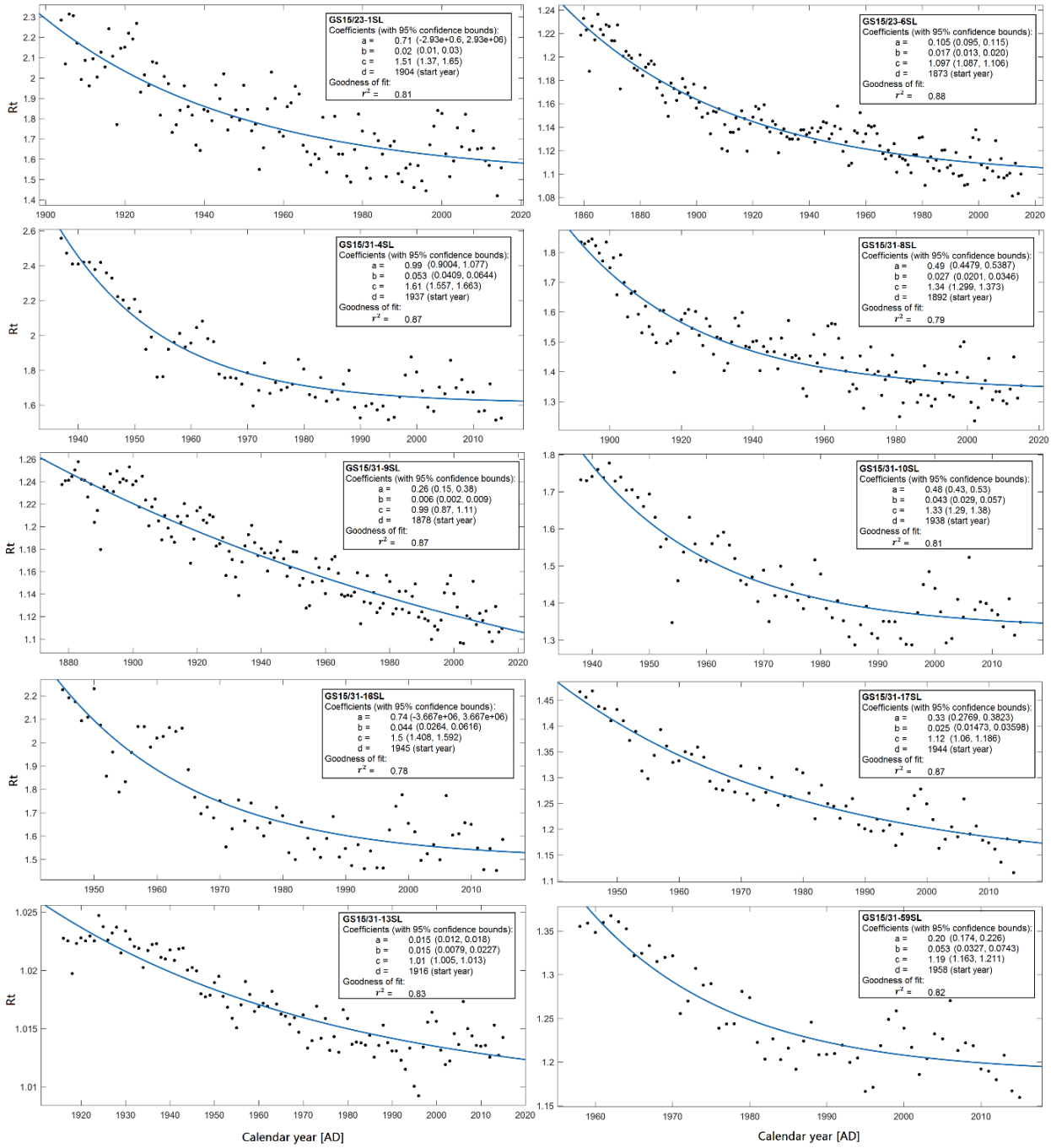

Figure E3: Data-adaptive power transformed (APT) data with fitted exponential curve for the ten individual specimens calculated using MATLAB. The fitted curve was: $f'(x) = a * exp(-b * (x - d) + c$.

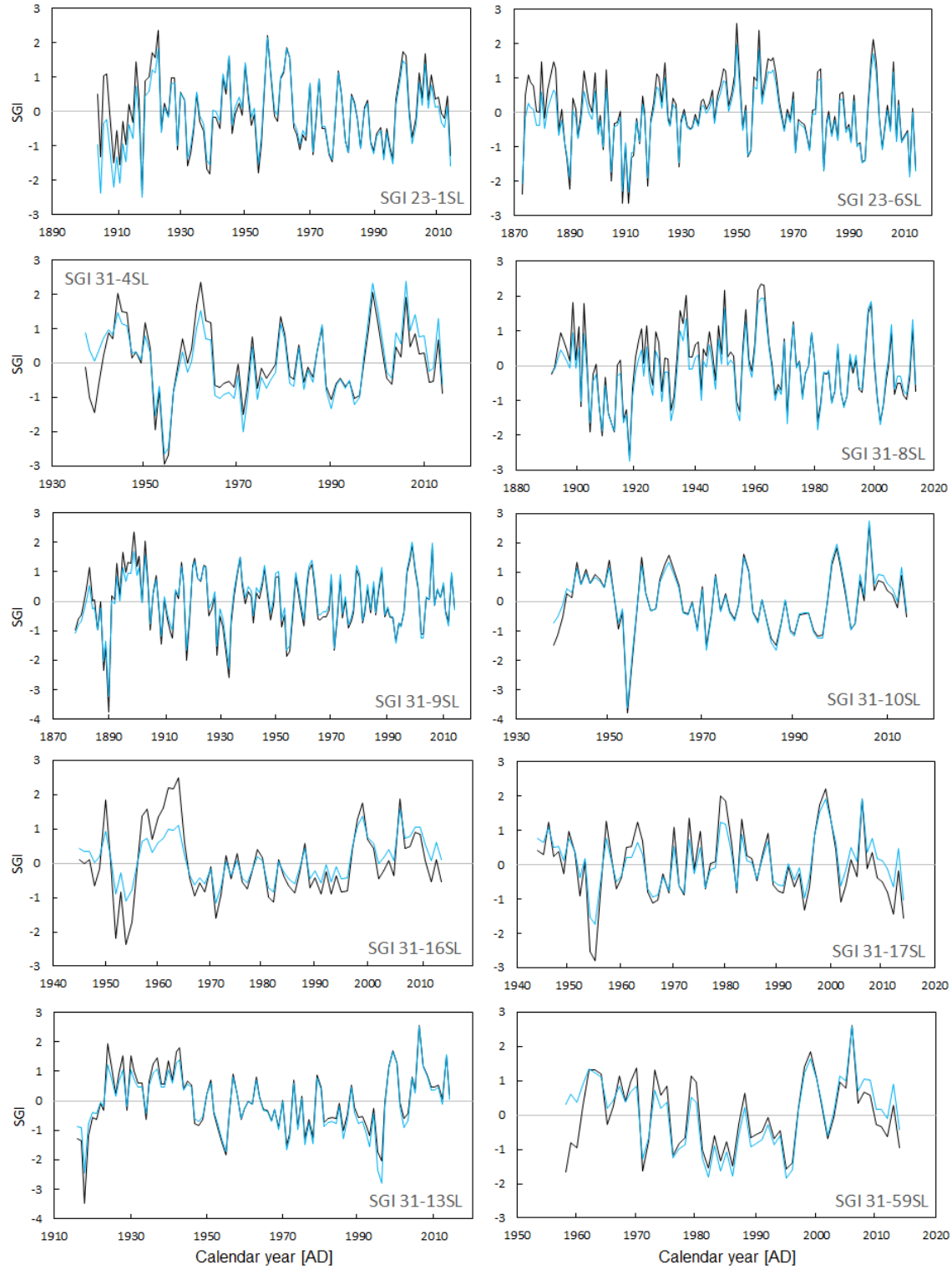

Figure E4: Standardized growth index curves calculated from the curve and data in Figure E3 (blue line) and similar obtained growth data using the ARSTAN software (black line).

Appendix F – Individual growth increment width data

Year	*GS15 23 6SL*	*GS15 31 9SL*	*GS15 31 8SL*	*GS15 23 1SL*	*GS1531 13SL*	*GS15314SL*	*GS15 31 10SL*	*GS15 31 17SL*	*GS15 31 16SL*	*GS15 31 59SL*
1873	0.43718									
1874	1.067958048									
1875	1.21943									
1876	1.09755									
1877	1.01161									
1878	0.76872	0.703538904								
1879	0.72964	0.762905072								
1880	1.108	0.771105271								
1881	0.62868	0.835348438								
1882	0.79105	0.9650097								
1883	0.86505	1.157296246								
1884	0.94452	0.785684094								
1885	0.85358	0.770503221								
1886	0.445984339	0.530706006								
1887	0.532603129	0.70454								
1888	0.362399928	0.30095069								
1889	0.29723349	0.392349239								
1890	0.202215534	0.161026592								
1891	0.513044787	0.665030637								
1892	0.438888806	0.614266771	0.911033223							
1893	0.315588974	0.890863673	0.881568885							
1894	0.389471587	0.599249231	0.92836256							
1895	0.576289987	0.944081369	0.971528069							
1896	0.456409036	0.735339597	0.846021815							
1897	0.389306904	0.79358495	0.725869005							
1898	0.341082938	0.764236472	0.614412196							
1899	0.496885133	1.030704844	0.912375608							
1900	0.255054814	0.697073762	0.531781325							
1901	0.299617228	0.752917246	0.65790218							
1902	0.19688535	0.426307461	0.293267438							
1903	0.451058036	0.844182519	0.698788887							
1904	0.217498179	0.495224218	0.387064056	0.87563						
1905	0.12208649	0.276720983	0.174080521	0.38765						
1906	0.231782104	0.425637581	0.301681504	0.97299						
1907	0.227509132	0.507469834	0.315414591	0.94597						
1908	0.248312486	0.309410315	0.186538337	0.57567						
1909	0.079823628	0.201109347	0.118716033	0.283465371						
1910	0.16036	0.351163048	0.22405	0.415124199						
1911	0.074285542	0.264239225	0.138739255	0.250190623						
1912	0.128535795	0.214970762	0.1137413	0.427389617						
1913	0.127006622	0.190518081	0.093072823	0.298717129						
1914	0.193373479	0.344345311	0.204077645	0.486055702						
1915	0.140017771	0.301398691	0.203830398	0.36454983						
1916	0.235780588	0.458182154	0.090764407	0.746421827	0.9162					
1917	0.189260101	0.346936554	0.09706159	0.449244098	0.8523					
1918	0.07438461	0.117218665	0.04312869	0.108313853	0.37205					
1919	0.163584797	0.204986926	0.116932017	0.5231377	0.8038					
1920	0.197058219	0.390264469	0.163347299	0.5325953	0.92391					
1921	0.266172391	0.4199	0.189992009	0.689005513	0.85691					
1922	0.249786639	0.316234131	0.208596657	0.62231	0.96867					
1923	0.182669766	0.296278036	0.13349	0.82464	0.85492					
1924	0.27936	0.35577665	0.19921	0.21949	1.63806					
1925	0.147206761	0.340330923	0.111644059	0.311083584	1.22373					
1926	0.129432573	0.173952283	0.086579088	0.251344489	0.8726304					
1927	0.175982477	0.184658583	0.167531528	0.40405259	1.0438947					
1928	0.15948673	0.212054045	0.13981	0.392502295	1.210604					
1929	0.070562725	0.087670385	0.06921086	0.13306544	0.6272819					
1930	0.124780594	0.154367808	0.106999666	0.30140244	1.1007255					
1931	0.140919967	0.127172571	0.103095964	0.260431294	0.8909518					
1932	0.112012477	0.084419525	0.044975033	0.089954517	0.74248					
1933	0.105672741	0.054395084	0.054552573	0.107261205	0.7082159					
1934	0.105737588	0.120432108	0.095192713	0.149070931	0.4331134					
1935	0.120728434	0.175474511	0.16981286	0.249590204	0.6680314					
1936	0.104330007	0.227327012	0.14074977	0.160920646	0.7800481					
1937	0.136305345	0.280724024	0.193175801	0.133559849	0.7971168	1.85486				
1938	0.13732	0.18923	0.084847607	0.06677444	0.5628574	1.41502	1.147717983			
1939	0.119128014	0.139998054	0.082417508	0.058484265	0.5394478	1.147232773	1.124790914			
1940	0.126433997	0.163920997	0.095542653	0.151103528	0.6794337	1.151533348	1.221645434			
1941	0.144344934	0.147944271	0.097683895	0.145195915	0.5218354	1.192675129	1.407929224			
1942	0.096238164	0.097176067	0.04482031	0.117654282	0.69853	1.192889374	1.199407518			
1943	0.13040284	0.14849392	0.084444218	0.253141487	0.710275	1.032911759	1.59576178			
1944	0.145979564	0.132966634	0.074014932	0.190528809	0.405786	1.186281084	1.117732728	1.48984		
1945	0.172797045	0.157015135	0.103073865	0.31849	0.4337782	0.972818176	1.20972	1.28865	0.97802	
1946	0.167390501	0.192976467	0.073899969	0.095263012	0.397325	0.877962342	0.930615796	1.51933	0.85434	
1947	0.10636324	0.129670409	0.047459951	0.128596773	0.2220308	0.600124373	0.941790319	1.020727231	0.799972443	
1948	0.122691044	0.085812715	0.10466347	0.149399864	0.20492	0.562008437	0.802168945	0.962635249	0.576367601	
1949	0.151990722	0.105405264	0.068400397	0.119694293	0.2138165	0.4724061	0.664369323	0.702988738	0.611668538	
1950	0.269364248	0.15336	0.160507006	0.25291894	0.2959786	0.571975139	0.858396699	0.939428869	0.99545	
1951	0.141460165	0.152657588	0.063716341	0.151576201	0.3461384	0.436882925	0.529396764	0.702997974	0.533169756	
1952	0.073600337	0.069298032	0.067555511	0.093293489	0.2071861	0.186019302	0.278242736	0.416577481	0.205037531	
1953	0.09759	0.082116152	0.061886529	0.10845	0.1573166	0.250057797	0.331371034	0.532005245	0.326989839	
1954	0.04833	0.04015052	0.027559168	0.036260873	0.1188114	0.09369783	0.045635807	0.180594685	0.14851349	
1955	0.0522538	0.042581573	0.022240142	0.062322615	0.0925806	0.093965079	0.12796	0.145019861	0.183840825	
1956	0.132982415	0.074833738	0.066422263	0.152714361	0.1667751	0.186395815	0.247974345	0.277741667	0.323888627	
1957	0.125462128	0.130594972	0.114324851	0.328590157	0.30247	0.219996125	0.527745119	0.55731	0.51989	
1958	0.22387	0.105720809	0.05514	0.191857741	0.21856	0.271389992	0.2973	0.35812	0.51968	1.17377
1959	0.097670721	0.076822626	0.04427805	0.090956126	0.1414684	0.197540545	0.205845468	0.228576712	0.357785777	1.25114
1960	0.122056253	0.05673293	0.068802161	0.08212388	0.159273	0.216025189	0.19972301	0.23934	0.421998578	1.043042924

1961	0.155139239	0.1022	0.14003	0.161048091	0.1738242	0.307737774	0.299841123	0.30665	0.436340247	1.26390603
1962	0.149520001	0.127917773	0.1496	0.174601632	0.1612966	0.357380218	0.354266742	0.2864467	0.50919	1.44828919
1963	0.153669863	0.136537012	0.14677612	0.246903486	0.2351834	0.240125326	0.385771419	0.348921334	0.47672	1.287697149
1964	0.122924939	0.092001949	0.103488745	0.210926101	0.17027	0.22342	0.290660031	0.263079482	0.5044	1.116185527
1965	0.086829622	0.055555048	0.063065534	0.066076736	0.1314283	0.101055969	0.21476	0.13364862	0.23286	0.653784305
1966	0.069244115	0.053332446	0.044643471	0.056631452	0.1252231	0.091713711	0.12861	0.108264109	0.1337	0.689425874
1967	0.0587	0.05485	0.025390328	0.040815505	0.1012764	0.091841727	0.117091529	0.103837099	0.093995646	0.803315795
1968	0.07576	0.05363	0.030967023	0.05359	0.119934	0.09005143	0.139339314	0.135165347	0.108480618	0.581255852
1969	0.065313057	0.058829479	0.027366801	0.04742	0.0827329	0.077648285	0.077128782	0.09872	0.086195347	0.632625613
1970	0.09207	0.093710045	0.0665	0.126710401	0.1290342	0.103809019	0.163165012	0.20673	0.124216424	0.653722891
1971	0.0399	0.027311995	0.01566	0.033682567	0.0550176	0.042557876	0.046855038	0.09414	0.044358592	0.197778757
1972	0.06324	0.04671	0.04578	0.063606175	0.066306	0.065188484	0.089379102	0.07798	0.067263946	0.258787876
1973	0.05998	0.087240867	0.083800408	0.129703907	0.1617116	0.133383262	0.180160673	0.19418	0.125777544	0.506446487
1974	0.05721	0.045029805	0.040488777	0.053620548	0.0710303	0.060291419	0.087445523	0.097450925	0.080646642	0.359097124
1975	0.04985	0.058566716	0.043912062	0.053324537	0.1179828	0.080711546	0.116732836	0.150257083	0.118392962	0.370377068
1976	0.03927506	0.035977862	0.02269	0.030481426	0.051986	0.066217753	0.079989493	0.066779105	0.068490229	0.145618076
1977	0.067056204	0.040030165	0.03506	0.025948925	0.0737356	0.070870688	0.064660852	0.088777055	0.057145735	0.158919517
1978	0.067130119	0.044936557	0.039632778	0.060121785	0.0496076	0.077588502	0.086682983	0.086099029	0.077183469	0.159305366
1979	0.108843577	0.088197642	0.067775914	0.136767539	0.1477185	0.145714635	0.207167153	0.188114378	0.10796888	0.31559687
1980	0.111439493	0.076015842	0.043289118	0.092861255	0.1175908	0.114545446	0.149724592	0.170260964	0.090027801	0.277072312
1981	0.027039868	0.034795759	0.01211	0.037587166	0.0608359	0.058262789	0.065436133	0.095741227	0.038806506	0.10683673
1982	0.055141506	0.039613197	0.01829	0.028422586	0.064035	0.0541315	0.05148227	0.044966835	0.032703293	0.074106808
1983	0.062883108	0.060022759	0.033548663	0.087621089	0.0629455	0.092297804	0.079189049	0.12003268	0.07789	0.115277726
1984	0.044781791	0.039052357	0.032591958	0.074303716	0.0592732	0.048630733	0.047835359	0.070317652	0.054488222	0.073074619
1985	0.057103729	0.060417899	0.033838146	0.053467162	0.0766968	0.062467923	0.031324943	0.064984386	0.042236428	0.094360154
1986	0.041625182	0.035714356	0.018464547	0.029872688	0.0436037	0.050879736	0.025317903	0.045206454	0.034552051	0.059125121
1987	0.07615729	0.053341346	0.0231231	0.065197366	0.0591659	0.077563381	0.042961392	0.065279174	0.054164505	0.110018472
1988	0.076816146	0.071582251	0.051305576	0.073170369	0.099456	0.110985787	0.068777292	0.081652925	0.088730913	0.16481805
1989	0.045716922	0.032146878	0.022565549	0.032520404	0.0634066	0.040589989	0.034143696	0.037223194	0.034825728	0.081574852
1990	0.048913979	0.036397144	0.016597123	0.026088121	0.0510922	0.029866757	0.030281698	0.032734984	0.04265798	0.082158408
1991	0.038254738	0.030835511	0.020274192	0.037373905	0.0510885	0.042149809	0.047134352	0.030486685	0.028152138	0.083226298
1992	0.071602231	0.029431847	0.04178	0.041494319	0.0402531	0.045189919	0.046898497	0.04394875	0.046821612	0.100560135
1993	0.035527109	0.018589959	0.032263441	0.022312547	0.0318754	0.037804077	0.046425782	0.031026341	0.026217762	0.068767924
1994	0.036473745	0.025657096	0.040553825	0.040006744	0.0549046	0.042069129	0.029930368	0.037066572	0.040281285	0.075792047
1995	0.027076639	0.023633413	0.022898236	0.026727367	0.0206147	0.028007936	0.02567	0.019499707	0.026641468	0.0356184
1996	0.02784	0.029840526	0.021869239	0.020346875	0.0160685	0.030255781	0.02537	0.028058729	0.026602014	0.039198339
1997	0.06221	0.058118163	0.042849125	0.067346459	0.0565056	0.05498782	0.058304628	0.060128016	0.06595859	0.099564328
1998	0.109816412	0.071637901	0.08441	0.104138322	0.1074596	0.097884254	0.116989922	0.088648373	0.110259649	0.175300123
1999	0.13788884	0.087669251	0.09476	0.147734936	0.1385282	0.155063288	0.158509537	0.107485378	0.140379061	0.209340685
2000	0.103421932	0.057032744	0.037327681	0.138553785	0.1098363	0.106073696	0.106896213	0.069845828	0.076332788	0.14485445
2001	0.049802322	0.041151167	0.01867212	0.053747295	0.0524368	0.064689935	0.059684829	0.043854548	0.062854683	0.095917557
2002	0.031544942	0.017149161	0.010667189	0.029996983	0.0361207	0.040720283	0.026688704	0.017926559	0.031996849	0.052452999
2003	0.045491727	0.016745915	0.01584	0.04484951	0.0393639	0.036341638	0.030132568	0.023716841	0.037678603	0.074976242
2004	0.057516704	0.033218979	0.02766	0.10008705	0.079829	0.071177913	0.081610216	0.034953441	0.046873032	0.128446548
2005	0.041239003	0.030852602	0.034420568	0.064073539	0.0601692	0.059715626	0.052249852	0.025643531	0.032449013	0.115083621
2006	0.100395408	0.076189581	0.062068608	0.135794473	0.1816417	0.142457668	0.219699595	0.080730034	0.138391324	0.260262664
2007	0.034501781	0.026883552	0.020034635	0.059709702	0.090856	0.070425694	0.062897568	0.028015929	0.058356734	0.089110545
2008	0.059957657	0.035249731	0.025326122	0.093631271	0.0754315	0.086807948	0.077081917	0.035639067	0.060435973	0.105544807
2009	0.033565328	0.029608768	0.025240852	0.060614953	0.0589954	0.062386382	0.07400435	0.023044888	0.07715	0.099151262
2010	0.036167763	0.037331809	0.019432629	0.062156409	0.0577363	0.062604055	0.062210125	0.021224722	0.07446	0.05943727
2011	0.038673031	0.022388177	0.01785536	0.045351153	0.0589959	0.035801109	0.055658301	0.01737825	0.043165413	0.056478013
2012	0.019557449	0.01756956	0.027097998	0.040123609	0.043646	0.036682394	0.041032289	0.011396615	0.025511977	0.046661569
2013	0.052292976	0.041790887	0.064436782	0.061693463	0.0990576	0.077938093	0.082558459	0.023955993	0.042763579	0.080571
2014	0.021119272	0.022400639	0.020957474	0.017632213	0.0459523	0.027803448	0.032725951	0.008089956	0.024867233	0.036224176

Appendix G - Isotope measurements

GS15/31-68SL			GS16/10-10SL			GS16/10-11SL		
Year	*δ18O (‰)*	*internal precision 1σ*	*Year*	*δ18O (‰)*	*internal precision 1σ*	*Year*	*δ18O (‰)*	*internal precision 1σ*
2004	2.69398030	0.128211299	2004	2.12820384	0.027475196	2004	2.17121279	0.03247798
2004/2005	2.78433444	0.028864965	2004/2005	2.06937257	0.025044508	2004/2005	2.58096646	0.04226432
2005	2.73746238	0.016882499	2005	2.44723884	0.045721243	2005	2.72787098	0.0274028
2005	2.62286746	0.078006206	2005	2.43368243	0.020960132	2005	2.54141959	0.0241501
2005	2.67285974	0.026607406	2005	2.43468495	0.022845411	2005	2.50932437	0.03551364
2005	2.61935236	0.031407815	2005	2.30230664	0.036237724	2005	2.46626987	0.03806245
2005	2.5992918	0.034717254	2005	2.29353142	0.023646472	2005	2.61977103	0.02630445
2005	2.54314339	0.031938575	2005	2.4069499	0.032810004	2005	2.30913066	0.03274828
2005	2.4788318	0.024657287	2005	2.26386509	0.021470808	2005	2.44754623	0.03314035
2005/2006	2.69882742	0.024658937	2005	2.28312007	0.0216129	2005	2.35470467	0.03306593
2006	2.92466942	0.016900969	2005	2.30385367	0.021891306	2005	2.29802828	0.01349715
2006	2.88224671	0.021072478	2005	2.43557749	0.042762572	2005	2.42568883	0.03329295
2006	2.7946987	0.048782871	2005/2006	2.40304306	0.037112596	2005	2.39052016	0.02719568
2006	2.76282585	0.023763424	2006	2.6655197	0.037943369	2005/2006	2.7883836	0.01759763
2006	2.72310279	0.030528135	2006	2.75873072	0.025722477	2006	2.80013677	0.03061522
2006	2.56924527	0.02141138	2006	2.88299648	0.037360897	2006	2.75375007	0.04064431
2006	2.66217974	0.032234586	2006	2.77048982	0.034956044	2006	2.56620087	0.02424372
2006	2.69858959	0.030163009	2006	2.70170517	0.035167912	2006	2.81840634	0.18647264
2006	2.47061352	0.030096374	2006	2.66113343	0.028457325	2006	3.33526619	0.16027057
2006	2.45490976	0.040141778	2006	2.74273217	0.044073786	2006	2.53835738	0.03343264
2006	2.35898607	0.024510298	2006	2.62373223	0.028512255	2006	2.55360212	0.04310929
2006	2.49527434	0.019821198	2006	2.38390701	0.037280593	2006	2.60040946	0.05273101
2006	2.27859516	0.024769999	2006	2.4005159	0.046676149	2006	2.31122552	0.05086851
2006/2007	2.46418138	0.014392375	2006	2.1766969	0.032457981	2006	2.43446786	0.03739243
2007	2.68897934	0.073997608	2006	2.28197467	0.024337426	2006	2.37859429	0.07566957
2007	2.67623088	0.083163847	2006	2.39329847	0.029470559	2006	2.39757879	0.05608824
2007	2.58249173	0.074431657	2006	2.40287963	0.025025343	2006/2007	2.32103094	0.07614179
2007	2.34575385	0.019442444	2006/2007	2.68148411	0.029733024	2007	2.52910572	0.0431106
2007	2.38771512	0.017301009	2007	2.54703346	0.027688883	2007	2.41763585	0.04585269
2007	2.20888933	0.009568347	2007	2.45026786	0.25100306	2007	2.44524312	0.0470316
2007/2008	2.01890309	0.059951098	2007	2.43318219	0.038782897	2007	x	x
2008	2.69874442	0.034297215	2007	2.46163308	0.042612248	2007	x	x
2008	2.64116667	0.032694285	2007	2.18731661	0.040501039	2007	2.47504579	0.07758121
2008	2.6706003	0.024081742	2007	2.26246801	0.028290334	2007	2.18037741	0.03065362
2008	2.60108091	0.026329135	2007	2.21609507	0.02192889	2007	2.30839299	0.09286824
2008	2.53118672	0.021175391	2007	2.70779491	0.135634641	2007/2008	2.3761675	0.06234347
2008	2.39073946	0.025224903	2007/2008	2.31958881	0.029241027	2008	2.97471715	0.06698481
2008/2009	2.38431471	0.072066371	2008	2.55818106	0.034827021	2008	2.73835285	0.05190709
2009	2.58937067	0.030169222	2008	2.62485791	0.027355561	2008	2.75736782	0.03584959
2009	2.85285051	0.019617322	2008	2.33702488	0.032870418	2008	2.46168659	0.07758185
2009	2.48496413	0.026885645	2008	2.34414916	0.018527144	2008	2.35172826	0.09896816
2009	2.36415277	0.036157113	2008	2.44166854	0.032500948	2008	2.20596337	0.03825729
2009	2.27438355	0.02621466	2008	2.39033571	0.018837045	2008/2009	2.4758071	0.04272455
2009/2010	2.59603886	0.032144593	2008	2.41171454	0.023406423	2009	2.56215982	0.02423598
2010	2.80109346	0.022088743	2008	2.1968075	0.030157629	2009	2.5353054	0.08892729
			2008/2009	2.26108764	0.046435434	2009	2.48594544	0.06389098
			2009	2.46954658	0.021646214	2009	2.31048242	0.03564281
			2009	2.46548004	0.041781611	2009	2.20809581	0.03813347
			2009	2.44130845	0.023620602	2009/2010	2.36090838	0.05859145
			2009	2.37386869	0.035786611	2010	2.72675348	0.03635281
			2009	2.29747788	0.037466612			
			2009	2.01535488	0.048643106			
			2009/2010	2.18956989	0.034906716			
			2010	2.59127528	0.027987799			

x = samples lost during IRMS analysis

Appendix H – ARSTAN output

```
                    ***********************************
                    ***********************************
                    ***                             ***
                    ***     Program ARSTAN_41d      ***
                    ***                             ***
                    ***      Creation Date:         ***
                    ***        03/18/07             ***
                    ***                             ***
                    ***      Programmed by:         ***
                    ***     Dr. Edward R. Cook      ***
                    ***      Paul J. Krusic         ***
                    ***    Tree-Ring Laboratory     ***
                    ***  Lamont-Doherty Earth Obs.  ***
                    ***    Palisades, N.Y. 10964    ***
                    *** drdendro@ldeo.columbia.edu  ***
                    ***    pjk@ldeo.columbia.edu    ***
                    ***  www.ldeo.columbia.edu/trl  ***
                    ***                             ***
                    ***********************************
                    ***********************************

                 MAXIMUM tree-ring chronology length:          5000
                 MAXIMUM number of tree-ring series:           1500

                   <ret> to run, / to exit, h for more info:

open the file listing the data file names
type h for help or <ret> to enter them     ==>

okay, so enter your data file name(s)
which will be stored in the new file: arstan.files
when done, hit <ret> to process the data file(s).

file name # 1: Iceland2014.cmp
file name # 2:

number of files to be processed:     1

okay, enter your overall run title:
==> IcelandChronology2014

run in batch mode from log file? y/<n>/h   ==>

|*************** arstan run time menu and current options settings
***************|

                        opt         plt
 [1] tree-ring data type    1              !tucson ring-width format
 [2] missing data in gap   -9           0   !missing values estimated (no plots)
 [3] data transformation    0           0   !no data transformation (no plots)
 [4] first detrending       1      0    0   !1st-neg expon curve (k>0), no = opt 4
 [5] second detrending      0      0    0   !2nd-no detrending performed
 [6] robust detrending      1              !non-robust detrending methods used
 [7] interactive detrend    0              !no interactive detrending
 [8] index calculation      1              !tree-ring indices or ratios (rt/gt)
 [9] ar modeling method     1           0   !non-robust autoregressive modeling
[10] pooled ar order        0           0   !minimum aic pooled ar model order fit
[11] series ar order        0              !pooled ar order fit to all series
[12] mean chronology        2   0    0   0  !robust (biweight) mean chronology
[13] stabilize variance     0              !no variance stabilization performed
[14] common period years        0    0      !no common period analysis performed
[15] site-tree-core mask        SSSTTCC     !site-tree-core separation mask
[16] running rbar              50   25   0   !running rbar window/overlap (no plots)
[17] printout option        2              !summary & series statistics printed
[18] core series save       0              !no individual core series saved
[19] summary plots          0              !no spaghetti and mean chronology plots
[20] stand dynamics stuff   0           0   !no stand dynamics analyses done
     running mean window    0              !running mean window width
     percent growth change  0              !percent growth change threshold
     std error threshold    0             !standard error limit threshold

enter the option to change (<ret> = go)    ==> 1

input control parameters from keyboard
hit <ret> for any specified default <parameters>

tree-ring measurement types (/ to exit, h for help):
raw measurements  (tucson format)   <1>
tree-ring series (uea cru format)    2
tree-ring indices (tucson format)    3
tree-ring series in compact format   4
enter your data format type                ==> 4

|*************** arstan run time menu and current options settings
***************|

                        opt         plt
 [1] tree-ring data type    4              !tree-ring compact data format
 [2] missing data in gap   -9           0   !missing values estimated (no plots)
 [3] data transformation    0           0   !no data transformation (no plots)
 [4] first detrending       1      0    0   !1st-neg expon curve (k>0), no = opt 4
 [5] second detrending      0      0    0   !2nd-no detrending performed
 [6] robust detrending      1              !non-robust detrending methods used
 [7] interactive detrend    0              !no interactive detrending
 [8] index calculation      1              !tree-ring indices or ratios (rt/gt)
 [9] ar modeling method     1           0   !non-robust autoregressive modeling
[10] pooled ar order        0           0   !minimum aic pooled ar model order fit
[11] series ar order        0              !pooled ar order fit to all series
[12] mean chronology        2   0    0   0  !robust (biweight) mean chronology
[13] stabilize variance     0              !no variance stabilization performed
[14] common period years        0    0      !no common period analysis performed
[15] site-tree-core mask        SSSTTCC     !site-tree-core separation mask
[16] running rbar              50   25   0   !running rbar window/overlap (no plots)
[17] printout option        2              !summary & series statistics printed
[18] core series save       0              !no individual core series saved
[19] summary plots          0              !no spaghetti and mean chronology plots
[20] stand dynamics stuff   0           0   !no stand dynamics analyses done
     running mean window    0              !running mean window width
     percent growth change  0              !percent growth change threshold
     std error threshold    0             !standard error limit threshold

enter the option to change (<ret> = go)    ==> 3

input control parameters from keyboard
hit <ret> for any specified default <parameters>

data transformation options (/ to exit, h for help):
no data transformation              <0>
natural log (rt)                     1
natural log (rt+1/6)                 2
inverse hypersine (rt)               3
adaptive power transform (rt^p)      4          (*** experimental!!! ***)
enter transformation method                ==> 4

plot the transformed data? y/<n>           ==>

|*************** arstan run time menu and current options settings
***************|

                        opt         plt
 [1] tree-ring data type    4              !tree-ring compact data format
 [2] missing data in gap   -9           0   !missing values estimated (no plots)
 [3] data transformation    4           0   !spread/level power transform (no plots)
 [4] first detrending       1      0    0   !1st-neg expon curve (k>0), no = opt 4
 [5] second detrending      0      0    0   !2nd-no detrending performed
 [6] robust detrending      1              !non-robust detrending methods used
 [7] interactive detrend    0              !no interactive detrending
 [8] index calculation      2              !residuals or differences (rt-gt)
 [9] ar modeling method     1           0   !non-robust autoregressive modeling
[10] pooled ar order        0           0   !minimum aic pooled ar model order fit
[11] series ar order        0              !pooled ar order fit to all series
[12] mean chronology        2   0    0   0  !robust (biweight) mean chronology
[13] stabilize variance     0              !no variance stabilization performed
[14] common period years        0    0      !no common period analysis performed
[15] site-tree-core mask        SSSTTCC     !site-tree-core separation mask
[16] running rbar              50   25   0   !running rbar window/overlap (no plots)
[17] printout option        2              !summary & series statistics printed
[18] core series save       0              !no individual core series saved
[19] summary plots          0              !no spaghetti and mean chronology plots
[20] stand dynamics stuff   0           0   !no stand dynamics analyses done
     running mean window    0              !running mean window width
     percent growth change  0              !percent growth change threshold
     std error threshold    0             !standard error limit threshold

enter the option to change (<ret> = go)    ==> 4

input control parameters from keyboard
hit <ret> for any specified default <parameters>

first tree-ring detrending option:
the detrending options (/ to exit, h for help):
friedman variable span smoother     -5
lowess robust smoothing method      -4
median filter sharpening/smoothing  -3
regional curve (rcs) detrending     -2
first differences                   -1
no detrending applied                0
neg expon curve (k>0), no = opt 4    1
neg expon curve (k>0), no = opt 5    2
neg expon curve (any k)              3
linear regression (any slope)        4
linear regression (neg slope)        5
horizontal line (arithmetic mean)    6
hugershoff growth curve              7
general negative exponential curve   8
smoothing spline (fixed n cutoff)   >9
smoothing spline (pct n cutoff)     <-9    ==> 2

plot data with curve fits? y/<n>           ==>

|*************** arstan run time menu and current options settings
***************|

                        opt         plt
 [1] tree-ring data type    4              !tree-ring compact data format
 [2] missing data in gap   -9           0   !missing values estimated (no plots)
 [3] data transformation    4           0   !spread/level power transform (no plots)
 [4] first detrending       2      0    0   !1st-neg expon curve (k>0), no = opt 5
 [5] second detrending      0      0    0   !2nd-no detrending performed
 [6] robust detrending      1              !non-robust detrending methods used
```

```
 [7] interactive detrend   0          !no interactive detrending
 [8] index calculation     2          !residuals or differences (rt-gt)
 [9] ar modeling method    1       0  !non-robust autoregressive modeling
[10] pooled ar order       0       0  !minimum aic pooled ar model order fit
[11] series ar order       0          !pooled ar order fit to all series
[12] mean chronology       2  0  0  0  !robust (biweight) mean chronology
[13] stabilize variance    0          !no variance stabilization performed
[14] common period years   0  0       !no common period analysis performed
[15] site-tree-core mask   SSSTTCC    !site-tree-core separation mask
[16] running rbar          50  25  0  !running rbar window/overlap (no plots)
[17] printout option       2          !summary & series statistics printed
[18] core series save      0          !no individual core series saved
[19] summary plots         0          !no spaghetti and mean chronology plots
[20] stand dynamics stuff  0       0  !no stand dynamics analyses done
     running mean window   0          !running mean window width
     percent growth change 0          !percent growth change threshold
     std error threshold   0          !standard error limit threshold

enter the option to change (<ret> = go)    ==> 7

input control parameters from keyboard
hit <ret> for any specified default <parameters>

interactive detrending (/ to exit, h for help):
no interactive detrending          <0>
interactive gap filling            1
interactive detrending             2
interactive gap and detrend        3     ==> 2

|********** arstan run time menu and current options settings
**********|

                    opt        plt
 [1] tree-ring data type   4           !tree-ring compact data format
 [2] missing data in gap   -9       0  !missing values estimated (no plots)
 [3] data transformation   4        0  !spread/level power transform (no plots)
 [4] first detrending      2     0  0  !1st-neg expon curve (k>0), no = opt 5
 [5] second detrending     0     0  0  !2nd-no detrending performed
 [6] robust detrending     1          !non-robust detrending methods used
 [7] interactive detrend   2          !interactive detrending used
 [8] index calculation     2          !residuals or differences (rt-gt)
 [9] ar modeling method    1       0  !non-robust autoregressive modeling
[10] pooled ar order       0       0  !minimum aic pooled ar model order fit
[11] series ar order       0          !pooled ar order fit to all series
[12] mean chronology       2  0  0  0  !robust (biweight) mean chronology
[13] stabilize variance    0          !no variance stabilization performed
[14] common period years   0  0       !no common period analysis performed
[15] site-tree-core mask   SSSTTCC    !site-tree-core separation mask
[16] running rbar          50  25  0  !running rbar window/overlap (no plots)
[17] printout option       2          !summary & series statistics printed
[18] core series save      0          !no individual core series saved
[19] summary plots         0          !no spaghetti and mean chronology plots
[20] stand dynamics stuff  0       0  !no stand dynamics analyses done
     running mean window   0          !running mean window width
     percent growth change 0          !percent growth change threshold
     std error threshold   0          !standard error limit threshold

enter the option to change (<ret> = go)    ==> 12

input control parameters from keyboard
hit <ret> for any specified default <parameters>

mean chronology options (/ to exit, h for help):
no mean chronologies computed      0
non-robust (arithmetic) mean       1
robust (biweight) mean             <2>
quantile (min -1 to max -100)      <0    ==> 2

compute bootstrap confidence limits?
be advised that no mean chronology
variance stabilization is allowed if
bootstrop limits are computed . . so
compute bootstrap confidence limits? y/<n> ==>

|********** arstan run time menu and current options settings
**********|

                    opt        plt
 [1] tree-ring data type   4           !tree-ring compact data format
 [2] missing data in gap   -9       0  !missing values estimated (no plots)
 [3] data transformation   4        0  !spread/level power transform (no plots)
 [4] first detrending      2     0  0  !1st-neg expon curve (k>0), no = opt 5
 [5] second detrending     0     0  0  !2nd-no detrending performed
 [6] robust detrending     1          !non-robust detrending methods used
 [7] interactive detrend   2          !interactive detrending used
 [8] index calculation     2          !residuals or differences (rt-gt)
 [9] ar modeling method    1       0  !non-robust autoregressive modeling
[10] pooled ar order       0       0  !minimum aic pooled ar model order fit
[11] series ar order       0          !pooled ar order fit to all series
[12] mean chronology       2  0  0  0  !robust (biweight) mean chronology
[13] stabilize variance    0          !no variance stabilization performed
[14] common period years   0  0       !no common period analysis performed
[15] site-tree-core mask   SSSTTCC    !site-tree-core separation mask
[16] running rbar          50  25  0  !running rbar window/overlap (no plots)
[17] printout option       2          !summary & series statistics printed
[18] core series save      0          !no individual core series saved
[19] summary plots         0          !no spaghetti and mean chronology plots
[20] stand dynamics stuff  0       0  !no stand dynamics analyses done
     running mean window   0          !running mean window width
     percent growth change 0          !percent growth change threshold
     std error threshold   0          !standard error limit threshold

enter the option to change (<ret> = go)    ==> 16

input control parameters from keyboard
hit <ret> for any specified default <parameters>

running rbar options (/ to exit, h for help):
enter rbar window length, <ret> for none   ==> 30
enter the running rbar window overlap      ==> 29

plot running rbar and eps? y/<n>           ==>

|********** arstan run time menu and current options settings
**********|

                    opt        plt
 [1] tree-ring data type   4           !tree-ring compact data format
 [2] missing data in gap   -9       0  !missing values estimated (no plots)
 [3] data transformation   4        0  !spread/level power transform (no plots)
 [4] first detrending      2     0  0  !1st-neg expon curve (k>0), no = opt 5
 [5] second detrending     0     0  0  !2nd-no detrending performed
 [6] robust detrending     1          !non-robust detrending methods used
 [7] interactive detrend   2          !interactive detrending used
 [8] index calculation     2          !residuals or differences (rt-gt)
 [9] ar modeling method    1       0  !non-robust autoregressive modeling
[10] pooled ar order       0       0  !minimum aic pooled ar model order fit
[11] series ar order       0          !pooled ar order fit to all series
[12] mean chronology       2  0  0  0  !robust (biweight) mean chronology
[13] stabilize variance    0          !no variance stabilization performed
[14] common period years   0  0       !no common period analysis performed
[15] site-tree-core mask   SSSTTCC    !site-tree-core separation mask
[16] running rbar          30  29  0  !running rbar window/overlap (no plots)
[17] printout option       2          !summary & series statistics printed
[18] core series save      0          !no individual core series saved
[19] summary plots         0          !no spaghetti and mean chronology plots
[20] stand dynamics stuff  0       0  !no stand dynamics analyses done
     running mean window   0          !running mean window width
     percent growth change 0          !percent growth change threshold
     std error threshold   0          !standard error limit threshold

enter the option to change (<ret> = go)    ==> 18

input control parameters from keyboard
hit <ret> for any specified default <parameters>

save core series (/ to exit, h for help):
no core series saved               <0>
save in tucson raw data format     1
save in tucson index format        2
save in uea cru index format       3
save in rlh compact data format    4
save in sas space-delimited columns  5
save in tab-delimited columns      6
save in comma-delimited columns    7     ==> 6

|********** arstan run time menu and current options settings
**********|

                    opt        plt
 [1] tree-ring data type   4           !tree-ring compact data format
 [2] missing data in gap   -9       0  !missing values estimated (no plots)
 [3] data transformation   4        0  !spread/level power transform (no plots)
 [4] first detrending      2     0  0  !1st-neg expon curve (k>0), no = opt 5
 [5] second detrending     0     0  0  !2nd-no detrending performed
 [6] robust detrending     1          !non-robust detrending methods used
 [7] interactive detrend   2          !interactive detrending used
 [8] index calculation     2          !residuals or differences (rt-gt)
 [9] ar modeling method    1       0  !non-robust autoregressive modeling
[10] pooled ar order       0       0  !minimum aic pooled ar model order fit
[11] series ar order       0          !pooled ar order fit to all series
[12] mean chronology       2  0  0  0  !robust (biweight) mean chronology
[13] stabilize variance    0          !no variance stabilization performed
[14] common period years   0  0       !no common period analysis performed
[15] site-tree-core mask   SSSTTCC    !site-tree-core separation mask
[16] running rbar          30  29  0  !running rbar window/overlap (no plots)
[17] printout option       2          !summary & series statistics printed
[18] core series save      6          !series saved in tab-delimited columns
[19] summary plots         0          !no spaghetti and mean chronology plots
[20] stand dynamics stuff  0       0  !no stand dynamics analyses done
     running mean window   0          !running mean window width
     percent growth change 0          !percent growth change threshold
     std error threshold   0          !standard error limit threshold

enter the option to change (<ret> = go)    ==> 19

input control parameters from keyboard
hit <ret> for any specified default <parameters>

summary hi-res plot options (/ to exit, h for help):
no summary hi-res plots            <0>
spaghetti plots of all series      1
various summary plots (try it!)    2
all of the above (lots!!!)         3     ==> 3

|********** arstan run time menu and current options settings
**********|

                    opt        plt
 [1] tree-ring data type   4           !tree-ring compact data format
 [2] missing data in gap   -9       0  !missing values estimated (no plots)
 [3] data transformation   4        0  !spread/level power transform (no plots)
```

```
 [4] first detrending      2     0    0   !1st-neg expon curve (k>0), no = opt 5
 [5] second detrending     0     0    0   !2nd-no detrending performed
 [6] robust detrending     1              !non-robust detrending methods used
 [7] interactive detrend   2              !interactive detrending used
 [8] index calculation     2              !residuals or differences (rt-gt)
 [9] ar modeling method    1          0   !non-robust autoregressive modeling
[10] pooled ar order       0          0   !minimum aic pooled ar model order fit
[11] series ar order       0              !pooled ar order fit to all series
[12] mean chronology       2  0   0   0   !robust (biweight) mean chronology
[13] stabilize variance    0              !no variance stabilization performed
[14] common period years       0    0      !no common period analysis performed
[15] site-tree-core mask       SSSTTCC      !site-tree-core separation mask
[16] running rbar              30   29   0   !running rbar window/overlap (no plots)
[17] printout option       2              !summary & series statistics printed
[18] core series save      6              !series saved in tab-delimited columns
[19] summary plots         3              !spaghetti and mean chronology plots
[20] stand dynamics stuff  0          0   !no stand dynamics analyses done
     running mean window   0              !running mean window width
     percent growth change 0              !percent growth change threshold
     std error threshold   0              !standard error limit threshold

enter the option to change (<ret> = go)    ==>

==> writing batch commands for: Iceland2014.cmp

  1  batch command files created

the log files have been created now.
continue with run? <y>/n/h                 ==>

data file #  1  --  Iceland2014.cmp
batch file inputs:
inputs.....!input indentification
4                !tree-ring compact data format
-9          0    !missing values estimated (no plots)
4           0    !spread/level power transform (no plots)
2     0     0    !1st-neg expon curve (k>0), no = opt 5
0     0     0    !2nd-no detrending performed
1                !non-robust detrending methods used
2                !interactive detrending used
2                !residuals or differences (rt-gt)
1           0    !non-robust autoregressive modeling
0           0    !minimum aic pooled ar model order fit (no plots)
0                !pooled ar order fit to all series
2  0  0   0      !robust (biweight) mean chronology
0                !no variance stabilization performed
0    0           !no common period analysis performed
SSSTTCC          !site-tree-core separation mask
30    29     0   !running rbar window/overlap (no plots)
2                !summary & series statistics printed
6                !series saved in tab-delimited columns
3                !spaghetti and mean chronology plots
0           0    !no stand dynamics analyses done

   10 series from   1873 to   2014     142 years

all possible series rbar:  0.8022  +/-  0.1330 1sd
percent of all possible cross-correlations:    100.00
percent of all possible tree-ring years used:   55.31

calculate raw data chronology running rbar
window length:        30
window overlap:       29
segments calculated:  105

transform the individual tree-ring series

   1  GS15 31 8SL
   2  GS15 31 9SL
   3  GS15 31 10SL
   4  GS15 31 13SL
   5  GS15 31 16SL
   6  GS15 31 17SL
   7  GS15 31 59SL
   8  GS15 23 1SL
   9  GS15 23 6SL
  10  GS15 31 14SL


        |************** plot options menu **************|
        | replot           [0] line color        [4] |
        | background color  [1] bar fill  color   [21] |
        | frame color       [2] curve style       [6] |
        | text color        [3] curve width       [7] |
        |                                             |
        |          reset plot options   [99]          |
        |---------------------------------------------|
        |             [s]ave  [c]ontinue              |
        |_____________________________________________|

         enter option number >

all possible series rbar:  0.8460  +/-  0.0848 1sd
percent of all possible cross-correlations:    100.00
percent of all possible tree-ring years used:   55.31

calculate transformed data running rbar
window length:        30
window overlap:       29
segments calculated:  105

calculate the robust raw data chronology
  year:  1873
  year:  1900
  year:  2000
  year:  2014


        |************** plot options menu **************|
        | replot           [0]  minor ticks y  [11] |
        | background color   [1]  major ticks z  [12] |
        | frame color        [2]  minor ticks z  [13] |
        | text color         [3]  max. x         [14] |
        | line color         [4]  min. x         [15] |
        | fit  color         [5]  max. y         [16] |
        | line style         [6]  min. y         [17] |
        | curve width        [7]                 [ ] |
        | major ticks x      [8]                 [ ] |
        | minor ticks x      [9]                 [ ] |
        | major ticks y     [10]                 [ ] |
        |                                             |
        |          reset plot options  [99]           |
        |---------------------------------------------|
        |   [s]ave   <[c]ontinue>  [n]o more plots    |
        |_____________________________________________|

         enter option number >


        |************** plot options menu **************|
        | replot           [0]  minor ticks  y  [11] |
        | background color  [1]  major ticks  z  [12] |
        | frame color       [2]  minor ticks  z  [13] |
        | text color        [3]  max. x         [14] |
        | line color        [4]  min. x         [15] |
        | curve  color      [5]  max. y         [16] |
        | line style        [6]  min. y         [17] |
        | curve width       [7]                 [ ] |
        | major ticks  x    [8]                 [ ] |
        | minor ticks  x    [9]                 [ ] |
        | major ticks  y   [10]                 [ ] |
        |                                             |
        |          reset plot options  [99]           |
        |---------------------------------------------|
        |   [s]ave   <[c]ontinue>  [n]o more plots    |
        |_____________________________________________|

         enter option number >

first detrending of individual tree-ring series


        |************** plot options menu **************|
        | replot           [0]  minor ticks y  [11] |
        | background color   [1]  major ticks z  [12] |
        | frame color        [2]  minor ticks z  [13] |
        | text color         [3]  max. x         [14] |
        | line color         [4]  min. x         [15] |
        | curve  color       [5]  max. y         [16] |
        | line style         [6]  min. y         [17] |
        | curve width        [7]  max. z         [18] |
        | major ticks x      [8]  min. z         [19] |
        | minor ticks x      [9]  symbol type    [20] |
        | major ticks y     [10]  symbol color   [21] |
        |                                             |
        |           reset options  [99]               |
        |---------------------------------------------|
        |   [s]ave   <[c]ontinue>  [n]o more plots    |
        |_____________________________________________|

         enter option number >

change curve fit? y/<n>                    ==>
continue interactive detrending? <y>/n     ==>


        |************** plot options menu **************|
        | replot           [0]  minor ticks y  [11] |
        | background color   [1]  major ticks z  [12] |
        | frame color        [2]  minor ticks z  [13] |
        | text color         [3]  max. x         [14] |
        | line color         [4]  min. x         [15] |
        | curve  color       [5]  max. y         [16] |
        | line style         [6]  min. y         [17] |
        | curve width        [7]  max. z         [18] |
        | major ticks x      [8]  min. z         [19] |
        | minor ticks x      [9]  symbol type    [20] |
        | major ticks y     [10]  symbol color   [21] |
        |                                             |
        |           reset options  [99]               |
        |---------------------------------------------|
        |   [s]ave   <[c]ontinue>  [n]o more plots    |
        |_____________________________________________|

         enter option number >

change curve fit? y/<n>                    ==> y

you can change the current curve fit with any one of the following options:

 -5:  friedman super smoother        lower alpha (0-9) gives more local fit
```

```
 -4:  robust lowess smoother         integer percent or fixed length of n
 -3:  median smoothing               must have odd window length
  1:  neg expon curve, no = opt 4    f(i) = a*exp(-b*t(i)) + d    (d>0)
  2:  neg expon curve, no = opt 5    f(i) = a*exp(-b*t(i)) + d    (d>0)
  3:  neg expon curve  (general)     f(i) = a*exp(-b*t(i)) + d   (any d)
  4:  linear regression (any slope)  f(i) = +/-c*t(i) + d
  5:  linear regression (neg slope)  f(i) = -c*t(i) + d
  6:  horizontal line through mean   f(i) = mean(y(i)) = d
  7:  hugershoff growth function     f(i) = a*t(i+p)**b * exp(-c*t(i+p)) + d
  8:  general exponential (b = 1)    f(i) = a*t(i+p)**b * exp(-c*t(i+p)) + d
 >9:  cubic smoothing spline         fixed 50 pct variance cutoff
<-9:  cubic smoothing spline         pct n 50 pct variance cutoff

enter new option (h for help)            ==> 3


        |************* plot options menu **************|
        | replot            [0]  minor ticks y   [11] |
        | background color   [1]  major ticks z   [12] |
        | frame color        [2]  minor ticks z   [13] |
        | text color         [3]  max. x          [14] |
        | line color         [4]  min. x          [15] |
        | curve  color       [5]  max. y          [16] |
        | line style         [6]  min. y          [17] |
        | curve width        [7]  max. z          [18] |
        | major ticks x      [8]  min. z          [19] |
        | minor ticks x      [9]  symbol type     [20] |
        | major ticks y     [10]  symbol color    [21] |
        |                                              |
        |            reset options  [99]               |
        |----------------------------------------------|
        |   [s]ave   <[c]ontinue>  [n]o more plots     |
        |______________________________________________|

        enter option number >

change curve fit? y/<n>                ==>
continue interactive detrending? <y>/n    ==>


        |************* plot options menu **************|
        | replot            [0]  minor ticks y   [11] |
        | background color   [1]  major ticks z   [12] |
        | frame color        [2]  minor ticks z   [13] |
        | text color         [3]  max. x          [14] |
        | line color         [4]  min. x          [15] |
        | curve  color       [5]  max. y          [16] |
        | line style         [6]  min. y          [17] |
        | curve width        [7]  max. z          [18] |
        | major ticks x      [8]  min. z          [19] |
        | minor ticks x      [9]  symbol type     [20] |
        | major ticks y     [10]  symbol color    [21] |
        |                                              |
        |            reset options  [99]               |
        |----------------------------------------------|
        |   [s]ave   <[c]ontinue>  [n]o more plots     |
        |______________________________________________|

        enter option number >

change curve fit? y/<n>                ==>
continue interactive detrending? <y>/n    ==>


        |************* plot options menu **************|
        | replot            [0]  minor ticks y   [11] |
        | background color   [1]  major ticks z   [12] |
        | frame color        [2]  minor ticks z   [13] |
        | text color         [3]  max. x          [14] |
        | line color         [4]  min. x          [15] |
        | curve  color       [5]  max. y          [16] |
        | line style         [6]  min. y          [17] |
        | curve width        [7]  max. z          [18] |
        | major ticks x      [8]  min. z          [19] |
        | minor ticks x      [9]  symbol type     [20] |
        | major ticks y     [10]  symbol color    [21] |
        |                                              |
        |            reset options  [99]               |
        |----------------------------------------------|
        |   [s]ave   <[c]ontinue>  [n]o more plots     |
        |______________________________________________|

        enter option number >

change curve fit? y/<n>                ==> y

you can change the current curve fit with any one of the following options:

 -5:  friedman super smoother        lower alpha (0-9) gives more local fit
 -4:  robust lowess smoother         integer percent or fixed length of n
 -3:  median smoothing               must have odd window length
  1:  neg expon curve, no = opt 4    f(i) = a*exp(-b*t(i)) + d    (d>0)
  2:  neg expon curve, no = opt 5    f(i) = a*exp(-b*t(i)) + d    (d>0)
  3:  neg expon curve  (general)     f(i) = a*exp(-b*t(i)) + d   (any d)
  4:  linear regression (any slope)  f(i) = +/-c*t(i) + d
  5:  linear regression (neg slope)  f(i) = -c*t(i) + d
  6:  horizontal line through mean   f(i) = mean(y(i)) = d
  7:  hugershoff growth function     f(i) = a*t(i+p)**b * exp(-c*t(i+p)) + d
  8:  general exponential (b = 1)    f(i) = a*t(i+p)**b * exp(-c*t(i+p)) + d
 >9:  cubic smoothing spline         fixed 50 pct variance cutoff
<-9:  cubic smoothing spline         pct n 50 pct variance cutoff

enter new option (h for help)            ==> 3


        |************* plot options menu **************|
        | replot            [0]  minor ticks y   [11] |
        | background color   [1]  major ticks z   [12] |
        | frame color        [2]  minor ticks z   [13] |
        | text color         [3]  max. x          [14] |
        | line color         [4]  min. x          [15] |
        | curve  color       [5]  max. y          [16] |
        | line style         [6]  min. y          [17] |
        | curve width        [7]  max. z          [18] |
        | major ticks x      [8]  min. z          [19] |
        | minor ticks x      [9]  symbol type     [20] |
        | major ticks y     [10]  symbol color    [21] |
        |                                              |
        |            reset options  [99]               |
        |----------------------------------------------|
        |   [s]ave   <[c]ontinue>  [n]o more plots     |
        |______________________________________________|

        enter option number >

change curve fit? y/<n>                ==>
continue interactive detrending? <y>/n    ==>


        |************* plot options menu **************|
        | replot            [0]  minor ticks y   [11] |
        | background color   [1]  major ticks z   [12] |
        | frame color        [2]  minor ticks z   [13] |
        | text color         [3]  max. x          [14] |
        | line color         [4]  min. x          [15] |
        | curve  color       [5]  max. y          [16] |
        | line style         [6]  min. y          [17] |
        | curve width        [7]  max. z          [18] |
        | major ticks x      [8]  min. z          [19] |
        | minor ticks x      [9]  symbol type     [20] |
        | major ticks y     [10]  symbol color    [21] |
        |                                              |
        |            reset options  [99]               |
        |----------------------------------------------|
        |   [s]ave   <[c]ontinue>  [n]o more plots     |
        |______________________________________________|

        enter option number >

change curve fit? y/<n>                ==>
continue interactive detrending? <y>/n    ==>


        |************* plot options menu **************|
        | replot            [0]  minor ticks y   [11] |
        | background color   [1]  major ticks z   [12] |
        | frame color        [2]  minor ticks z   [13] |
        | text color         [3]  max. x          [14] |
        | line color         [4]  min. x          [15] |
        | curve  color       [5]  max. y          [16] |
        | line style         [6]  min. y          [17] |
        | curve width        [7]  max. z          [18] |
        | major ticks x      [8]  min. z          [19] |
        | minor ticks x      [9]  symbol type     [20] |
        | major ticks y     [10]  symbol color    [21] |
        |                                              |
        |            reset options  [99]               |
        |----------------------------------------------|
        |   [s]ave   <[c]ontinue>  [n]o more plots     |
        |______________________________________________|

        enter option number >

change curve fit? y/<n>                ==>
continue interactive detrending? <y>/n    ==>


        |************* plot options menu **************|
        | replot            [0]  minor ticks y   [11] |
        | background color   [1]  major ticks z   [12] |
        | frame color        [2]  minor ticks z   [13] |
        | text color         [3]  max. x          [14] |
        | line color         [4]  min. x          [15] |
        | curve  color       [5]  max. y          [16] |
        | line style         [6]  min. y          [17] |
        | curve width        [7]  max. z          [18] |
        | major ticks x      [8]  min. z          [19] |
        | minor ticks x      [9]  symbol type     [20] |
        | major ticks y     [10]  symbol color    [21] |
        |                                              |
        |            reset options  [99]               |
        |----------------------------------------------|
        |   [s]ave   <[c]ontinue>  [n]o more plots     |
        |______________________________________________|

        enter option number >

change curve fit? y/<n>                ==>
continue interactive detrending? <y>/n    ==>


        |************* plot options menu **************|
```

```
    | replot            [0]  minor ticks y   [11] |
    | background color   [1]  major ticks z   [12] |
    | frame color        [2]  minor ticks z   [13] |
    | text color         [3]  max. x          [14] |
    | line color         [4]  min. x          [15] |
    | curve  color       [5]  max. y          [16] |
    | line style         [6]  min. y          [17] |
    | curve width        [7]  max. z          [18] |
    | major ticks x      [8]  min. z          [19] |
    | minor ticks x      [9]  symbol type     [20] |
    | major ticks y     [10]  symbol color    [21] |
    |                                              |
    |             reset options  [99]              |
    |----------------------------------------------|
    |   [s]ave   <[c]ontinue>  [n]o more plots     |
    |______________________________________________|

    enter option number >

change curve fit? y/<n>                 ==>
continue interactive detrending? <y>/n     ==>


    |************* plot options menu **************|
    | replot            [0]  minor ticks y   [11] |
    | background color   [1]  major ticks z   [12] |
    | frame color        [2]  minor ticks z   [13] |
    | text color         [3]  max. x          [14] |
    | line color         [4]  min. x          [15] |
    | curve  color       [5]  max. y          [16] |
    | line style         [6]  min. y          [17] |
    | curve width        [7]  max. z          [18] |
    | major ticks x      [8]  min. z          [19] |
    | minor ticks x      [9]  symbol type     [20] |
    | major ticks y     [10]  symbol color    [21] |
    |                                              |
    |             reset options  [99]              |
    |----------------------------------------------|
    |   [s]ave   <[c]ontinue>  [n]o more plots     |
    |______________________________________________|

    enter option number >

change curve fit? y/<n>                 ==>
continue interactive detrending? <y>/n     ==>


    |************* plot options menu **************|
    | replot            [0]  minor ticks y   [11] |
    | background color   [1]  major ticks z   [12] |
    | frame color        [2]  minor ticks z   [13] |
    | text color         [3]  max. x          [14] |
    | line color         [4]  min. x          [15] |
    | curve  color       [5]  max. y          [16] |
    | line style         [6]  min. y          [17] |
    | curve width        [7]  max. z          [18] |
    | major ticks x      [8]  min. z          [19] |
    | minor ticks x      [9]  symbol type     [20] |
    | major ticks y     [10]  symbol color    [21] |
    |                                              |
    |             reset options  [99]              |
    |----------------------------------------------|
    |   [s]ave   <[c]ontinue>  [n]o more plots     |
    |______________________________________________|

    enter option number >

change curve fit? y/<n>                 ==>
continue interactive detrending? <y>/n     ==>

    |************* plot options menu *************|
    | replot           [0]  minor ticks  y  [11] |
    | background color  [1]  major ticks  z  [12] |
    | frame color       [2]  minor ticks  z  [13] |
    | text color        [3]  max. x         [14] |
    | line color        [4]  min. x         [15] |
    | curve  color      [5]  max. y         [16] |
    | line style        [6]  min. y         [17] |
    | curve width       [7]                 [  ] |
    | major ticks  x    [8]                 [  ] |
    | minor ticks  x    [9]                 [  ] |
    | major ticks  y   [10]                 [  ] |
    |                                            |
    |          reset plot options  [99]          |
    |--------------------------------------------|
    |   [s]ave   <[c]ontinue>  [n]o more plots   |
    |____________________________________________|

    enter option number >

all possible series rbar:  0.6823  +/-   0.0941 1sd
percent of all possible cross-correlations:    100.00
percent of all possible tree-ring years used:   55.31

calculate standard chronology running rbar
window length:        30
window overlap:       29
segments calculated:  105

calculate the robust standard tree-ring chronology
   year:   1873
   year:   1900
   year:   2000
   year:   2014

    |************* plot options menu **************|
    | replot            [0]  minor ticks y   [11] |
    | background color   [1]  major ticks z   [12] |
    | frame color        [2]  minor ticks z   [13] |
    | text color         [3]  max. x          [14] |
    | line color         [4]  min. x          [15] |
    | fit  color         [5]  max. y          [16] |
    | line style         [6]  min. y          [17] |
    | curve width        [7]                  [  ] |
    | major ticks x      [8]                  [  ] |
    | minor ticks x      [9]                  [  ] |
    | major ticks y     [10]                  [  ] |
    |                                              |
    |           reset plot options  [99]           |
    |----------------------------------------------|
    |   [s]ave   <[c]ontinue>  [n]o more plots     |
    |______________________________________________|

    enter option number >


    |************* plot options menu *************|
    | replot           [0]  minor ticks  y  [11] |
    | background color  [1]  major ticks  z  [12] |
    | frame color       [2]  minor ticks  z  [13] |
    | text color        [3]  max. x         [14] |
    | line color        [4]  min. x         [15] |
    | curve  color      [5]  max. y         [16] |
    | line style        [6]  min. y         [17] |
    | curve width       [7]                 [  ] |
    | major ticks  x    [8]                 [  ] |
    | minor ticks  x    [9]                 [  ] |
    | major ticks  y   [10]                 [  ] |
    |                                            |
    |          reset plot options  [99]          |
    |--------------------------------------------|
    |   [s]ave   <[c]ontinue>  [n]o more plots   |
    |____________________________________________|

    enter option number >

computing pooled autoregression

selected autoregression order:   1
r-squared due to pooled autoregression:   18.19 pct
variance inflation from autoregression:  122.23 pct


    |************* plot options menu ***************|
    | replot            [0] line color        [4] |
    | background color   [1] bar fill  color   [5] |
    | frame color        [2] curve style       [6] |
    | text color         [3] curve width       [7] |
    |                                               |
    |              reset options  [99]              |
    |-----------------------------------------------|
    |            [s]ave   <[c]ontinue>              |
    |_______________________________________________|

    enter option number >

calculate individual series autoregressions


all possible series rbar:  0.7280  +/-   0.0668 1sd
percent of all possible cross-correlations:    100.00
percent of all possible tree-ring years used:   55.31

calculate residual chronology running rbar
window length:        30
window overlap:       29
segments calculated:  105

calculate the robust residual tree-ring chronology
   year:   1873
   year:   1900
   year:   2000
   year:   2014

--------------------

batch detail file saved: Iceland2014.cmp_detail

|===== as jim morrison would say, "this is the end." =====|
```